(12) PATENT
(19) AUSTRALIAN PATENT OFFICE

(11) Application No. **AU 200034833 B2**
(10) Patent No. **774889**

(54) Title
A method and apparatus for predicting the presence of haemostatic dysfunction in a patient sample

(51)[7] International Patent Classification(s)
G01N 033/86

(21) Application No: **200034833**

(22) Application Date: **2000.02.04**

(87) WIPO No: **WO00/46603**

(30) Priority Data

(31) Number	(32) Date	(33) Country
09/244340	**1999.02.04**	**US**

(43) Publication Date : **2000.08.25**
(43) Publication Journal Date : **2000.10.26**
(44) Accepted Journal Date : **2004.07.08**

(71) Applicant(s)
bioMerieux, Inc.

(72) Inventor(s)
Cheng Hock Toh; Colin Downey; Timothy J. Fischer

(74) Agent/Attorney
WATERMARK PATENT and TRADEMARK ATTORNEYS,Locked Bag 5,HAWTHORN VIC 3122

(56) Related Art
US 5708591

34833/800

PCT WORLD INTELLECTUAL PROPERTY ORGANIZATION
International Bureau

INTERNATIONAL APPLICATION PUBLISHED UNDER THE PATENT COOPERATION TREATY (PCT)

(51) International Patent Classification 7 : G01N 33/86 — A1

(11) International Publication Number: WO 00/46603

(43) International Publication Date: 10 August 2000 (10.08.00)

(21) International Application Number: PCT/US00/02987

(22) International Filing Date: 4 February 2000 (04.02.00)

(30) Priority Data:
09/244,340 4 February 1999 (04.02.99) US

(71) Applicant *(for all designated States except US)*: ~~AKZO NOBEL N.V. [NL/NL]; Velperweg 76, P.O. Box 186, NL-6800 LS Arnhem (NL).~~ bioMerieux, Inc. 595 Anglum Drive, Hazelwood Missouri 63042 (US)

(72) Inventors; and

(75) Inventors/Applicants *(for US only)*: TOH, Cheng, Hock [MY/GB]; 35 Beaconsfield Road, Liverpool L25 6EQ (GB). DOWNEY, Colin [GB/GB]; 23 Grieve Road, Liverpool L10 7NH (GB). FISCHER, Timothy, J. [US/US]; 4825 Winterwood Drive, Raleigh, NC 22613 (US).

(74) Agents: BLACKSTONE, William, M. et al.; Akzo Nobel Patent Department, Suite 206, 1300 Piccard Drive, Rockville, MD 20850 (US).

(81) Designated States: AU, CA, JP, KR, US, European patent (AT, BE, CH, CY, DE, DK, ES, FI, FR, GB, GR, IE, IT, LU, MC, NL, PT, SE).

Published
With international search report.
Before the expiration of the time limit for amending the claims and to be republished in the event of the receipt of amendments.

(54) Title: A METHOD AND APPARATUS FOR PREDICTING THE PRESENCE OF HAEMOSTATIC DYSFUNCTION IN A PATIENT SAMPLE

(57) Abstract

A method is disclosed for predicting the presence of haemostatic dysfunction. At least one time-dependent measurement (101) on an unknown sample (103) is performed and a respective property of the sample (103) is measured over time so as to derive a time-dependent measurement profile. One or more predictor variables (110), including initial slope, are defined which sufficiently define the data of the time-dependent measurement profile. A model (113) is then derived that represents the relationship between an abnormality and a set of predictor variables (110). Subsequently, the model (113) is utilized to predict haemostatic dysfunction.

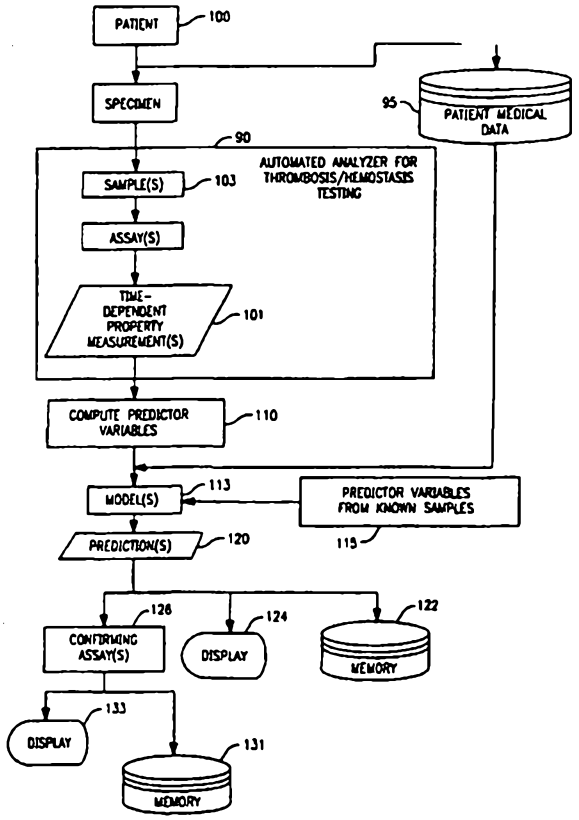

FOR THE PURPOSES OF INFORMATION ONLY

Codes used to identify States party to the PCT on the front pages of pamphlets publishing international applications under the PCT.

AL	Albania	**ES**	Spain	**LS**	Lesotho	**SI**	Slovenia
AM	Armenia	**FI**	Finland	**LT**	Lithuania	**SK**	Slovakia
AT	Austria	**FR**	France	**LU**	Luxembourg	**SN**	Senegal
AU	Australia	**GA**	Gabon	**LV**	Latvia	**SZ**	Swaziland
AZ	Azerbaijan	**GB**	United Kingdom	**MC**	Monaco	**TD**	Chad
BA	Bosnia and Herzegovina	**GE**	Georgia	**MD**	Republic of Moldova	**TG**	Togo
BB	Barbados	**GH**	Ghana	**MG**	Madagascar	**TJ**	Tajikistan
BE	Belgium	**GN**	Guinea	**MK**	The former Yugoslav Republic of Macedonia	**TM**	Turkmenistan
BF	Burkina Faso	**GR**	Greece			**TR**	Turkey
BG	Bulgaria	**HU**	Hungary	**ML**	Mali	**TT**	Trinidad and Tobago
BJ	Benin	**IE**	Ireland	**MN**	Mongolia	**UA**	Ukraine
BR	Brazil	**IL**	Israel	**MR**	Mauritania	**UG**	Uganda
BY	Belarus	**IS**	Iceland	**MW**	Malawi	**US**	United States of America
CA	Canada	**IT**	Italy	**MX**	Mexico	**UZ**	Uzbekistan
CF	Central African Republic	**JP**	Japan	**NE**	Niger	**VN**	Viet Nam
CG	Congo	**KE**	Kenya	**NL**	Netherlands	**YU**	Yugoslavia
CH	Switzerland	**KG**	Kyrgyzstan	**NO**	Norway	**ZW**	Zimbabwe
CI	Côte d'Ivoire	**KP**	Democratic People's Republic of Korea	**NZ**	New Zealand		
CM	Cameroon			**PL**	Poland		
CN	China	**KR**	Republic of Korea	**PT**	Portugal		
CU	Cuba	**KZ**	Kazakstan	**RO**	Romania		
CZ	Czech Republic	**LC**	Saint Lucia	**RU**	Russian Federation		
DE	Germany	**LI**	Liechtenstein	**SD**	Sudan		
DK	Denmark	**LK**	Sri Lanka	**SE**	Sweden		
EE	Estonia	**LR**	Liberia	**SG**	Singapore		

A Method and Apparatus for Predicting the Presence of Haemostatic Dysfunction in a Patient Sample

BACKGROUND OF THE INVENTION

This application is a continuation-in-part of U.S. patent application 09/001,647, filed December 31, 1997, which is a continuation-in-part of U.S. patent application 08/859,773 to Givens et al. filed May 21, 1997, which is a continuation of U.S. patent application 08/477,839 to Givens et al. filed June 7, 1995, all of which are incorporated by reference. This application also relates to U.S. patent 5,646,046 to Fischer et al, the subject matter of which is incorporated herein by reference. This application is further related to the following publications, the subject matter of each also being incorporated herein by reference:

1. B. Pohl, C. Beringer, M. Bomhard, F. Keller, The quick machine - a mathematical model for the extrinsic activation of coagulation, *Haemostasis*, **24**, 325-337 (1994).

2. J. Brandt, D. Triplett, W. Rock, E. Bovill, C. Arkin, Effect of lupus anticoagulants on the activated partial thromboplastin time, *Arch Pathol Lab Med*, **115**, 109-14 (1991).

3. I. Talstad, Which coagulation factors interfere with the one-stage prothrombin time?, *Haemostasis*, **23**, 19-25 (1993).

4. P. Baumann, T. Jurgensen, C. Heuck,

Computerized analysis of the in vitro activation of the plasmatic clotting system, *Haemostasis*, **19**, 309-321 (1989).

5. C. Heuck, P. Baumann, Kinetic analysis of the clotting system in the presence of heparin and depolymerized heparin, *Haemostasis*, **21**, 10-18 (1991).

6. M. Astion and P. Wilding, The application of backpropagation neural networks to problems in pathology and laboratory medicine, *Arch Pathol Lab Med*, **116**, 995-1001 (1992).

7. M. Astion, M. Wener, R. Thomas, G. Hunder, and D. Bloch, Overtraining in neural networks that interpret clinical data, *Clinical Chemistry*, **39**, 1998-2004 (1993).

8. J. Furlong, M. Dupuy, and J. Heinsimer, Neural network analysis of serial cardiac enzyme data, *A.J.C.P.*, **96**, 134-141 (1991).

9. W. Dassen, R. Mulleneers, J. Smeets, K. den Dulk, F. Cruz, P. Brugada, and H. Wellens, Self-learning neural networks in electrocardiography, *J. Electrocardiol*, **23**, 200-202 (1990).

10. E. Baum and D. Haussler, What size net gives valid generalization? *Advances in Neural Information Processing Systems*, Morgan Kauffman Publishers, San Mateo, CA, 81-90 (1989).

11. A. Blum, *Neural Networks in C++*, John Wiley & Sons, New York, (1992).

12. S. Haykin, *Neural Networks A Comprehensive Foundation*, Macmillan College Publishing Company, New York, (1994).

13. J. Swets, Measuring the accuracy of diagnostic systems, *Science*, **240**, 1285-1293 (1988).

14. M. Zweig and G. Campbell, Receiver-operating characteristic (ROC) plots: a fundamental evaluation tool in clinical medicine, *Clinical Chemistry*, 39, 561-577 (1993).

15. D. Bluestein, L. Archer, The sensitivity, specificity and predictive value of diagnostic information: a guide for clinicians, *Nurse Practitioner*, 16, 39-45 (1991).

16. C. Schweiger, G. Soeregi, S. Spitzauer, G. Maenner, and A. Pohl, Evaluation of laboratory data by conventional statistics and by three types of neural networks, *Clinical Chemistry*, **39**, 1966-1971 (1993).

Blood clots are the end product of a complex chain reaction where proteins form an enzyme cascade acting as a biologic amplification system. This system enables relatively few molecules of initiator products to induce sequential activation of a series of inactive proteins, known as factors, culminating in the production of the fibrin clot. Mathematical models of the kinetics of the cascade's pathways have been previously proposed.

In [1], a dynamic model of the extrinsic

coagulation cascade was described where data were collected for 20 samples using quick percent, activated partial thromboplastin time (APTT), thrombin time (TT), fibrinogen, factor(F) II, FV, FVII, FX, anti-thrombin III (ATIII), and factor degradation product (FDP) assays. These data were used as input to the model and the predictive output compared to actual recovered prothrombin time (PT) screening assay results. The model accurately predicted the PT result in only 11 of 20 cases. These coagulation cascade models demonstrate: (1) the complexity of the clot formation process, and (2) the difficulty in associating PT clot times alone with specific conditions.

Thrombosis and hemostasis testing is the in vitro study of the ability of blood to form clots and to break clots in vivo. Coagulation (hemostasis) assays began as manual methods where clot formation was observed in a test tube either by tilting the tube or removing fibrin strands by a wire loop. The goal was to determine if a patient's blood sample would clot after certain materials were added. It was later determined that the amount of time from initiation of the reaction to the point of clot formation in vitro is related to congenital disorders, acquired disorders, and therapeutic monitoring. In order to remove the inherent variability associated with the subjective endpoint determinations of manual techniques, instrumentation has been developed to measure *clot time*, based on (1) electromechanical properties, (2) clot elasticity, (3) light scattering, (4) fibrin adhesion, and (5) impedance. For light scattering methods, data is gathered that represents the transmission of light through the specimen as a function of time (an *optical time-dependent*

measurement profile).

Two assays, the PT and APTT, are widely used to screen for abnormalities in the coagulation system, although several other screening assays can be used, e.g. protein C, fibrinogen, protein S and/or thrombin time. If screening assays show an abnormal result, one or several additional tests are needed to isolate the exact source of the abnormality. The PT and APTT assays rely primarily upon measurement of time required for clot time, although some variations of the PT also use the amplitude of the change in optical signal in estimating fibrinogen concentration.

Blood coagulation is affected by administration of drugs, in addition to the vast array of internal factors and proteins that normally influence clot formation. For example, heparin is a widely-used therapeutic drug that is used to prevent thrombosis following surgery or under other conditions, or is used to combat existing thrombosis. The administration of heparin is typically monitored using the APTT assay, which gives a prolonged clot time in the presence of heparin. Clot times for PT assays are affected to a much smaller degree. Since a number of other plasma abnormalities may also cause prolonged APTT results, the ability to discriminate between these effectors from screening assay results may be clinically significant.

Using a sigmoidal curve fit to a profile, Baumann, et al [4] showed that a ratio of two coefficients was unique for a select group of blood factor deficiencies when fibrinogen was artificially maintained by addition of exogenous fibrinogen to a fixed concentration, and that same ratio also correlates heparin to FII deficiency and FXa deficiencies. However, the requirement for

artificially fixed fibrinogen makes this approach inappropriate for analysis of clinical specimens. The present invention makes it possible to predict haemostatic dysfunction for clinical samples from a time-dependent measurement profile without artificial manipulation of samples.

The present invention was conceived of and developed for predicting haemostatic dysfunction in an unknown sample based on one or more time-dependent measurement profiles, such as optical time-dependent measurement profiles, where one or more predictor variables are provided which define characteristics of profile, and where in turn a model is derived that represents the relationship between the haemostatic dysfunction and the one or more predictor variables (so as to, in turn, utilise this model to predict the haemostatic dysfunction in the unknown sample). In addition, the present invention is directed to predicting the presence of Disseminated Intravascular Coagulation in a patient based on a time-dependent profile, such as an optical transmission profile, from a clotting assay run on the patient's blood or plasma sample.

Any discussion of documents, devices, acts or knowledge in this specification is included to explain the context of the invention. It should not be taken as an admission that any of the material formed part of the prior art base or the common general knowledge in the relevant art in Australia on or before the priority date of the claims herein.

SUMMARY OF THE INVENTION

In one aspect, the present provides a method for predicting the presence of disseminated intravascular coagulation in a patient from a time-dependent measurement profile, including:

a) performing a time-dependent measurement on an unknown sample and measuring a respective property over time so as to derive a time-dependent measurement profile;

b) computing the slope of the time-dependent measurement profile prior to clot formation;

c) detecting a biphasic waveform in the time-dependent measurement profile based on the computed slope; and

d) predicting the presence of disseminated intravascular coagulation in the patient based on the detected biphasic waveform.

In another aspect, the present invention provides a method for predicting the presence of haemostatic dysfunction in a patient from at least one time-dependent measurement profile, including:

performing at least one time-dependent measurement on an unknown sample and measuring a respective property over time so as to derive a time-dependent measurement profile;

computing the slope of the time-dependent measurement profile prior to clot formation;

detecting a biphasic waveform in the time-dependent measurement profile based on the computed slope; and

predicting the presence of haemostatic dysfunction in the patient based on the biphasic waveform.

In another aspect, the present invention provides a method for predicting the presence of haemostatic dysfunction in a patient utilising an automated or semi-automated optical analyser including:

conducting a prothrombin time (PT) clot time assay on an unknown patient sample to provide a time-dependent optical measurement profile;

detecting a biphasic waveform in the time-dependent optical measurement profile; and

predicting the presence of haemostatic dysfunction in the patient based on the biphasic waveform.

In another aspect, the present invention provides a method for predicting the presence of disseminated intravascular coagulation in a patient utilising an automated or semi-automated analyser including:

a) conducting an activated partial thromboplastin time (APTT) clot time assay on an unknown patient sample utilising said analyser;

b) profiling said APTT clot time assay results utilising an optical time-dependent measurement profile;

c) causing said analyser to distinguish between a normal sigmoidal appearance from a normal APTT clot time assay profile and an abnormal biphasic waveform associated with an abnormal APTT clot time assay profile associated with disseminated intravascular coagulation to produce a flag on a monitor or print out of the analyser; and

d) utilising the flag to predict the presence of disseminated intravascular coagulation by alerting an operator of the analyser.

In another aspect, the present invention provides an automated analyser for predicting the presence of haemostatic dysfunction in a patient from at least one time-dependent measurement profile, including:

means for performing at least one time-dependent measurement on an unknown sample and measuring a respective property over time so as to derive a time-dependent measurement profile;

means for computing the slope of the time-dependent measurement profile prior to clot formation;

means for detecting a biphasic waveform in the time-dependent measurement profile based on the computed slope; and

means for alerting an operator that a haemostatic dysfunction may be present in the patient responsive to detection of a biphasic waveform.

In a final aspect, the present invention provides an automated analyser for predicting the presence of haemostatic dysfunction in a patient including:

means for conducting a prothrombin time (PT) clot time assay on an unknown patient sample to provide a time-dependent optical measurement profile;

means for detecting a biphasic waveform in the time-dependent optical measurement profile; and

means for predicting the presence of haemostatic dysfunction in the patient based on the biphasic waveform.

The term "comprises", and grammatical variations thereof such as "comprising" when used in the description and claims does not preclude the presence of additional features, integers, steps or components; or groups thereof.

BRIEF DESCRIPTION OF THE DRAWINGS

Figure 1 is a general neuron diagram relating to the embodiment of the present invention utilizing a neural network;

Figure 2 is a diagram of a multilayer perceptron for predicting congenital or acquired imbalances or therapeutic conditions, relating to the neural network embodiment of the present invention;

Figure 3 is an optical profile with first and second derivatives of a normal clotting sample;

Figure 4 is an illustration of two learning curves;

Figure 5 is an illustration of an unstable learning curve;

Figure 6 is a graph showing a comparison of training and cross-validation learning curves;

Figure 7 is a graph showing a comparison of training error for training tolerances of 0.0 and 0.1;

Figure 8 is a ROC illustrating the effect of decision boundary on classification;

Figure 9 is a Table comparing hidden layer size with prediction error;

Figure 10 is a receiver operator characteristic plot related to predicting an abnormality in relation to Factor VIII;

Figure 11 is a graph demonstrating the ability to predict actual Factor VIII activity;

Figure 12 is a receiver operator characteristic plot related to predicting an abnormality in relation to Factor X;

Figure 13 is a chart listing examples of predictor variables for use in the present invention;

Figures 14 - 21 show ROC curves for neural networks trained to predict FII, FV, FVII, FVIII, FIX, FX, FXI, and FXII deficiencies from PT parameters alone, from APTT parameters alone, or from combined APTT and PT parameters;

Figure 22 shows the constituency of the training and cross-validation sets with regard to each factor deficiency;

Figure 23 shows results of classification of coagulation factor deficiencies as determined from area under ROC curves;

Figure 24 shows areas under ROC curves for three networks trained to classify factor deficiencies based on three different diagnostic cutoffs;

Figure 25 shows results from linear regressions comparing factor concentrations estimated using neural network with measured factor concentrations;

Figure 26 shows the correlation between neural network output and measured fibrinogen concentration for cross-validation data set from neural networks trained to estimate fibrinogen concentration;

Figure 27 shows the correlation between neural network output and measured FX concentration for cross-validation data set from neural networks trained

to estimate FX concentration;

Figure 28 shows SOM contour plots derived from APTT optical data for the six specimen categories;

Figure 29 shows contour plots for self-organizing feature maps trained with PT data; and

Figure 30 shows the sensitivity, specificity, efficiency and predictive value of positive test (PPV) and the predictive value of negative test (NPV), based on either APTT or PT parameters.

Figure 31 is a chart illustrating steps of one embodiment of the invention;

Figure 32(A) and (B) illustrate transmittance waveforms on the APTT assay with (A) showing a normal appearance, and (B) a bi-phasic appearance, as derived on the MDA-180, an automated Haemostasis-Thrombosis analyzer. The arrow signifies the point on the waveform where the clot time is recorded (in seconds) in relation to the X-axis. The dotted line indicates the light transmittance level at 25 seconds into the reaction;

Figure 33 illustrates transmittance levels at 25 seconds in relation to diagnosis in the 54 patients with bi-phasic waveform abnormalities. The horizontal dotted line represents the normal transmittance level. When more than one sequential analysis is available on a patient, the lowest transmittance level value is represented for that patient;

Figure 34 illustrates serial transmittance levels (upper panel) and waveforms (lower panel) on a patient who developed DIC following sepsis and recovered;

Figure 35 illustrates serial transmittance levels (upper panel) and waveforms (lower panel) on a patient who developed DIC following trauma and died;

Figure 36 illustrates ROC plots for the prediction of DIC for transmittance at 25 seconds (TR25), APTT clot time, and Slope1 (the slope up to initiation of clot formation);

Figures 37 and 38 show histograms for DIC, normal and abnormal/non-DIC populations for TR25 and slope 1 respectively;

Figures 39 and 41 show group distributions for slope 1 and TR25 respectively;

Figures 40 and 42 show partial subpopulations of the data shown in Figures 39 and 41;

Figure 43 is an optical transmission profile for an APTT assay; and

Figures 44 and 45 are optical transmission profiles for PT assays.

DESCRIPTION OF THE PREFERRED EMBODIMENTS

In the present invention, both a method and apparatus are provided for predicting the presence of the existence of haemostatic dysfunction in a patient sample. As can be seen in Figure 31, one or more time-dependent measurements (101) are performed on an unknown sample (103). The term "time-dependent measurement" is referred to herein to include

measurements derived from assays (e.g. PT, APTT, fibrinogen, protein C, protein S, TT, ATIII, plasminogen and factor assays). The terms "unknown sample" and "clinical sample" refer to a sample, such as one from a medical patient (100), where haemostatic dysfunction associated with thrombosis/hemostasis is not known (or, if suspected, has not been confirmed).

In the present invention, a coagulation property is measured over time so as to derive a time-dependent measurement profile. In a preferred embodiment, the time-dependent measurement is an optical measurement for deriving an optical profile. For example, a PT profile, a fibrinogen profile, a TT profile, an APTT profile and/or variations thereof can be provided where, an unknown sample is analyzed for clot formation based on light transmittance over time through the unknown sample. In another preferred embodiment, two (or more) optical profiles are provided, such as both a PT profile and an APTT profile.

After the time-dependent measurement profiles are provided, a set of predictor variables are defined (110) which sufficiently define the data of the time-dependent profile. One or more predictor variables comprise the set. And, in one embodiment, three or more, and in a preferred embodiment, four or more predictor variables were found to desirably make up the set. It was found that the characteristics of the time-dependent measurement profile could best be defined by one or more predictor variables, including the minimum of the first derivative of the optical profile, the time index of this minimum, the minimum of the second derivative of the optical profile, the time index of this minimum, the maximum of the second

derivative, the time index of this maximum, the overall change in transmittance during the time-dependent measurement, clotting time, slope of the optical profile prior to clot formation, and slope of the optical profile after clot formation.

After defining the set of predictor variables, a model (113) is derived which represents the relationship between a congenital or acquired imbalance or therapeutic condition and the set of predictor variables. This model can be derived from a neural network in one embodiment of the present invention. In another embodiment, the model is derived via a set of statistical equations.

Neural networks represent a branch of artificial intelligence that can be used to learn and model complex, unknown systems given some known data (115) from which it can train. Among the features of neural networks that make them an attractive alternative for modeling complex systems are :

1. They can handle noisy data well and recognize patterns even when some of the input data are obscured or missing.

2. It is unnecessary to determine what factors are relevant a priori since the network will determine during the training phase what data are relevant, assuming there are at least some meaningful parameters in the set.

Neural networks are formed from multiple layers of interconnected neurons like that shown in Figure 1. Each neuron has one output and receives input $i_1 \ldots i_n$ from multiple other neurons over connecting links, or

synapses. Each synapse is associated with a synaptic weight, w_j. An adder Σ or linear combiner sums the products of the input signals and synaptic weights $i_j * w_j$. The linear combiner output sum_l and θ_l (a threshold which lowers or a bias which raises the output) are the input to the activation function $f()$. The synaptic weights are learned by adjusting their values through a learning algorithm.

After deriving the model (113), whether based on neural networks or statistical equations, the model is utilized to predict (120) the existence of a congenital or acquired imbalance or therapeutic condition in the unknown sample relative to the time-dependent measurement profile(s). As such, a congenital or acquired imbalance or therapeutic condition can be predicted. Conditions which can be predicted as being abnormal in the present invention can include, among others, a) factor deficiencies, e.g. fibrinogen, Factors II, V, VII, VIII, IX, X, XI and XII, as well as ATIII, plasminogen, protein C, protein S, etc., b) therapeutic conditions, e.g. heparin, coumadin, etc., and c) conditions such as lupus anticoagulant. In one embodiment of the present invention, the method is performed on an automated analyzer (90). The time-dependent measurement profile, such as an optical data profile, can be provided automatically by the automated analyzer, where the unknown sample is automatically removed by an automated probe from a sample container to a test well, one or more reagents are automatically added to the test well so as to initiate the reaction within the sample. A property over time is automatically optically monitored so as to derive the optical profile. The predicted congenital or therapeutic

condition (120) can be automatically stored in a memory (122) of an automated analyzer and/or displayed (124) on the automated analyzer, such as on a computer monitor, or printed out on paper. As a further feature of the invention, if the predicted congenital or acquired imbalance or therapeutic condition (128) is an abnormal condition, then one or more assays for confirming the existence of the abnormal condition are performed on the automated analyzer. In fact, in a preferred embodiment, the one or more confirming assays are automatically ordered and performed on the analyzer once the predicted condition is determined, with the results of the one or more confirming assays being stored in a memory (131) of the automated analyzer and/or displayed (133) on the analyzer.

EXAMPLE 1: Prediction of Heparin in Sample

This example shows a set of predictor variables that adequately describe screening assay optical profiles, develops an optimal neural network design, and determines the predictive capabilities of an abnormal condition associated with thrombosis/hemostasis (in this case for the detection of heparin) with a substantial and well-quantified test data set.

Simplastin™ L, Platelin™ L, calcium chloride solution (0.025 M), imidazole buffer were obtained from Organon Teknika Corporation, Durham, NC, 27712, USA. All plasma specimens were collected in 3.2% or 3.8% sodium citrate in the ratio of one part

anticoagulant to nine parts whole blood. The tubes were centrifuged at 2000 g for 30 minutes and then decanted into polypropylene tubes and stored at -80°C until evaluated. 757 specimens were prepared from 200 samples. These specimens were tested by the following specific assays: FII, FV, FVII, FVIII, FIX, FX, FXI, FXII, heparin, fibrinogen, plasminogen, protein C, and AT-III. Samples represented normal patients, a variety of deficiencies, and therapeutic conditions. Of the specimen population 216 were positive for heparin determined by a heparin concentration greater than 0.05 units/ml measured with a chromogenic assay specific for heparin. The remaining specimens, classified as heparin-negative, included normal specimens, a variety of single or multiple factor deficiencies, and patients receiving other therapeutic drugs. Positive heparin samples ranged to 0.54 units/ml.

PT and APTT screening assays were performed on each specimen five days. When clot-based coagulation assays are performed by an automated optically-based analyzer such as the MDA 180, data are collected over time that represents the normalized level of light transmission through a sample as a clot forms (the optical profile). As the fibrin clot forms, the transmission of light is decreased. The optical profile was stored from each test.

The network configuration chosen, a multilayer perceptron (M condition. A similar network was also employed for PT-only variables and APTT-only variables. This specific MLP consists of three layers: the input layer, one hidden layer, and the output layer.

A normal optical profile is shown in Figure 3. The set of predictor variables were chosen with the intent of describing optical profiles as completely as

possible with a minimum number of variables. They are summarized in Table 1 where t is time from initiation of reaction, T is normalized light transmission through the reaction mixture, and pv_{jk} is the kth predictor variable of assay j.

The predictor variables were scaled to values between 0 and 1, based on the range of values observed for each variable for assay type k

$$i_j = f\left(pv_{jk}, \left(pv_{j\_n,k}\right)_{\min}, \left(pv_{j\_n,k}\right)_{\max}\right).$$

The input variable set includes $i_{1\ldots7}$ for both a PT assay and APTT assay for each specimen. For known output variable values, heparin samples with results of greater than 0.05 units/ml were considered positive and assigned a value of 1 while negative samples were assigned a value of 0.

As the ratio of training set sample to the number of weights samples taken from the same distribution as the training set. Thus, small samples sizes, then can lead to artificially high classification rates. This phenomenon is known as overtraining. In order to achieve a true accuracy rate of 80%, a guideline for the number of samples in the training set is approximately five times the number of weights in the network. For most of this work, a 14-6-1 network was used, leading to an upward bound on the sample size of $O(450)$. To monitor and evaluate the performance of the network and its ability to generalize, a cross-validation set is processed at the end of each training epoch. This cross-validation set is a randomly determined subset of the known test set that is excluded from the training set.

Once the input predictor variables and output values were determined for all specimen optical profiles, the 757 sets of data were randomly distributed into two groups: 387 were used in the training set and 370 were used in the cross-validation set. These same two randomly determined sets were used throughout all the experiments.

All synaptic weights and threshold values were initialized at the beginning of each training session to small random numbers.

The error-correction learning rule is an iterative process used to update the synaptic weights by a method of gradient descent in which the network minimizes the error as pattern associations (known input-output pairs) in the training set are presented to the network. Each cycle through the training set is known as an epoch. The order or presentation of the pattern associations was the same for all epochs.

The learning algorithm consists of six steps which make up the forward pass and the backward pass. In the forward pass, the hidden layer neuron activations are first determined

$$h = F(iW1 + \theta_h)$$

where h is the vector of hidden-layer neurons, i the vector of input-layer neurons, W1 the weight matrix between the input and hidden layers, and $F()$ the activation function. A logistic function is used as the activation function

$$F(x) = \frac{1}{1+e^{-x}}.$$

Then the output-layer neurons are computed

$$o = F(hW2 + \theta_0)$$

where o represents the output layer, h the hidden layer and W2 the matrix of synapses connecting the hidden layer and output layers. The backward pass begins with the computation of the output-layer error

$$e_0 = (o - d),$$

where d is the desired output. If each element of e_o is less than some predefined training error tolerance vector TE_{tol}, than the weights are not updated during that pass and the process continues with the next pattern association. A training error tolerance of 0.1 was used in all experiments unless otherwise specified. Otherwise, the local gradient at the output layer is then computed:

$$g_o = o(1 - o)e_0.$$

Next, the hidden-layer local gradient is computed:

$$g_h = h(1 - h)W2g_o.$$

Once the hidden layer error is calculated, the second layer of weights is adjusted

$$W2_m = W2_{m-1} + \Delta W2$$

where

$$\Delta W2 = \eta h g_0 + \gamma \Delta W2_{m-1}$$

is the learning rate, γ is the momentum factor, and m is the learning iteration. The first layer of weights is adjusted in a similar manner

$$W1_m = W1_{m-1} + \Delta W1$$

where

$$\Delta W1 = \eta i e + \gamma \Delta W1_{m-1}.$$

The forward pass and backward pass are repeated for all of the pattern associations in the training set, referred to as an epoch, 1000 times . At the end of each epoch, the trained network is applied to the cross-validation set.

Several methods were employed to measure the performance of the network's training. Error, E, for each input set was defined as

$$E = \sqrt{\frac{1}{N}\sum_{q=1}^{N}\left(d_q - o_q\right)^2}$$

The learning curve is defined as the plot of E versus epoch. The percent classification φ, describes the percent of the total test set (training and cross-

validation) that is correctly classified based on some defined decision boundary, β. Receiver-Operating Characteristic (ROC) plots have also been utilized to describe trained networks' ability to discriminate between the alternative possible outcome states. In these plots, measures of sensitivity and specificity are shown for a complete range of decision boundaries. The sensitivity, or true-positive fraction is defined as

$$sensitivity = \frac{true\ positive}{true\ positive + false\ negative}$$

and the false-positive fraction , or (1-specificity) is defined as

$$(1 - specificity) = \frac{false\ positive}{false\ positive + true\ negative}$$

These ROC plots represent a common tool for evaluating clinical laboratory test performance.

Using the test set described, experiments were performed to determine if the presence of heparin could be predicted with this method. First, experiments were conducted to determine optimal error-correction backpropagation learning parameters: (1) hidden layer size, (2) learning rate, and (3) momentum. Additional experiments were also conducted to compare the performance of networks based on PT and APTT assays alone with that of one combining the results of both, the effect of the training error tolerance, and the decision boundary selection.

Figure 9 shows the effect of the hidden layer size on the training and cross validation error and the percent correct classification for the optimal decision boundary, defined as the decision boundary which yielded the lowest total number of false positives and false negatives from the total test set. As the hidden layer size is increased, the error is decreased. However, the ability to generalize does not increase after a hidden layer size of 6. The most significant benefit in terms of both error and percentage correct classification is between 4 and 6. A hidden layer size of 6 was used for the remainder of the experiments.

A series of experiments were conducted with $\eta = \{0.01, 0.1, 0.5, 0.9\}$ and $\gamma = \{0.0, 0.1, 0.5, 0.9\}$. Figure 4 shows the learning curves for two of the best combinations of parameters. Figure 5 shows an example learning curve when the learning rate is so high it leads to oscillations and convergence to a higher E. In general, as $\eta \rightarrow 0$ the network converged to a lower E and as $\gamma \rightarrow 1$, the rate of convergence improved. As $\eta \rightarrow 1$, the value of E converged too increased and oscillations increased. In addition, as $\eta \rightarrow 1$, $\gamma \rightarrow 1$ exacerbated the oscillations.

Figure 6 shows a comparison of the learning curve for the training set and cross-validation set for η=0.5 and γ=0.1. It is a primary concern when developing neural networks, and it has been previously shown that it is important to look not only at the error in the training set for each cycle, but also the

cross-validation error.

Figure 7 shows the learning curve η=0.5 and γ=0.1 and a learning tolerance of 0.0 and 0.1. These results suggest that a small learning tends to smoothen the convergence of the learning process.

Figure 8 shows the ROC plot for networks trained with the predictor variables from each of the two screening assays with that of them combined. In the single assay cases, the hidden layer size was 3. While using the data from one assay does lead to some success, using the information from both assays makes a significant improvement in the ability of the network to correctly predict the presence of heparin. This graph indicates that a 90% true positive proportion can be achieved with a false positive proportion of 15%. Using a single assay, a 60-70% true positive proportion can be achieved with a false positive proportion of approximately 15%.

EXAMPLE 2: Factor VIII

Similar tests were run as in Example 1. As can be seen in Figures 10 and 11, two training sessions were conducted for predicting a Factor VIII condition in an unknown sample. Figure 10 is a receiver operator characteristic plot related to predicting an abnormality in relation to Factor VIII. In Figure 10, everything below 30% activity was indicated as positive, and everything above 30% was indicated as negative. Cutoff values other than 30% could also be used. In this Example, the activity percentage has a known accuracy of approximately + or - 10%. In Figure 11, the actual percent activity was utilized as the output.

EXAMPLE 3: Factor X

As can be seen in Figure 12, the method of the present invention was run similar to that as in Example 2, where here an abnormality in Factor X concentration was predicted from unknown samples. Everything below 30% activity was indicated as positive, and everything above 30% was indicated as negative. Cutoff values other than 30% could also be used.

The results of the cross-validation sample sets throughout the experiments indicate that the sample size was sufficient for the network to generalize. While the random distribution of the training and cross-validation sets were held constant throughout the experiments presented, other distributions have been used. These distributions, while all yielding different results, still lead to the same general conclusion.

Many alternatives for or additions to the set of predictor variables were explored. This included coefficients of a curve fitted to the data profile, pattern recognition, and clot time-based parameters. Low order functions tend to lose information due to their poor fit, and high order functions tend to lose information in their multiple close solutions. Clot-based parameters, such as clot time, slope in the section prior to the initiation of clot formation, and afterwards, are often available, but not always (because in some samples, the clot time is not detectable). The successful results observed indicate that the set of predictor variables used are effective for predicting congenital or acquired imbalances or therapeutic conditions.

The optimization of the network learning algorithm's parameters made significant differences in its performance. In general, performance was best with low learning rates, high momentum rates, some small training error tolerance, and a hidden layer size approximately half of the size of the input layer.

ADDITIONAL EXAMPLES:

Optical measurements for APTT and PT assays were performed on MDA 180 instruments at a wavelength of 580 nm. Plasma specimens (n= 200) included normal patients, patients with a variety of coagulation factor deficiencies and patients undergoing heparin or other anticoagulant therapy. Duplicate APTT and PT screening assays were performed on each specimen with two MDA 180s using single lots of APTT and PT reagents. These specimens were also analyzed using specific assays for FII, FV, FVII, FVIII, FIX, FX, FXI, FXII, heparin, fibrinogen, plasminogen, protein C and antithrombin-III.

Data Processing and Neural Networks

Optical profile data files were exported from the MDA 180s and processed off-line. A set of nine parameters was derived to describe the timing, rate and magnitude of coagulation events. These parameters were calculated for all APTT and PT tests. The parameter set is modified slightly from that for Example 1. In this approach, the optical data for a PT or APTT assay was divided into three segments (a pre-coagulation segment, a coagulation segment and a

post-coagulation segment) using divisions based on the minimum and maximum value of the second derivative for changes in optical signal with respect to time. The parameters that were analyzed included: (1) the times at which the onset, midpoint and end of the coagulation phase occur (*tmin2*, *tmin1* and *tmax2*; respectively); (2) mean slopes for the pre-coagulation phase and the post-coagulation phase (*slope1* and *slope3*, respectively) and the slope at the mid-point of coagulation (*min1*, the coagulation "velocity" at reaction midpoint, which is analogous to *slope2*); (3) terms for coagulation "acceleration" and "deceleration" (*min2* and *max2*, respectively); and (4) the magnitude of signal change during coagulation (*delta*).

Three different sets of data parameters were used as input to the neural network: (1) the nine parameters from PT assays, (2) the nine parameters from APTT assays, and (3) the combined parameters from the APTT and PT assays. Each specimen was run in duplicate on two instruments, to give a total of approximately 800 parameter sets from the 200 specimens. The total number varied slightly because of missing data due to insufficient sample, mechanical failure or unspecified failures. The data parameter sets were divided into training and cross-validation sets randomly by specimen where all replicates for a given specimen were grouped either in the cross-validation set or training set. The same training and cross-validation sets were used throughout this study. The method for training and cross-validation of the back-propagation neural networks has been described in relation to Example 1. Each neural network was trained for 1000 epochs. Training parameters were learning

rate, 0.01; momentum, 0.5; learning tolerance, 0.10; decay, 0.05; input layer size, 18 (or 9 for single assays); hidden layer size, 9 (or 5 for single assays); and output layer size, 1. Three types of networks were trained. These included networks that classified specimens as deficient or non-deficient based on a single diagnostic cut-off, sets of networks that used diagnostic cut-offs at different levels of the same factor, and networks trained to estimate the actual concentration of a specific factor.

Classification of Factor Deficiencies Based on a Single Diagnostic Cut-off Level

In the first set of tests, neural networks were trained to classify plasma samples into two groups, positive (factor-deficient) and negative (non-deficient), and results were compared to classification based on the measured factor concentration for the specimens. In most testing, the diagnostic cut-off for defining factor deficiencies was set as 30%; that is, specimens with a measured concentration of less that 30% of normal for a specific factor were defined as deficient and those with greater than 30% activity were defined as non-deficient. These diagnostic cut-off levels were arbitrarily defined, but are based on clinical requirements and reagent sensitivity. The desired output from positive samples and negative samples were defined as '1' and '0', respectively; the actual output for each specimen was a floating point value, a, where $0 \leq a \leq 1$. Figure 22 shows the constituency of the training and cross-validation sets with regard to each factor deficiency. Classification of specimens was evaluated at varying "decision boundaries" that divided the neural network outputs into

positive and negative groups. This positive or negative classification was then compared to the desired output (the known classification) for each input data set. Results were plotted as nonparametric receiver-operating characteristic (ROC) curves and the areas under the curves were computed along with their associated standard errors. ROC curves were also derived for APTT and PT clot time values for comparison. Data points on the ROC curves represent the proportion of true-positive and false-positive classifications at various decision boundaries. Optimum results are obtained as the true-positive proportion approaches 1.0 and the false-positive proportion approaches 0.0 (upper-left corner of graph). The optimum global measure of the ROC curve is an area of 1.0.

Classification of Factor Deficiencies at Multiple Diagnostic Cut-off Levels

A second set of networks was trained for FX classification in a similar manner to the first set except that the diagnostic cut-off level was varied (10%, 30%, and 50%). FX was chosen for this experiment because the data set contained a greater number of positive samples at all cut-off levels than other factors.

Estimation of Factor Concentration Using Neural Networks

A third set of networks were trained to approximate actual specific factor activities (FII, FV, FVII, FVIII, FIX, FX, FXI and FXII) and fibrinogen levels from combined PT and APTT parameters from unknown samples. In these cases, the desired output of the training and cross-validation sets was the measured activity for a

specific factor for each specimen and the actual output of the neural network was a predicted concentration for this specific factor activity. The coefficients of linear regressions using the desired outputs versus the actual neural network outputs for the cross-validation set were used to describe the performance of these networks. The Pearson product moment correlation coefficient, *r*, was used to estimate the correlation between the two data sets.

Classification of Factor Deficiencies Based on a Single Diagnostic Cut-off Level

Neural networks were trained to classify samples as deficient (positive result) or non-deficient (negative result) for individual plasma factors, using a value of 30% activity as the diagnostic cut-off to define deficiencies. Results were examined graphically using receiver-operating curves (ROC). These graphs plot the true-positive proportion (number of positives detected divided by the total number of positives) versus the false-positive proportion (number of negative specimens incorrectly diagnosed as positive divided by the total number of negatives). An ROC curve is generated by determining true-positive and false-positive proportions at different "decision boundaries" for the diagnostic test. For example, an ROC plot for diagnosis of FII deficiencies using PT clot time was generated by varying the decision boundary (value of PT clot time) used to differentiate between deficient and non-deficient specimens. When a short clot time is used as the decision boundary, most deficient specimens can be identified but a significant proportion of non-deficient specimens may also be flagged (false-positives). When a long clot time is used as the decision boundary, the

proportion of false-positives decreases, but the number of true-positive specimens that are not diagnosed may also increase. Under ideal conditions, a decision boundary can be identified from an ROC curve that produces a very high proportion of true-positives and a very low proportion of false-positives. This condition corresponds to the upper left region of the ROC plot. Two related terms that are often applied to clinical diagnostic tests are "sensitivity" and "specificity". Sensitivity refers to the ability to detect positive specimens and corresponds to the y-axis of the ROC plots. Specificity refers to the proportion of specimens diagnosed as negative which are correctly identified. The ROC x-axis equals (1-specificity). Visual assessment of the ROC curves is one method used to evaluate the performance of the neural networks and compare them to the diagnostic power of PT and APTT clot times. Another method is to measure the diagnostic performance by using the area under the ROC curves. The area under the ROC curve is equivalent to an estimate of the probability that a randomly chosen positive specimen will have a more positive result than a randomly chosen negative specimen. In the event that ROC curves overlap, the shape of the curves as well as the areas beneath them becomes important. An ROC curve encompassing a smaller area may be preferable to an overlapping curve with greater area depending on the desired performance for a given diagnostic system.

Figures 14 - 21 show ROC curves for neural networks trained to predict FII, FV, FVII, FVIII, FIX, FX, FXI, and FXII deficiencies from PT parameters alone, from APTT parameters alone, or from combined APTT and PT parameters. ROC plots based on classification using APTT and PT clot times are included for comparison.

Figure 23 shows the area under these curves and their associated standard errors.

Results for classification of FII deficiencies are shown in Figure 14. Best results were observed for neural networks using APTT parameters alone or combined with PT parameters, with area under ROC curves greater than 0.99 in both cases (Figure 23). Classification based on PT or APTT clot times, or from neural networks using PT data alone resulted in less successful classification and reduced area under curves.

Results from classification of FV deficiencies showed somewhat different characteristics (Figures 15 and 23). Best results were observed for classification from a neural network using APTT data parameters, based on visual inspection and area under the ROC curve. Less successful classification were obtained from neural networks using PT data parameters alone or combined with APTT data, and from PT clot time, as judged from areas under ROC curves. Classification based on PT clot time was qualitatively different from neural networks using PT data, however, and tended toward higher sensitivity rather than specificity. This type of pattern was observed for classification of several coagulation factors, especially factors VIII, X and XI. In situations where overlapping ROC curves were obtained, consideration of the relative value of specificity and sensitivity, as well as the area under ROC curves, becomes important in comparing diagnostic results.

For several of these plasma factors, including FV, FVIII, FIX, FX, FXI and FXII (Figures 15, 17, 18, 19, 20 and 21), it appeared that it would be possible to achieve a moderately high true-positive proportion (> 0.6) while maintaining a low false-positive proportion

(< 0.1) from neural networks using PT, APTT or combined parameters. This corresponds to a situation where a significant proportion of deficient specimens are not detected (moderate sensitivity), but those that are detected are correctly classified as deficient for that specific factor (high specificity). In contrast, using PT or APTT clot times it was possible for most factors to adjust decision boundaries to identify most deficiencies (true-positive proportion approaching 1.0, high sensitivity), but with a relatively high rate of false-positives (low specificity). This corresponds to a situation where most or all deficient specimens are detected, but where the specific factor deficiency is frequently not correctly identified. The first scenario involving moderate or high true-positive rates with very low false positive rates may be preferable in the diagnostic scheme shown in Figure 13.

For factors II, V, IX and XII, it appeared that an appropriate choice of neural network gave best diagnostic performance, as judged from the area under curves. For factors VIII, X and XI, neural networks were not visibly superior to diagnosis based on clot times when areas under ROC curves were the only consideration; however, neural networks for these factors did provide better specificity. For one factor (FVII, Figure 16), neural network classification was less effective than for other factors, at least in this test system.

The performance of networks using data parameters from PT or APTT assays alone or in combination varied for different factors. For factors VIII and XII, best performance (significantly greater area with no overlap) was observed when the combined sets of APTT-PT data parameters were used. For several other factors, use of a single parameter set provided results that were

comparable to or better than the combined APTT and PT parameters. A network using only APTT data parameters (APTT NN) was equivalent (similar area) to a network using combined APTT-PT data (APTT-PT NN) for FII and FX; and superior for FV (greater area and no overlap). Networks using only PT parameters provided results that were comparable (similar area) to the combined parameters for FV classification and better (greater area and insignificant overlap) for FIX classification.

The data for misclassified positive specimens were examined more closely. Misclassified positive specimens were clustered in several categories: 1) Specimens with "no clot" APTT or PT results (specimens with very prolonged or very weak coagulation reaction for which no clot time can be reliably calculated); 2) specimens with multiple deficiencies or abnormalities; 3) specimens with borderline deficiencies (factor activity marginally lower than the diagnostic cut-off of 30%); and 4) specimens with atypically steep slope during the pre-coagulation phase for APTT assays that were not characteristic of other specimens in the same classification (FX deficiencies were not detected for two specimens exhibiting this characteristic with FX activities of 26.8% and 16.8%, respectively).

Classification of Factor Deficiencies at Multiple Diagnostic Cut-off Levels

The ability of neural networks to classify FX-deficient specimens was tested at varying diagnostic cut-offs. Areas under the ROC curves for cut-off levels of 10%, 30% and 50% FX activity are shown in Figure 24. Results indicate that progressively poorer classification (as expressed in smaller areas under ROC curves) was observed as higher cut-off levels were used.

This was true for classification based on neural networks or PT clot times.

Neural Network Estimation of Factor Concentration

Neural networks were also trained to estimate actual protein concentrations (as opposed to a positive/negative classification at a defined cut-off) for FII, FV, FVII, FVIII, FIX, FX, FXI, FXII and fibrinogen. Linear correlation coefficients for the estimated and measured concentrations are shown in Figure 25 for all experiments, and plots of the correlation data are shown in Figure 26 for fibrinogen and Figure 27 for FX. Correlation data between PT and APTT clot time and measured concentrations are also shown in Figure 25 for comparison.

Example: Self-Organizing Feature Maps

Neural networks using self-organizing feature maps and learning vector quantization were used to analyze optical data from clinical coagulation tests. Self-organizing feature maps using an unsupervised learning algorithm were trained with data from normal donors, patients with abnormal levels of coagulation proteins and patients undergoing anticoagulant therapy. Specimen categories were distinguishable in these maps with varying levels of resolution. A supervised neural network method, learning vector quantization, was used to train maps to classify coagulation data. These networks showed sensitivity greater than 0.6 and specificity greater than 0.85 for detection of several factor deficiencies and heparin.

An alternative approach to analyzing PT and APTT data with artificial neural networks (as set forth in

Example 1) is by using self-organizing feature maps. Self-organizing feature maps contain layers of input and output neurons only and contain no hidden layers. Training is based on competitive learning where the output neurons compete with one another to be activated and only one output neuron is activated for any given set of inputs. Output neurons become selectively tuned to certain input patterns, and data with similar features tend to be grouped together spatially. This type of neural network may use either an unsupervised or supervised learning algorithm. When an unsupervised method is used, such as the self-organizing map (SOM) algorithm, unidentified input patterns are presented to the network during training and the output for each input pattern is the coordinates of the winning neuron in the output layer, or map. When a supervised method is used, such as learning vector quantization (LVQ), input patterns are presented along with a known sample classification to the network during training and the output is a unique predicted classification. The LVQ method is similar to SOM, except that the map is divided into classes, and the algorithm attempts to move outputs away from the boundaries between these classes.

MDA Simplastin L (PT reagent), MDA Platelin L (APTT reagent) and other reagents were obtained from Organon Teknika Corporation, Durham, NC 27712, USA, unless otherwise indicated. Factor-deficient plasmas for factor assays were obtained from Organon Teknika and George King Bio-Medical Corporation, Overland Park, Kansas 66210, USA. Additional factor-deficient plasmas were obtained from HRF, Raleigh, NC 27612, USA. Random samples, specimens from patients receiving heparin or oral anticoagulant therapy, and other specimens were obtained from Duke University Medical

Center Coagulation Laboratory.

All testing was performed on MDA 180 coagulation analyzers (Organon Teknika). Optical measurements for PT and APTT assays were performed at a wavelength of 580 nm. Plasma specimens (n= 200) included normal patients, patients with a variety of deficiencies, and patients undergoing heparin or other anticoagulant therapy. Duplicate PT and APTT assays were performed on each specimen using two MDA 180s to give a total of approximately 800 parameter sets from the 200 specimens. The total number varied slightly because of missing data due to insufficient sample, mechanical failure or unspecified failures. These specimens were also tested to determine the concentration of coagulation factors (FII, FV, FVII, FVIII, FIX, FX, FXI, FXII) heparin, and fibrinogen. The diagnostic cut-off for defining factor deficiencies was set at 30%; that is, specimens with a measured concentration of less that 30% of normal for a specific factor were defined as deficient and those with greater than 30% activity were defined as non-deficient. Samples were defined as positive for heparin if the measured heparin concentration was greater than 0.05 IU/ml.

Optical Data Processing

Optical profile data files were exported from MDA 180s and processed off-line. A set of nine parameters was derived to describe the timing, rate and magnitude of coagulation events for PT and APTT tests, as described previously. In this approach, the optical data for a PT or APTT assay was divided into three segments (a pre-coagulation segment, a coagulation segment and a post-coagulation segment) using divisions based on the minimum and maximum value of the second

derivative for changes in optical signal with respect to time. Parameters included: 1) the times at which the onset, midpoint and end of the coagulation phase occur; 2) mean slopes for the pre-coagulation phase and the post-coagulation phase and the slope at the mid-point of coagulation; 3) terms for coagulation "acceleration" and "deceleration"; and 4) the magnitude of signal change during coagulation.

Self-Organizing Map Algorithm

A self-organizing feature map neural network consists of input and output layers of neurons. The self-organizing map (SOM) algorithm transforms an input vector (a set of data parameters from PT or APTT optical data for a single test) to an individual output neuron whose location in the output layer, or map, corresponds to features of the input data. These features tend to be spatially correlated in the map. There are five steps in the SOM learning process:

1. Unique weight vectors $w_j(0)$, are randomly chosen.

2. A sample from the training set is selected.

3. The best-matching winning neuron $i(x)$ at time n, using the minimum-distance Euclidean criterion

$$i(x) = \arg\min_j \left\{ \left\| x(n) - w_j(n) \right\| \right\}$$

is identified.

4. The weight vectors of all neurons are updated with the formula

$$w_j(n+1) = \begin{cases} w_j(n) + \alpha(n)\left[x(n) - w_j(n)\right], & j \in N_c(n) \\ w_j(n), & j \notin N_c(n) \end{cases}$$

where $\alpha(n)$ is the learning rate parameter, and $N_c(n)$

is the neighborhood function centered around the winning neuron $i(x)$; both $\alpha(n)$ and $N_c(n)$ vary dynamically during training.

5. Steps 2 through 4 are repeated until the map reaches equilibrium.

The SOM tests were performed using the Self-Organizing Map Program Package (SOM_PAK) available from the Helsinki University of Technology, Laboratory of Computer Sciences. Two different sets of parameters were used as input to the SOMs: (1) the nine parameters from a PT assay, and (2) the nine parameters from the APTT assay. All data sets (786) were used to train the SOMs. A 10x10 map was trained using a hexagonal neighborhood in two stages. In the first stage, the map was trained for 1000 epochs (an epoch is one cycle through all data sets) with an initial learning rate parameter of 0.5 (decreasing linearly to zero during training) and a neighborhood radius of 10 (decreasing linearly to 1 during training). In the second stage, the map was trained for 10000 epochs using a learning rate parameter of 0.1 and a radius of 3.

Learning Vector Quantization

Learning vector quantization (LVQ) is a supervised learning algorithm often used to fine-tune self-organizing feature maps in order to use them in the role of a pattern classifier. The classification accuracy of the map is improved by pulling the weight vectors away from the decision surfaces that demarcate the class borders in the topological map. There are several variations of the LVQ algorithm; the one used here is referred to as LVQ1. The learning process is similar to

the SOM algorithm described above, except that known sample classifications are included when weight vectors are updated (step 4):

1. Initial weight vectors $w_j(0)$, are randomly chosen.

2. A sample from the training set with a known classification is selected.

3. The best-matching winning neuron $i(x)$ at time n, using the minimum-distance Euclidean criterion

$$i(x) = \arg\min_j \left\{ \left\| \mathbf{x}(n) - \mathbf{w}_j(n) \right\| \right\}$$

is identified.

4. The weight vectors of all neurons are updated with the formula

$$\mathbf{w}_j(n+1) = \begin{cases} \mathbf{w}_j(n) + \alpha(n)\left[\mathbf{x}(n) - \mathbf{w}_j(n)\right], & j = i, C_{w_i} = C_x \\ \mathbf{w}_j(n) - \alpha(n)\left[\mathbf{x}(n) - \mathbf{w}_j(n)\right], & j = i, C_{w_i} \neq C_x \\ \mathbf{w}_j(n), & j \neq i \end{cases}$$

where C_{w_i} is the class associated with the vector W_i and C_x is the class associated with the input vector **x**.

5. Steps 2 through 4 are repeated until the map reaches equilibrium.

The LVQ tests were performed using the Learning Vector Quantization Program Package (LVQ_PAK), also available from the Helsinki University of Technology, Laboratory of Computer Sciences. The sets of parameters from the APTT assay or PT assays were used for the LVQ networks. The data parameter sets were divided evenly into training and cross-validation sets randomly by specimen, where all replicates for a given specimen were grouped either in the cross-validation set or training set. The same training and cross-validation sets were

used throughout this study. The LVQ networks were trained to classify plasma samples into two categories, positive (factor-deficient specimens or specimens from patients undergoing anticoagulant therapy) and negative (non-deficient or no anticoagulant therapy), and results were compared to classification based on the measured factor concentration or therapeutic condition for the specimens. LVQ training was performed using 200 weight vectors, 10000 epochs, initial learning rate parameter of 0.5 (decreasing linearly to 0), and 7 neighbors used in knn-classification.

LVQ networks were evaluated using sensitivity (the proportion of known positive specimens that were correctly classified as positive by the network), specificity (the proportion of known negative specimens that were correctly classified as negative by the network), positive predictive value (PPV), negative predictive value (NPV) and efficiency. These terms are defined below, where TP, TN, FP and FN correspond to true positive, true negative, false positive and false negative classifications, respectively.

$$sensitivity = \frac{TP}{TP + FN}$$

$$specificity = \frac{TN}{FP + TN}$$

$$PPV = \frac{TP}{TP + FP}$$

$$NPV = \frac{TN}{TN + FN}$$

$$efficiency = \frac{TN + TP}{TP + FP + FN + TN}$$

Self-Organizing Map Algorithm

Self-organizing feature maps were trained using optical data parameters from either PT or APTT data for 200 specimens as input. Network output consisted of map coordinates for each specimen. Contour plots were constructed for six categories of known specimen classifications: normal donors, specimens with heparin > 0.05 IU/ml, fibrinogen >600mg/dl, fibrinogen <200 mg/dl, patients receiving oral anticoagulants, and factor-deficient specimens (specimens with <30% of normal activity for FII, FV, FVII, FVIII, FIX, FX, FXI, or FXII). These contour plots depict the distribution of specimens within a category according to their map coordinates.

Figure 28: Contour plots for populations of samples used in training a self-organizing feature map using the unsupervised training method SOM based on data from APTT assays. Optical data parameters from 765 APTT assays were used to train this self-organizing feature map. The shaded areas represent the distribution of output neurons for specific specimen populations within the feature map. Each contour line represents an incremental step of one test result located at a given set of map coordinates.

Figure 28 shows SOM contour plots derived from APTT optical data for the six specimen categories. Specimens containing low fibrinogen and high fibrinogen were classified at opposite borders of the SOM with no overlap. Normal populations showed some overlapping

with low fibrinogen, factor deficient and oral anticoagulated categories. Overlap between normal specimens and edges of the high and low fibrinogen populations is expected, since some proportion of healthy donors have fibrinogen levels that are lower or higher than normal. Overlap between mapping of normal specimens and factor-deficient plasmas is also not surprising, since APTT tests are sensitive to some factor-deficiencies (but not others), whereas PT assays are sensitive to a separate subset of factor deficiencies. The low fibrinogen category tended to overlap the factor-deficient category, consistent with our observation that many factor-deficient specimens also had reduced fibrinogen levels. The heparin category tended to overlap the high fibrinogen category, again consistent with measured levels of fibrinogen for these specimens. Little or no overlap was observed between normal specimens and specimens containing heparin. Specimens from patients receiving oral anticoagulant therapy show significant overlap with both normal and heparin populations. This is consistent with known properties of APTT assays, which are sensitive to heparin therapy but relatively insensitive to oral anticoagulant therapy.

Figure 29: Contour plots for populations of samples used in training a self-organizing feature map using the unsupervised training method SOM based on optical data from 765 PT assays. Experimental details are as described in the Materials and Methods section and in Figure 28.

Contour plots for self-organizing feature maps trained with PT data are shown in Figure 29. Results are similar to maps from APTT data in several respects: (1) high and low fibrinogen were well resolved at

opposite sides of the map; (2) normal specimens were localized in a region that overlapped low fibrinogen specimens slightly; (3) factor-deficient specimens were distributed between non-overlapping regions and regions that overlapped low fibrinogen and normal populations. Overlap was consistent with measured fibrinogen for some specimens, and with poor sensitivity of PT reagents to some factor deficiencies in other cases; (4) oral anticoagulated specimens showed some overlap with both normal and heparin populations; and (5) the heparinized population was distributed over a large portion of the map. Overlap between heparinized specimens and high fibrinogen populations was consistent with measured fibrinogen levels. The resolution of the heparin population is somewhat surprising, considering that PT reagents are relatively insensitive to heparin.

These results indicate that self-organizing feature maps are capable of distinguishing differences in optical data parameters from APTT and PT assays even when no information regarding specimen diagnosis is presented to the neural network. Resolution of specimen populations was variable, depending on reagent properties and sensitivities, and on whether specimens belonged to a given category uniquely or to multiple overlapping categories.

Learning Vector Quantization

Eighteen LVQ networks were trained to predict the presence or absence of a specific factor deficiency or therapeutic condition from APTT or PT optical data. Results for the cross-validation data are summarized in Figure 30. Previous studies concluded that back-propagation neural networks were capable of sensitivity > 0.6 while maintaining specificity >0.9 for all factors

except FVII using an appropriate choice of PT and APTT data separately or in combination. In this study, LVQ networks using APTT data gave sensitivity > 0.6 with specificity > 0.85 for factors II, X, XI, and XII, and heparin. LVQ networks using PT data were able to achieve > 0.6 sensitivity while maintaining > 0.85 specificity for Factors II, X, and XI, and heparin (Figure 30). Results from LVQ networks showed less sensitivity for prediction of FVII deficiencies, consistent with results from back-propagation networks. For FV, FVIII and FIX, sensitivity for predicting deficiencies from LVQ cross-validation sets was generally less (<0.35) than for factors II, X, XI and XII.

Example: Haemostatic Dysfunction (e.g. Disseminated Intravascular Coagulation (DIC))

In a further embodiment of the invention, not only can a particular abnormality (Haemostatic Dysfunction) be detected, but in addition the progression of the disease can be monitored in a single patient. Haemostatic Dysfunction, as used herein, is the activation of coagulation prior to initiation of clot formation, which results in a biphasic waveform.

Disseminated intravascular coagulation (DIC - a type of Haemostatic Dysfunction) prognosis has been hampered by the lack of an early, useful and rapidly available diagnostic marker. The invention has been found to be not only useful as an early diagnostic and single monitoring marker of DIC, but in addition the quantifiable and standardizable changes also allow for prognostic applicability in clinical management.

Disseminated intravascular coagulation (DIC) is a

secondary response to a pre-existing pathology whereby the haemostatic response becomes perturbed and disseminated as opposed to the focused events of normal haemostasis. Despite improvements both in the intensive care management of patients and in our basic knowledge of haemostatic mechanisms in DIC, survival in this patient group is still very discouraging. Fundamental to the management of this complication is the implementation of aggressive therapy directed at forestalling or eradicating the primary pathology as the source of the initiating stimulus. However, in practical terms, the problem remains one of early identification of DIC to facilitate immediate and appropriate intervention. Although the technological armory available to the clinical investigator has expanded enormously, the pace of acute DIC precludes most of the more specific tests and reliance is still placed on traditional screening tests such as the prothrombin (PT), activated partial thromboplastin time (APTT) and platelet count. These tests lack specificity on an individual basis and are only useful in DIC if they lead on to further determinations of fibrinogen and fibrin breakdown products/D-dimers. However, changes in these parameters may not occur all at the same time and as such, serial testing is often needed which inevitably leads to a delay in diagnosis and clinically useful intervention.

The normal sigmoidal appearance from an APTT transmittance waveform (TW) changes to a "bi-phasic" appearance in DIC patients. This represents a loss in the plateau of a normal APTT-TW, with development of an initial low gradient slope followed by a much steeper slope (Figures 32a and b). In addition, this bi-phasic pattern can be seen even when the APTT clotting time

result is normal.

Freshly collected blood samples that required a PT or an APTT were analyzed prospectively over a two week working period. These were in 0.105M tri-sodium citrate in the ratio of 1 part anticoagulant to 9 parts whole blood and the platelet-poor plasma was analyzed on the MDA (Multichannel Discrete Analyzer) 180, an automated analyzer for performing clinical laboratory coagulation assays using an optical detection system (Organon Teknika Corporation, Durham, NC, USA). In addition, to deriving the clot times for both PT (normal 11.2-15s) using MDA Simplastin LS and APTT (normal 23-35s) using MDA Platelin LS with 0.025M calcium chloride (Organon Teknika Corporation, USA), an analysis of the TW for the APTT was performed on each occasion at a wavelength of 580nm. To quantitate the visual profile, the amount of light transmittance at 25 seconds was recorded. A normal waveform has a light transmittance of 100% which is represented on the analyzer and in Figure 32a without the decimal point as 10000. As such, a bi-phasic change will have a reduced light transmittance of less than 10000. Decreasing levels of light transmittance therefore correlates directly with increasing steepness of the bi-phasic slope. The recording of the light transmittance at 25 seconds also allows for standardization between patients and within the same patient with time. If the minimum level of light transmittance for each sample were to be used instead, this would be affected by variations in the clot time of the APTT and would therefore not be ideal for comparisons.

To ensure that no cases of DIC were overlooked, the following criteria was followed. If (a) an abnormal bi-phasic TW was encountered, or (b) a specific DIC screen

was requested, or (c) if there was a prolongation in either the PT or APTT in the absence of obvious anticoagulant therapy, a full DIC screen was performed. This would further include the thrombin time (TT) (normal 10.5-15.5 seconds), fibrinogen (Fgn) (normal 1.5-3.8 g/l) and estimation of D-dimer levels (normal < 0.5 mg/l) on the Nyocard D-Dimer (Nycomed Pharma AS, Oslo, Norway). Platelet counts (Plt) (normal 150-400 10^9/l) performed on an EDTA sample at the same time were recorded. In addition, clinical details were fully elucidated on any patient with a bi-phasic TW or coagulation abnormalities consistent with DIC.

The diagnosis of DIC was strictly defined in the context of both laboratory and clinical findings of at least 2 abnormalities in the screening tests (increased PT, increased APTT, reduced Fgn, increased TT or reduced Plt) plus the finding of an elevated D-dimer level (>0.5 mg/l) in association with a primary condition recognized in the pathogenesis of DIC. Serial screening tests were also available on those patients to chart progression and confirmation of the diagnosis of DIC as was direct clinical assessment and management. For statistical analysis, values for the sensitivity, specificity, positive and negative prediction of the APTT-TW for the diagnosis of DIC were calculated employing a two-by-two table. 95% confidence intervals (CI) were calculated by the exact binomial method.

A total of 1,470 samples were analyzed. These were from 747 patients. 174 samples (11.9%) from 54 patients had the bi-phasic waveform change. 22 of these 54 patients had more than 3 sequential samples available for analysis. DIC was diagnosed in 41 patients with 30 of these requiring transfusion support with fresh frozen plasma, cryoprecipitate or platelets. The underlying

clinical disorders as shown in Table 1

Table 1: Clinical disorders predisposing patients to DIC.

Disorder	No
Infections	17
Trauma or recent major surgery	16
Malignancy	2
Hepatic Disease	1
Obstetric Cause	1
Miscellaneous Additional Causes •	4

• Includes hypoxia, acidosis, Lithium overdosage and graft rejection

40 of the 41 patients with DIC had the bi-phasic TW. The one false negative result (DIC without a bi-phasic TW) occurred in a patient with pre-eclampsia (PET) where the single sample available for analysis showed a prolonged PT of 21.0s, APTT of 44.0s and raised D-dimers of 1.5mg/l. 5 other patients were identified in this study with PET and none had either DIC or a bi-phasic TW. Of the 14 patients with a bi-phasic TW which did not fulfil the criteria of DIC, all had some evidence of a coagulopathy with abnormalities in one or two of the screening tests. These abnormal results fell short of the criterion for DIC as defined above. 4 of these 14 patients had chronic liver disease with prolonged PT and mild thrombocytopaenia. A further 2 patients had atrial fibrillation with isolated elevation of D-dimer levels only. The remaining 8 patients were on the ICU with multiple organ dysfunction arising from trauma or suspected infection but without the classical laboratory changes of DIC. These patient profiles were described in the ICU as consistent with the "systemic inflammatory response syndrome" (SIRS). Based on these figures, the bi-phasic TW has a 97.6% sensitivity for the diagnosis of DIC with a specificity of 98%. Use of an optical

transmittance waveform was found to be helpful in detecting the biphasic waveform.

Table 2: Performance of the transmittance waveform (TW) analysis in patients with and without DIC

	Biphasic TW	Normal TW	Total
DIC positive	40	1	41
DIC negative	14	692	706
Total	54	693	747

Sensitivity 97.6% (CI 85.6-99.9%), Specificity 98.0% (CI 96.6-98.9%), Positive predictive value 74.0% (CI 60.1-84.6%), Negative predictive value 99.9% (CI 99.1-99.9%)

The positive predictive value of the test was 74%, which increased with increasing steepness of the bi-phasic slope and decreasing levels of light transmittance (Table 2 and Figure 33). In the first two days of the study, there were 12 patients who had an abnormality in the clotting tests plus elevation of D-dimer levels. These were patients who were clinically recovering from DIC that occurred in the week preceding the study. This led to the impression that TW changes might correlate more closely with clinical events than the standard markers of DIC.

Table 3: Serial results in a patient with sepsis

Day	Time	PT (11.2-15s)	APTT (23-35s)	TT (10.5-15.5s)	Fgn (1.5-3.8 g/l)	D-Dimer (<0.5 mg/l)	Plt (150-400 x 10^9/l)	TW
1	0923	14.7	32.9	12.0	4.7	0.00	193	B•
1	2022	20.8•	38.6•	12.4	5.7	6.00•	61•	B•
2	0920	18.0•	33.0	13.0	5.2	2.00•	66•	N
3	1011	16.3•	24.8	13.2	4.7	0.00	64•	N

PT = Prothrombin time, APTT = Activated Partial Thromboplastin Time, TT = Thrombin Time, Fgn = Fibrinogen, Plt = Platelet count, TW = Transmittance Waveform

• Indicates abnormal changes. B = bi-phasic; N = normal

The availability of more than 3 sequential samples in 22 patients allowed for further assessment. Table 3 illustrates one such example with serial test results from a patient with *E. coli* septicaemia.

The appearance of a bi-phasic TW preceded changes in the standard tests for the diagnosis of DIC. It was only later in the day that the PT, APTT, Plt and D-dimer levels became abnormal and fulfilled the diagnostic criteria of DIC. Treatment with intravenous antibiotics led to clinical improvement by Day 2 with normalization of her TW in advance of the standard parameters of DIC. D-dimers and Plt were still respectively abnormal 24 and 48 hours later.

This correlation between clinical events and TW changes was seen in all the DIC patients where samples were available to chart the course of clinical events. As the TW changes were quantifiable and standardizable through recording of the transmittance level at 25 seconds, this analysis provided a handle in assessing prognostic applicability. Figure 34 illustrates the results of a patient who initially presented with peritonitis following bowel perforation. This was further complicated by gram negative septicaemia post-operatively with initial worsening of DIC followed by a gradual recovery after appropriate therapy. As DIC progressed initially, there was increasing steepness in the bi-phasic slope of the TW and a fall in the light transmittance level. A reversal of this heralded clinical recovery. Figure 35 illustrates the results of a patient who sustained severe internal and external injuries following a jet-ski accident. Although initially stabilized with blood product support, his condition deteriorated with continuing blood loss and

development of fulminant DIC. The bi-phasic slope became increasingly steep with falls in transmittance level as the consequences of his injuries proved fatal.

As DIC can arise from a variety of primary disorders, the clinical and laboratory manifestations can be extremely variable not only from patient to patient but also in the same patient with time. There is therefore, a need for systems that are not only robust in their diagnosis but simple and rapid to perform. Although it has been shown that the bi-phasic TW appeared to be sensitive for Haemostatic Dysfunction (e.g. DIC) and was not seen in other selected patient groups with coagulation aberrations or influenced by either (i) pre-analytical variables, (ii) different silica-based APTT reagents, (iii) the use of thrombin as the initiator of the coagulation reaction or (iv) treatment in the form of heparin or plasma expanders, the robustness of this assay for DIC could only be addressed through a prospective study. This study has shown that the bi-phasic TW provides diagnostic accuracy in DIC with an overall sensitivity of 97.6% and specificity of 98%. In contrast, none of the standard parameters on an individual basis (i.e., PT, APTT, TT, Fgn, Plt, D-dimers) or even in combination, has ever reached the degree of sensitivity or specificity. The ready availability of TW data from the MDA-180 would also fulfil the criteria of simplicity and rapidity unlike the measurements of thrombin-antithrombin complexes or other markers that are dependent on ELISA technology. In addition, the advantages of TW analysis are that: (a) the bi-phasic TW change appears to be the single most useful correlate within an isolated sample for DIC and as such, reliance need no longer be placed

on serial estimations of a battery of tests, and (b) the appearance or resolution of the bi-phasic TW can precede changes in the standard, traditional parameters monitored in DIC with strong, clear correlation to clinical events and outcome.

Although the bi-phasic TW was also seen in patients who did not have DIC *per se* as defined by the above criteria, the clinical conditions were associated with Haemostatic Dysfunction - namely activated coagulation prior to initiation of clot formation resulting in a biphasic waveform (for example in chronic liver disease or in the very ill patients on the Intensive Care Unit who had multiple organ dysfunction). It appears that bi-phasic TW is sensitive to non-overt or compensated DIC and that a transmittance level of less than 90% (Figure 33) or sequential falls in that level (Figure 35), reflects decompensation towards a more overt manifestation and potentially fulminant form of DIC. This line of explanation is supported by the observation of only a mild bi-phasic TW (transmittance level of about 95%) in 2 patients with atrial fibrillation; a condition that is associated with mild coagulation activation and elevated D-dimer levels. As no follow-up samples were available on these 2 patients whose clinical details were otherwise unremarkable, their bi-phasic TW could well have been transient. Nonetheless, these cases illustrate that the lower the level of light transmittance, the more likely the bi-phasic TW becomes predictive of Haemostatic Dysfunction, particularly DIC.

The observation of a normal TW in a patient with PET and DIC needs further exploration as the study did not selectively aim to examine any particular patient groups and only had a total of 6 patients with PET; the

remaining 5 of which did not have DIC. One explanation which would be supported by other findings in this study is that the patient could have been recovering from PET and DIC at the time of the sample. There may already have been normalization in the bi-phasic TW in advance of the other parameters which were still abnormal and indicative of DIC. Another explanation is that the disturbed haemostatic process in PET is more localized and different from the DIC that arises from other conditions. Such patients respond dramatically to delivery of the fetus which suggests anatomical localization of the pathological process to the placenta despite standard laboratory clotting tests implying systemic evidence of the condition.

Example:

Though analysis of the transmittance at a time of 25 seconds is helpful in predicting DIC, a second embodiment of the invention has been found that greatly improves sensitivity and specificity. It has been found that looking at transmittance at a particular time can result in detecting an artifact or other decrease in transmittance at that point, even though the waveform is not a bi-phasic waveform. For example, a temporary dip in transmittance at 25 seconds would cause such a patient sample to be flagged as bi-phasic, even if the waveform was normal or at least not bi-phasic. Also, if a patient sample had a particularly short clotting time, then if clot formation begins e.g. prior to 25 seconds (or whatever time is preselected), then the waveform could be flagged as biphasic, even though the real reason for decreased transmittance at 25 seconds is because clot formation has already begun/occurred.

For this reason, it has been found that rather than analysis of transmittance at a particular time, it is

desirable to calculate the slope of the waveform prior to initiation of clot formation. This calculation can involve determination of clot time followed by determination of waveform slope prior to clot time. In an additional embodiment, the slope (not transmittance) is determined prior to clot time or prior to a preselected time period, whichever is less. As can be seen in Figure 42, when transmittance is used for determining e.g. DIC, there is poor specificity and sensitivity. However, as can be seen in Figure 40, when slope prior to initiation of clot formation is used, specificity and sensitivity are greatly improved, and are better than standard tests used in the diagnosis of Haemostatic Dysfunction, such as DIC.

Additional testing was performed on three sets of patients. The first set consisted of 91 APTT assays run on samples from 51 different confirmed DIC patients. The second set of data consisted of 110 APTT assays run on samples from 81 different confirmed normal patients. The third set of data included 37 APTT assays run on 22 abnormal, non-DIC samples. Fig. 36 illustrates ROC plots for the prediction of DIC for three different parameters derived from the APTT assay using the combined data sets described: (1) transmittance at 25 seconds (TR25), (2) APTT clot time, and (3) slope 1 (the slope up to initiation of clot formation). Slope 1 exhibited the best predictive power, followed by TR25. It has also been shown that transmittance at 18 seconds has predictive value, particularly when the APTT clot time is less than 25 seconds. The "cutoffs" associated with the highest efficiency for the three parameters are listed in Table 4:

Parameter	Cutoff
TR25	< 9700
Clot Time	> 35
Slope 1	< -0.0003

Table 4

It should be noted that these cutoffs have shifted with the addition of the third set, and would likely shift again, depending on the sample populations. Figures 37 and 38 show the histograms for the DIC, normal and abnormal/non-DIC populations for TR25 and slope 1 respectively. Tables 5 and 6 show the data for the histograms in Figures 37 and 38 respectively:

Bins	DIC	Normal	Abnormal/Non-DIC
-0.006	3	0	0
-0.005	2	0	0
-0.004	1	0	0
-0.003	10	0	0
-0.002	24	0	0
-0.001	33	0	0
-0.0005	12	0	0
-0.0002	5	5	2
-0.0001	1	37	13
More	0	68	22

Table 5

Bin	DIC	Normal	Abnormal/Non-DIC
7000	34	1	0
8000	18	2	0
9000	26	6	1
9500	8	3	0
9600	3	2	1
9700	1	0	0
9800	1	3	0
9900	0	21	4
10000	0	62	30
More	0	10	1

Table 6

Figures 39 and 41 show the group distributions for Slope 1 and TR25 respectively; and Figures 40 and 42 show the group distributions for Slope 1 and TR25 respectively. Figures 40 and 42 show partial subpopulations of the data shown in Figures 39 and 41.

When the prediction of Haemostatic Dysfunction is performed on an automated or semi-automated analyzer, the detected bi-phasic waveform can be flagged. In this way, the operator of the machine, or an individual interpreting the test results (e.g. a doctor or other medical practitioner) can be alerted to the existence of the biphasic waveform and the possibility/probability of Haemostatic Dysfunction such as DIC. The flag can be displayed on a monitor or printed out. A slope of less than about -0.0003 or less than about -0.0005 is the preferred cutoff for indicating a bi-phasic waveform.

An increasing steepness in slope prior to clot formation correlates to disease progression.

The above examples show that waveform analysis on the APTT assay can identify characteristic bi-phasic patterns in patients with haemostatic dysfunction. In the majority of cases, this dysfunction could be labelled as DIC. This diagnostic waveform profile was seen in all APTT reagents tested, which were either silica or ellagaic acid-based. It has also been surprisingly found that a bi-phasic waveform can also be seen on PT assays with particular reagents, and that the bi-phasic waveform is likewise indicative of haemostatic dysfunction, primarily DIC.

Using samples that give bi-phasic APTT waveforms, the PT waveform profile was derived using PT reagents (thromboplastin), namely Recombiplast™ (Ortho), Thromborel™ (Dade-Behring) and Innovin™ (Dade-Behring). Both Recombiplast and Thromborel were particularly good at showing bi-phasic responses. Innovin was intermediate in its sensitivity. Using the transmittance level at 10 seconds into the PT reaction as the quantitative index, Recombiplast and Thromborel objectively showed lower levels of light transmittance than Innovin. Thromborel can show a slight increase in initial light transmittance before the subsequent fall. This may be, in part, related to the relative opaqueness of Thromborel.

Further studies were performed comparing APTT profiles using Platelin™ and PT waveform profiles using Recombiplast™. Consecutive samples over a four week period from the intensive care unit were assessed. Visually, and on objective scores (comparing TL18 for APTT and TL10 for PT), the APTT profile was more sensitive to changes of haemostatic dysfunction and

clinical progression than the PT profile. This relative sensitivity can be seen in the APTT profile of Figure 43 (Platelin) compared to the PT profiles of Figure 44 (Recombiplast) and Figure 45 (Thromborel S). Invariably, at smaller changes in light transmittance, the APTT waveform detected abnormalites more easily than the PT waveform. Nonetheless, in severe degrees of haemostatic dysfunction, both bi-phasic profiles were concordant.

It is to be understood that the invention described and illustrated herein is to be taken as a preferred example of the same, and that various changes in the method and apparatus of the invention may be resorted to, without departing from the spirit of the invention or scope of the claims.

THE CLAIMS DEFINING THE INVENTION ARE AS FOLLOWS:

1. A method for predicting the presence of disseminated intravascular coagulation in a patient from a time-dependent measurement profile, including:

a) performing a time-dependent measurement on an unknown sample and measuring a respective property over time so as to derive a time-dependent measurement profile;

b) computing the slope of the time-dependent measurement profile prior to clot formation;

c) detecting a biphasic waveform in the time-dependent measurement profile based on the computed slope; and

d) predicting the presence of disseminated intravascular coagulation in the patient based on the detected biphasic waveform.

2. A method for predicting the presence of haemostatic dysfunction in a patient from at least one time-dependent measurement profile, including:

performing at least one time-dependent measurement on an unknown sample and measuring a respective property over time so as to derive a time-dependent measurement profile;

computing the slope of the time-dependent measurement profile prior to clot formation;

detecting a biphasic waveform in the time-dependent measurement profile based on the computed slope; and

predicting the presence of haemostatic dysfunction in the patient based on the biphasic waveform.

3. The method of claim 1 or 2, wherein the time-dependent measurement profile is at least one optical profile.

4. The method of claim 3, wherein the at least one optical profile is provided by an automated analyser for thrombosis and wherein detecting a biphasic waveform includes automatically detecting the biphasic waveform.

5. The method of claim 4, wherein the time-dependent measurement profile is of optical transmission through the unknown sample during an activated partial thromboplastin time (APTT) assay and wherein automatically detecting the biphasic waveform includes automatically detecting the biphasic waveform when the slope is less than about -0.0003.

6. The method of claim 4, wherein the time-dependent measurement profile is of optical transmission through the unknown sample during an activated partial thromboplastic time (APTT) assay and wherein automatically detecting the biphasic waveform includes automatically detecting the biphasic waveform when the slope is less that about -0.0005.

7. The method of claim 4, further including automatically generating a flag on an output device of the automated analyser responsive to detecting a biphasic waveform and wherein predicting the presence of haemostatic dysfunction comprises predicting the presence of haemostatic dysfunction in the patient based on the flag.

8. The method of claim 4, wherein a plurality of optical measurements at one or more wavelengths are taken over time so as to derive the at least one optical profile, the plurality of optical measurements corresponding to changes in light transmission through the unknown sample.

9. The method of claim 8, wherein the optical measurements are normalised.

10. The method of claim 4, wherein the at least one optical profile is provided automatically by said automated analyser based on optical transmission through the unknown sample, wherein the unknown sample is automatically removed by an automated probe from a sample container to a test well, one or more reagents are automatically added to the test well so as to initiate changes in the respective property within the unknown sample, and the development of the respective property over time is automatically optically monitored so as to derive the at least one optical profile.

11. The method of claim 1 or 2, wherein the time-dependent measurement profile is of optical transmission through the unknown sample during an activated partial thromboplastic time (APTT) assay.

12. The method of claim 1 or 2, wherein said time-dependent measurement profile is an optical transmission through the unknown sample during a prothrombin time (PT) assay.

13. The method of claim 1 or 2, wherein the slope of the time-dependent measurement profile is taken from an end of blank time up to immediately before the initiation of clot formation or a predetermined time period.

14. The method of claim 2, wherein the prediction of the presence of haemostatic dysfunction includes flagging the presence of the haemostatic dysfunction and wherein predicting the presence of the haemostatic dysfunction includes predicting the presence of the haemostatic dysfunction based on the flagging.

15. The method of claim 2, wherein the predicted haemostatic dysfunction is due to one or more of infection, trauma, major surgery, malignancy, hepatic disease, pregnancy and/or child birth, hypoxia, acidosis, lithium overdose, and graft rejection.

16. The method of claim 15 wherein performing at least one time-dependent measurement, computing the slope and detecting a biphasic waveform are performed on an automated or semi-automated analyser and wherein predicting the presence of haemostatic dysfunction further includes flagging the presence of likelihood of the haemostatic dysfunction and wherein said flagging is an alert to at least one of an individual operating said automated or semi-automated analyser or an individual reading or evaluating the results of a test run on said automated or semi-automated analyser, that there is a possibility and/or

probability of haemostatic dysfunction of a patient whose test sample has been run on the automated or semi-automated analyser and flagged.

17. The method of claim 16, wherein a slope of less than about -0.0003 causes flagging of the unknown sample and wherein an increase in steepness of the slope from test to test corresponds to disease progression.

18. The method of claim 1 or 2, wherein the unknown sample includes whole blood or a portion thereof.

19. The method of claim 1 or 2, wherein the unknown sample includes a plasma sample.

20. A method for predicting the presence of haemostatic dysfunction in a patient utilising an automated or semi-automated optical analyser including:

conducting a prothrombin time (PT) clot time assay on an unknown patient sample to provide a time-dependent optical measurement profile;

detecting a biphasic waveform in the time-dependent optical measurement profile; and

predicting the presence of haemostatic dysfunction in the patient based on the biphasic waveform.

21. The method of claim 20, further including computing a slope of the time-dependent measurement profile prior to clot formation and wherein detecting a biphasic waveform includes detecting the biphasic waveform based on the computed slope.

22. The method of claim 21, further including automatically generating a flag on an output device of the analyser responsive to detecting a biphasic waveform and wherein predicting the presence of haemostatic dysfunction includes predicting the presence of haemostatic dysfunction in the patient based on the flag.

23. The method of claim 22, wherein the output device includes at least one of a monitor or a printer.

24. The method of claim 20, wherein the haemostatic dysfunction includes disseminated intravascular coagulation.

25. A method for predicting the presence of disseminated intravascular coagulation in a patient utilising an automated or semi-automated analyser including:

a) conducting an activated partial thromboplastin time (APTT) clot time assay on an unknown patient sample utilising said analyser;

b) profiling said APTT clot time assay results utilising an optical time-dependent measurement profile;

c) causing said analyser to distinguish between a normal sigmoidal appearance from a normal APTT clot time assay profile and an abnormal biphasic waveform associated with an abnormal APTT clot time assay profile associated with disseminated intravascular coagulation to produce a flag on a monitor or print out of the analyser; and

d) utilising the flag to predict the presence of disseminated intravascular coagulation by alerting an operator of the analyser.

26. The method of claim 25, wherein the flag is produced in the monitor.

27. The method of claim 25, wherein the flag is produced on the print out of the analyser.

28. A method for predicting the presence of disseminated intravascular coagulation in a patient utilising an automated or semi-automated analyser including:

a) conducting an prothrombin time (PT) clot time assay on an unknown patient sample utilising said analyser;

b) profiling the PT clot time assay results utilising an optical time-dependent measurement profile;

c) causing the analyser to distinguish between a normal sigmoidal appearance from a normal PT clot time assay profile and an abnormal biphasic waveform associated with an abnormal PT clot time assay profile associated with disseminated intravascular coagulation to produce a flag on a monitor or print out of the analyser; and

d) utilising the flag to predict the presence of disseminated intravascular coagulation.

29. The method of claim 28, wherein the PT assay is performed utilising a reagent including thromboplastin.

30. A method according to any one of claims 1, 2, 20 or 25 substantially as hereinbefore described with reference to the accompanying Figures.

DATED this 21st day of May 2004

BIOMERIUX, INC

WATERMARK PATENT & TRADE MARK ATTORNEYS
290 BURWOOD ROAD
HAWTHORN VICTORIA 3122
AUSTRALIA

KJS/DMF

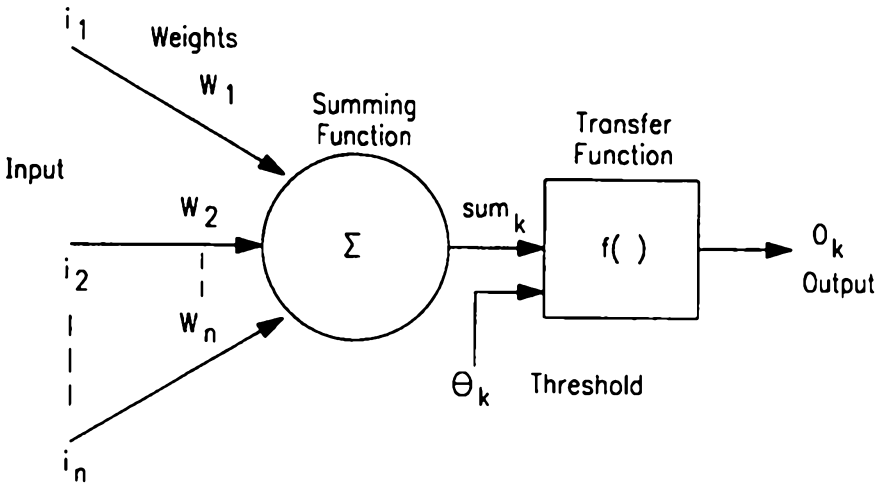
i 1
Weights
W 1
Summing
Function
Transfer
Function
Input
W 2
sum k
Σ
f( )
O k
Output
i 2
W n
Θ k
Threshold
i n

FIG. 1

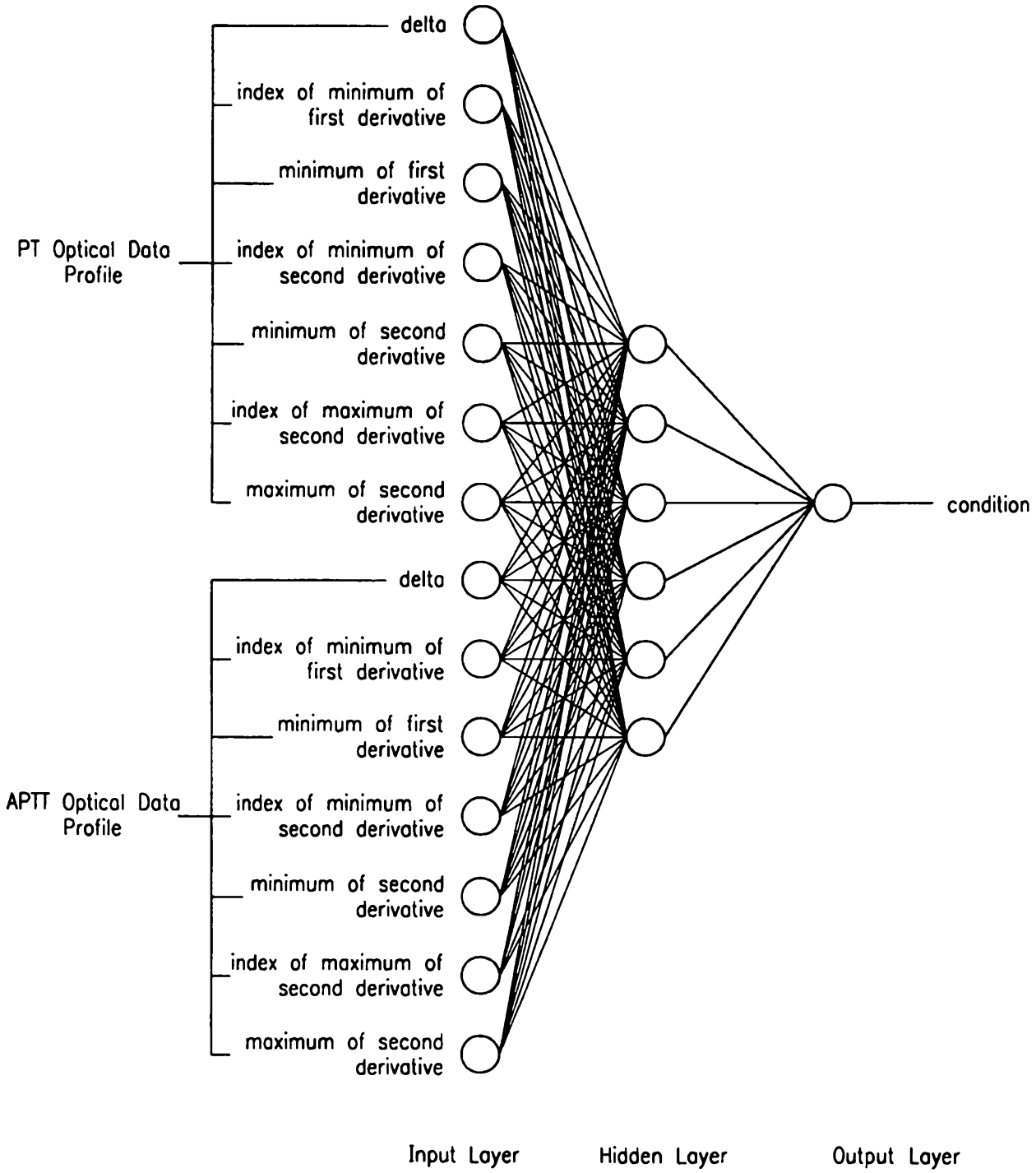
delta
index of minimum of first derivative
minimum of first derivative
PT Optical Data Profile
index of minimum of second derivative
minimum of second derivative
index of maximum of second derivative
maximum of second derivative
delta
index of minimum of first derivative
minimum of first derivative
APTT Optical Data Profile
index of minimum of second derivative
minimum of second derivative
index of maximum of second derivative
maximum of second derivative
condition
Input Layer
Hidden Layer
Output Layer

FIG. 2

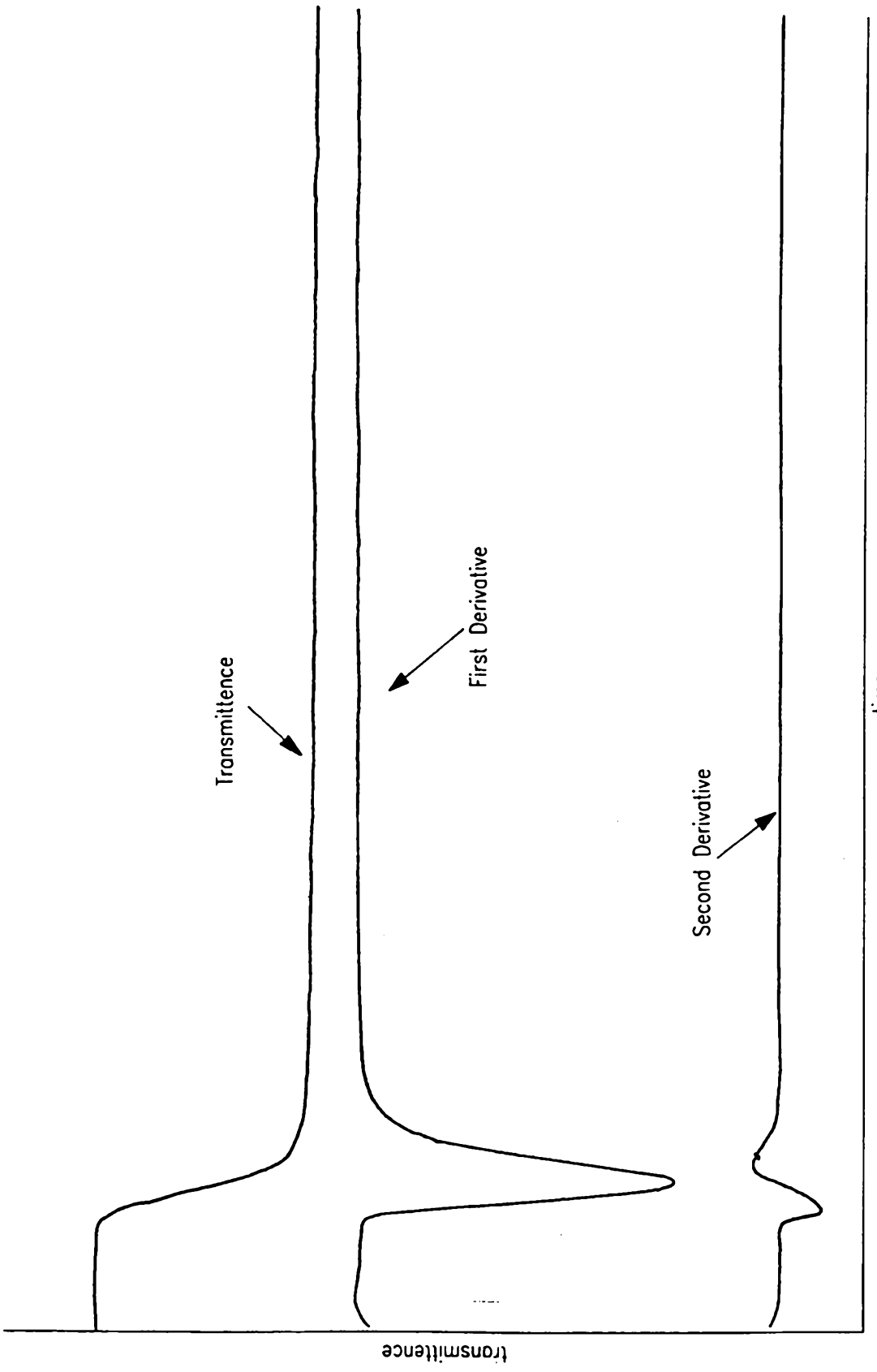
Transmittence
First Derivative
Second Derivative
time
transmittence

FIG. 3

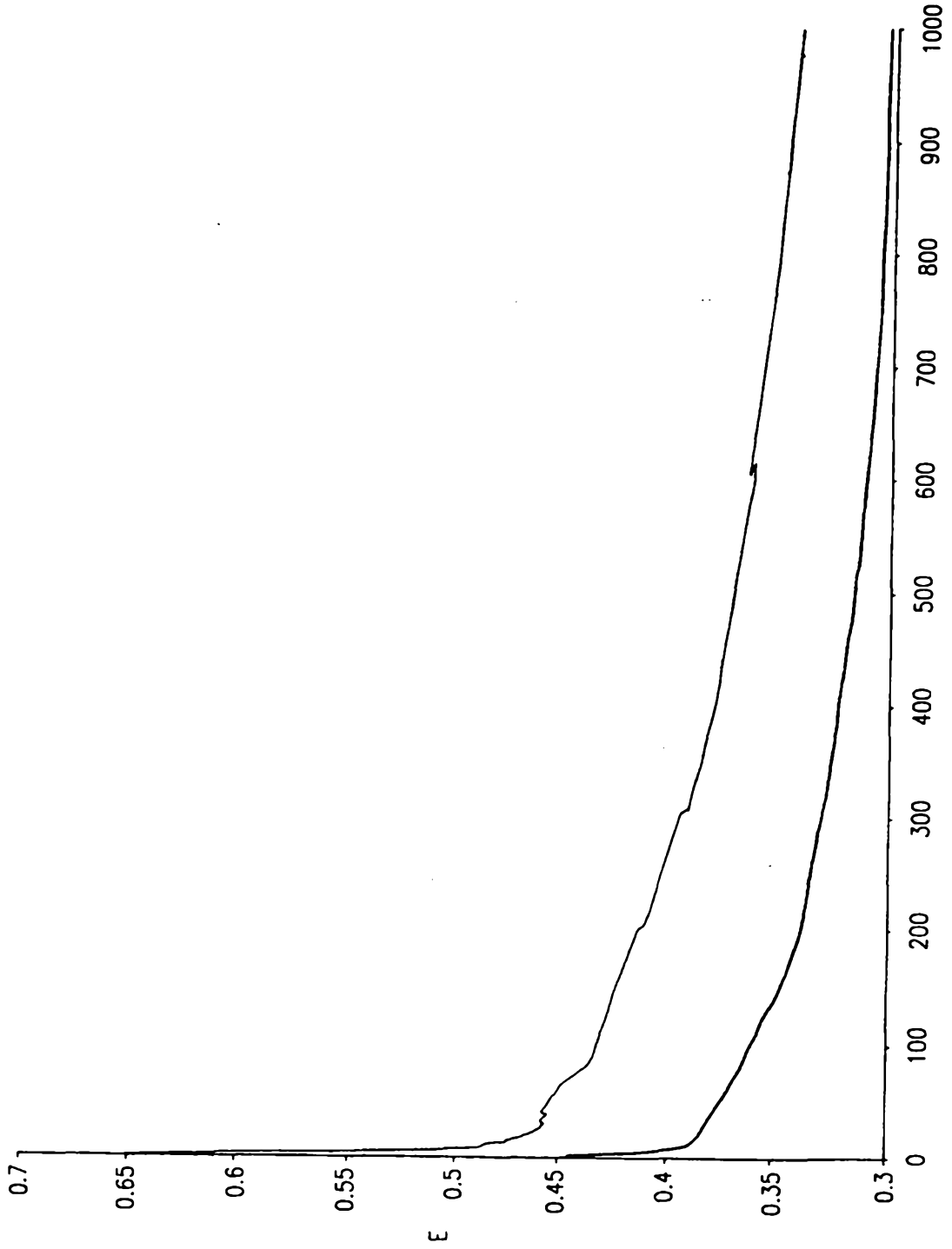
0.7
0.65
0.6
0.55
0.5
0.45
0.4
0.35
0.3
E
0
100
200
300
400
500
600
700
800
900
1000
Epoch
η=0.5, α=0.1
η=0.01, α=0.9

FIG. 4

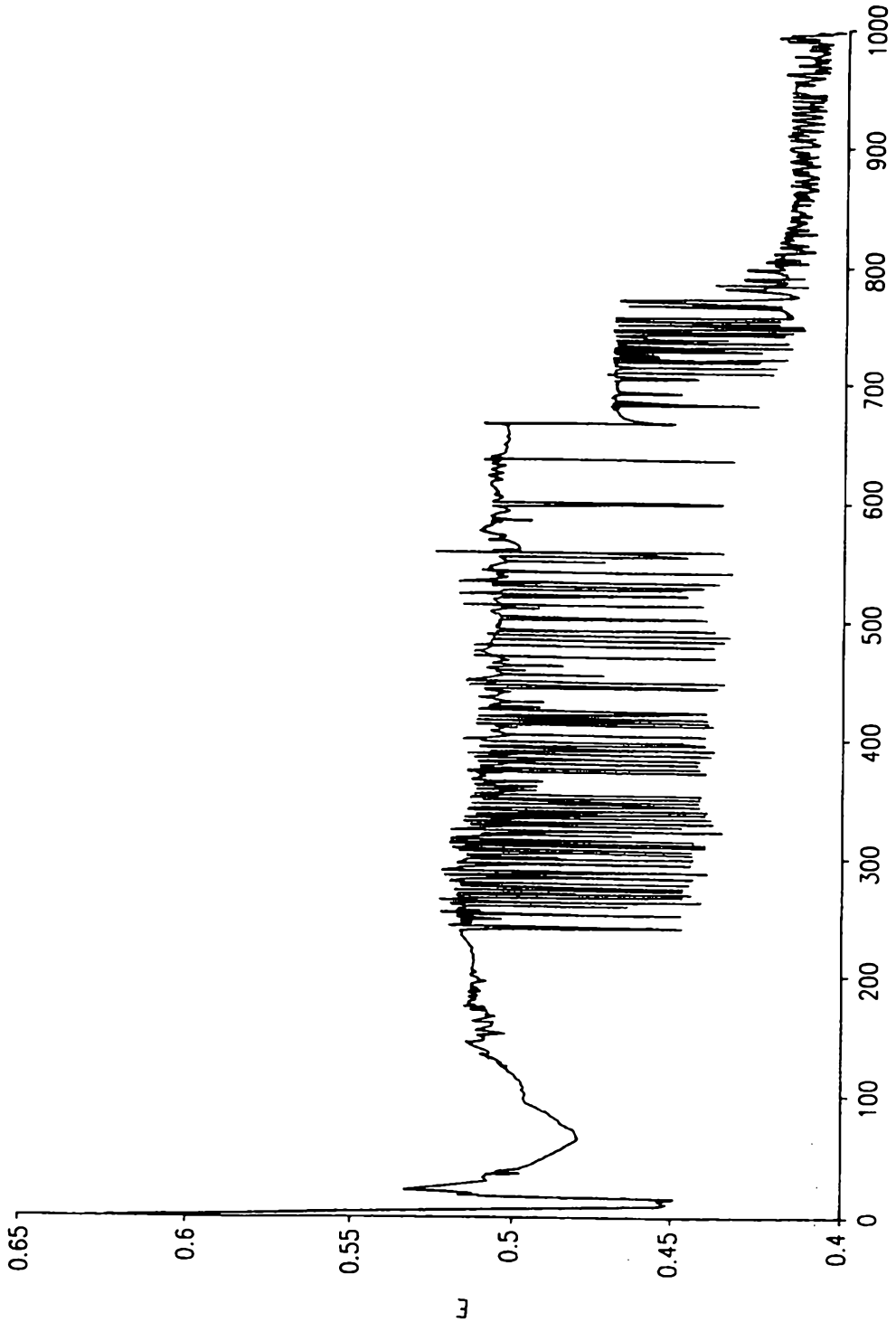
0.65
0.6
0.55
0.5
0.45
0.4
E
0
100
200
300
400
500
600
700
800
900
1000
Epoch
η=0.9, α=0.1

FIG. 5

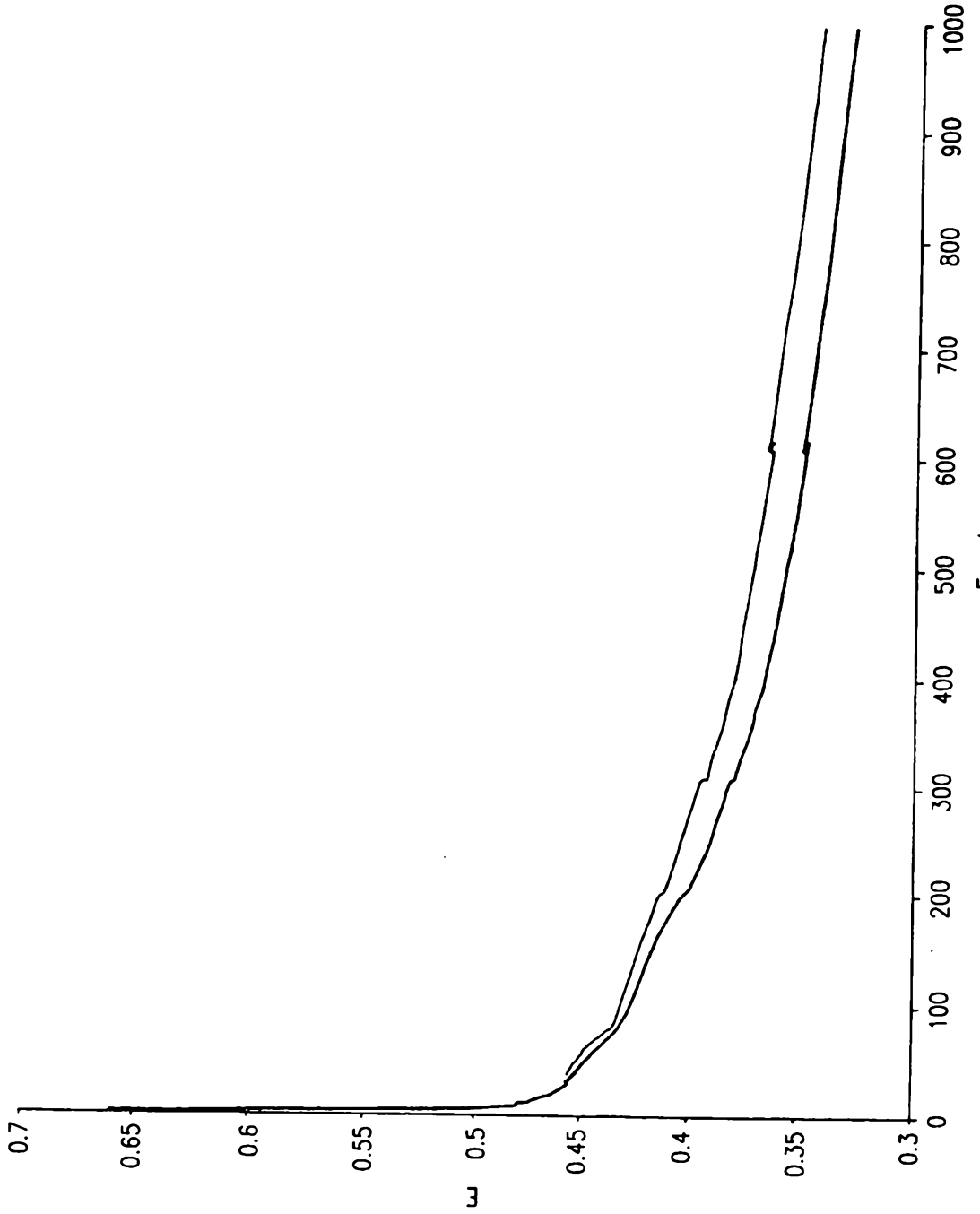
0.7
0.65
0.6
0.55
0.5
0.45
0.4
0.35
0.3
E
0
100
200
300
400
500
600
700
800
900
1000
Epoch
Training Set
Cross-Validation Set

FIG. 6


0.7
0.65
0.6
0.55
0.5
0.45
0.4
0.35
0.3
E
0
100
200
300
400
500
600
700
800
900
1000
Epoch
0 Tolerance
0.1 Tolerance

FIG. 7

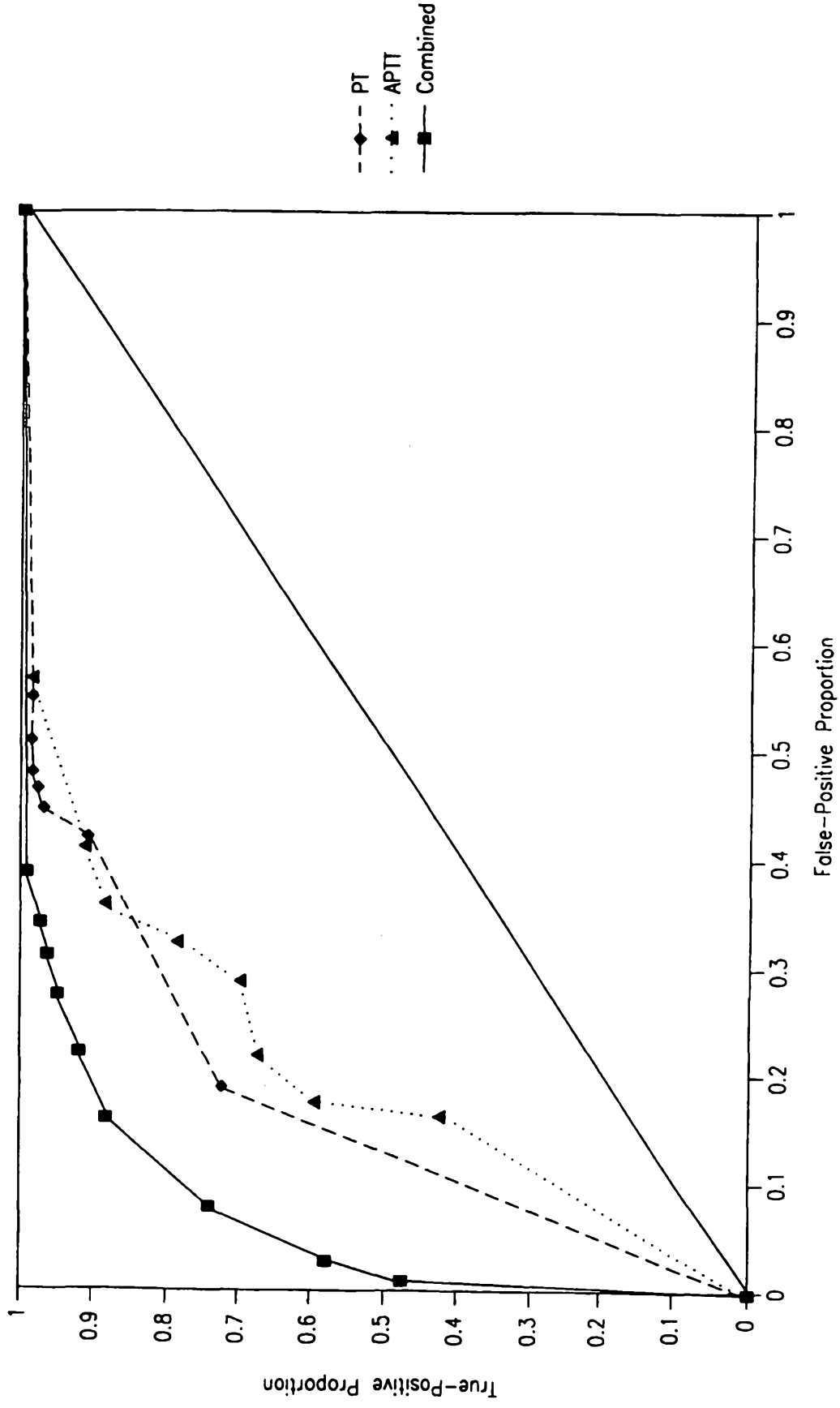
PT
APTT
Combined
True-Positive Proportion
False-Positive Proportion
0
0.1
0.2
0.3
0.4
0.5
0.6
0.7
0.8
0.9
1

FIG. 8

Hidden Layer Size	Error		
	E_{tr}	E_{DV}	φ_{ODB}
2	0.384	0.376	0.848
4	0.386	0.354	0.835
6	0.341	0.328	0.875
8	0.358	0.327	0.857
10	0.346	0.325	0.856
12	0.347	0.322	0.855

FIG. 9

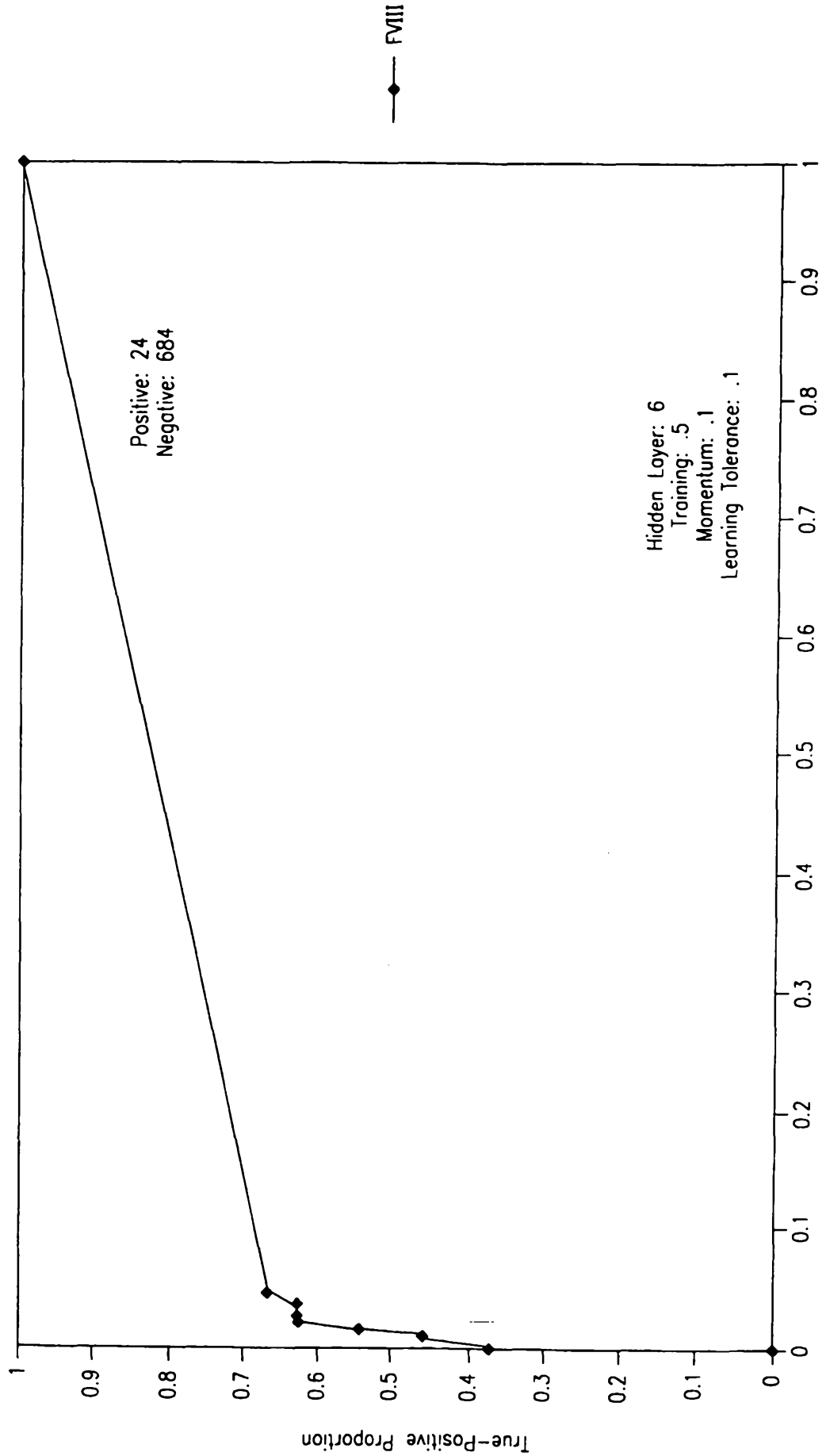
FVIII
Positive: 24
Negative: 684
Hidden Layer: 6
Training: .5
Momentum: .1
Learning Tolerance: .1
True-Positive Proportion
False-Positive Proportion
0
0.1
0.2
0.3
0.4
0.5
0.6
0.7
0.8
0.9
1

FIG. 10

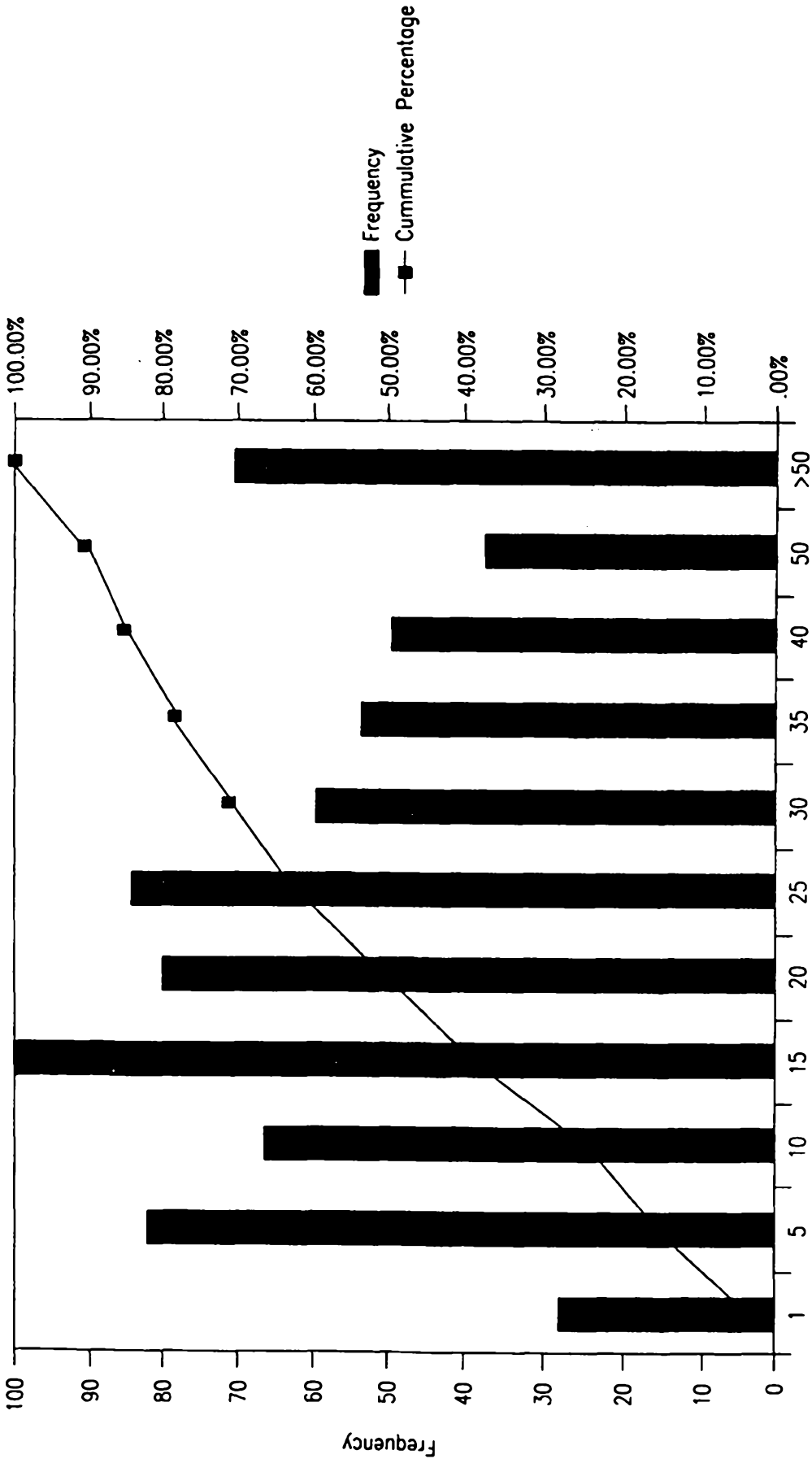
Frequency
Cummulative Percentage
100.00%
90.00%
80.00%
70.00%
60.00%
50.00%
40.00%
30.00%
20.00%
10.00%
.00%
100
90
80
70
60
50
40
30
20
10
0
Frequency
1
5
10
15
20
25
30
35
40
50
>50
% Difference

FIG. 11

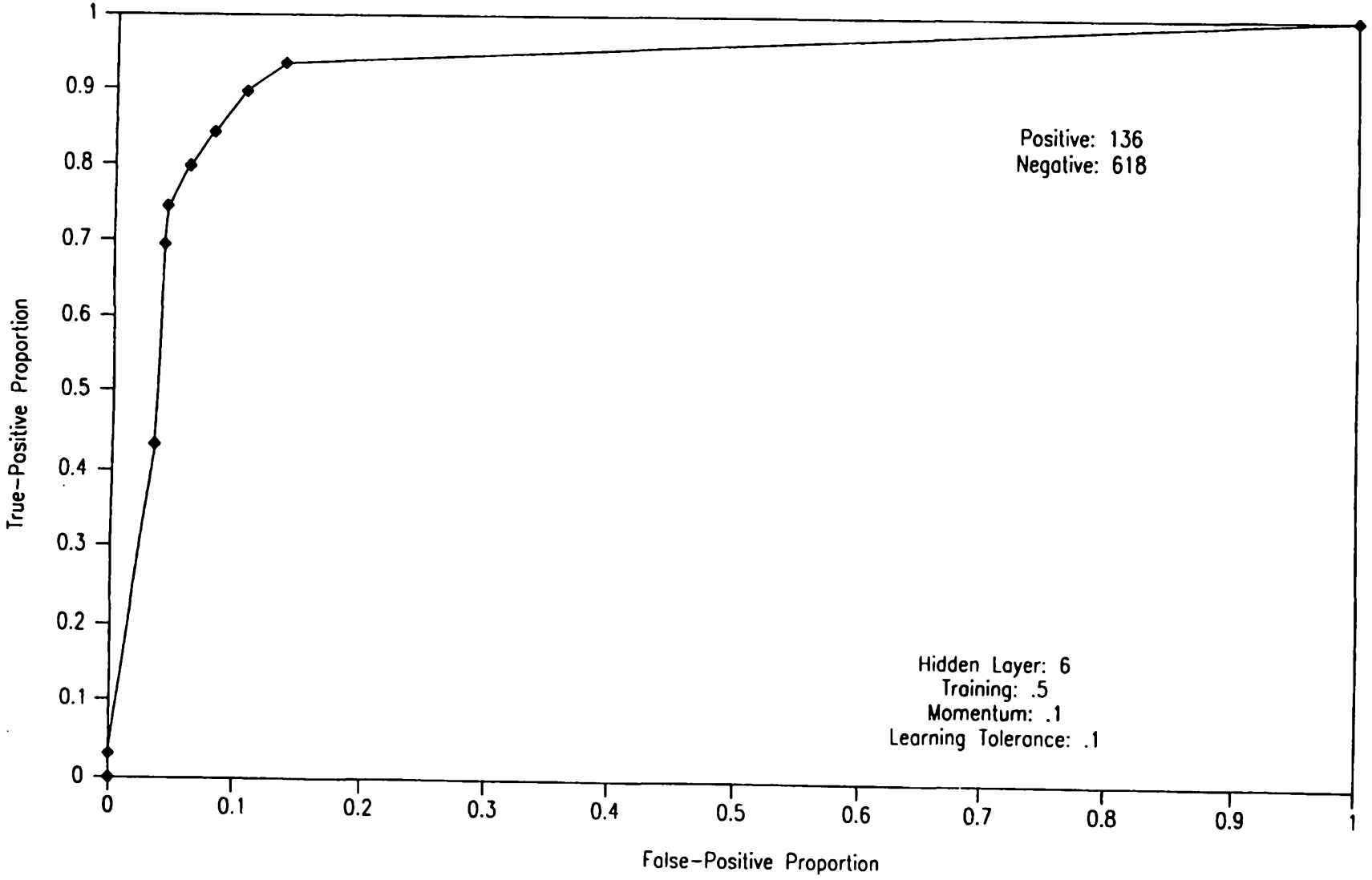
True-Positive Proportion
False-Positive Proportion
0
0.1
0.2
0.3
0.4
0.5
0.6
0.7
0.8
0.9
1
Positive: 136
Negative: 618
Hidden Layer: 6
Training: .5
Momentum: .1
Learning Tolerance: .1
FX

FIG. 12

Predictor Variables

Predictor Variable	Description
$pv_{j1} = \left(\frac{dT}{dt}\right)_{min}$	minimum of the first derivative
$pv_{j2} = t \text{ at } \left(\frac{dT}{dt}\right)_{min}$	time index of the minimum of the first derivative
$pv_{j3} = \left(\frac{d^2T}{dt^2}\right)_{min}$	minimum of the second derivative
$pv_{j4} = t \text{ at } \left(\frac{dT^2}{dt^2}\right)_{min}$	index of the minimum of the second derivative
$pv_{j5} = \left(\frac{d^2T}{dt^2}\right)_{max}$	moximum of the second derivative
$pv_{j6} = t \text{ at } \left(\frac{dT^2}{dt^2}\right)_{max}$	index of the maximum of the second derivative
$pv_{j7} = {}^{T}t_{0} - {}^{T}t_{R}$	overall change in transmittence during the reaction

FIG. 13

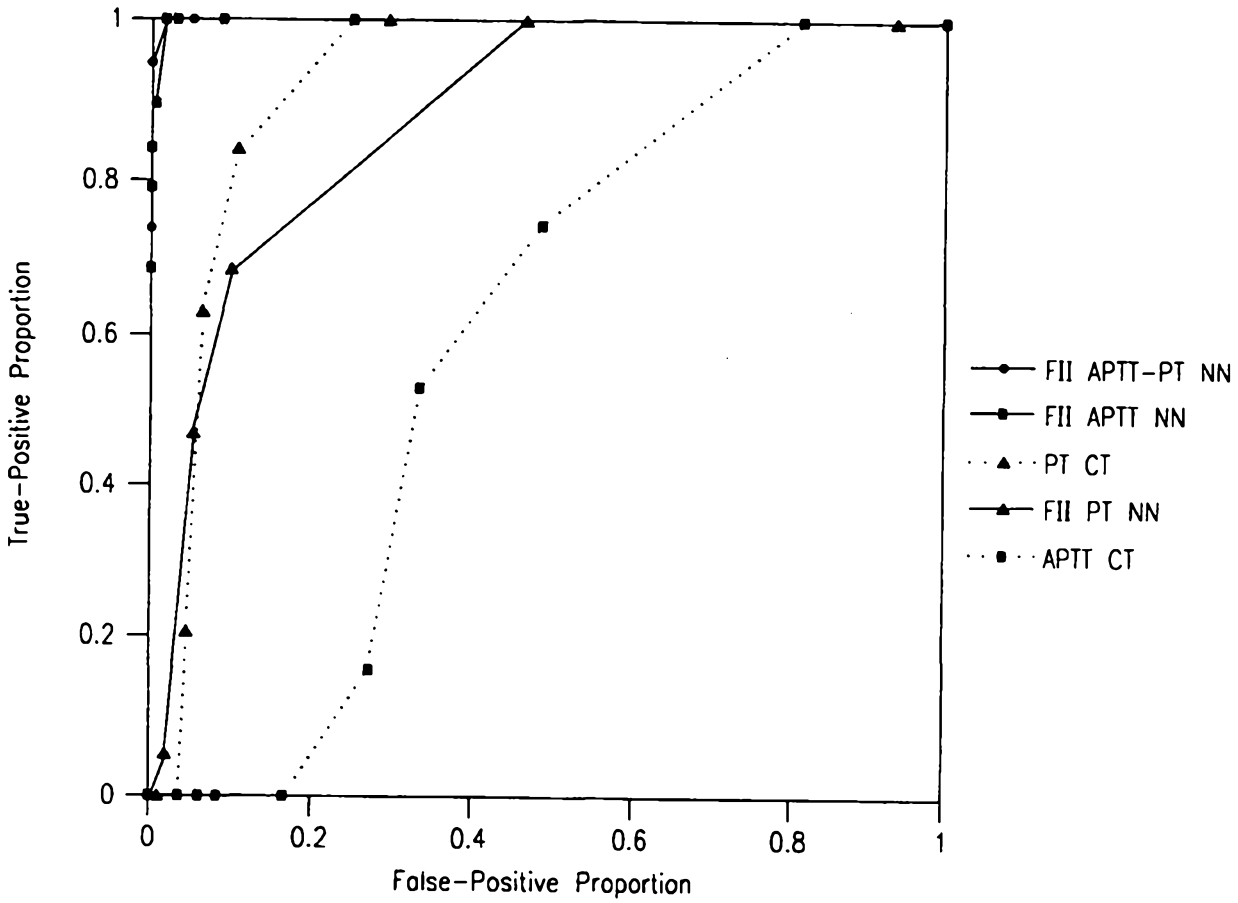
True-Positive Proportion
False-Positive Proportion
0
0.2
0.4
0.6
0.8
1
FII APTT-PT NN
FII APTT NN
PT CT
FII PT NN
APTT CT

FIG. 14

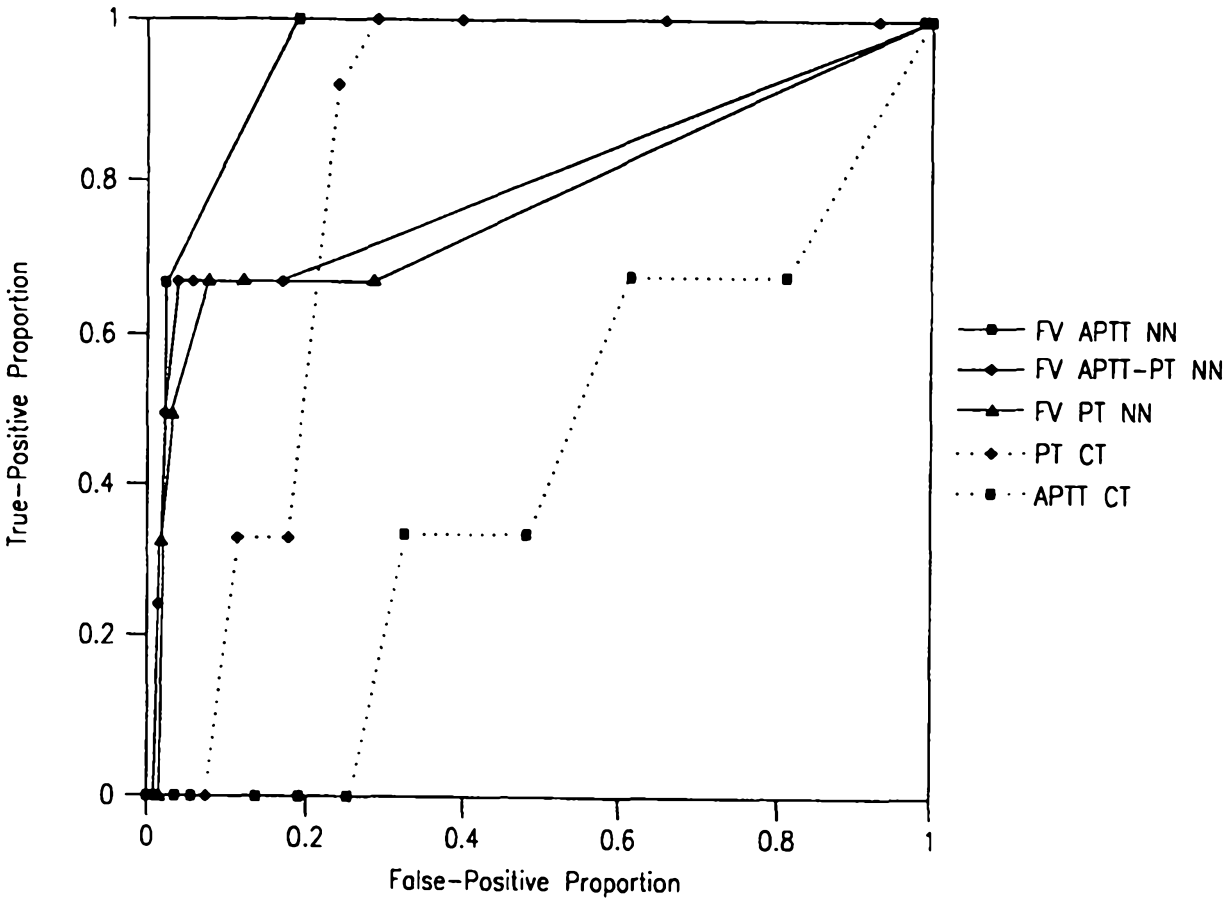
True-Positive Proportion
False-Positive Proportion
0
0.2
0.4
0.6
0.8
1
FV APTT NN
FV APTT-PT NN
FV PT NN
PT CT
APTT CT

FIG. 15

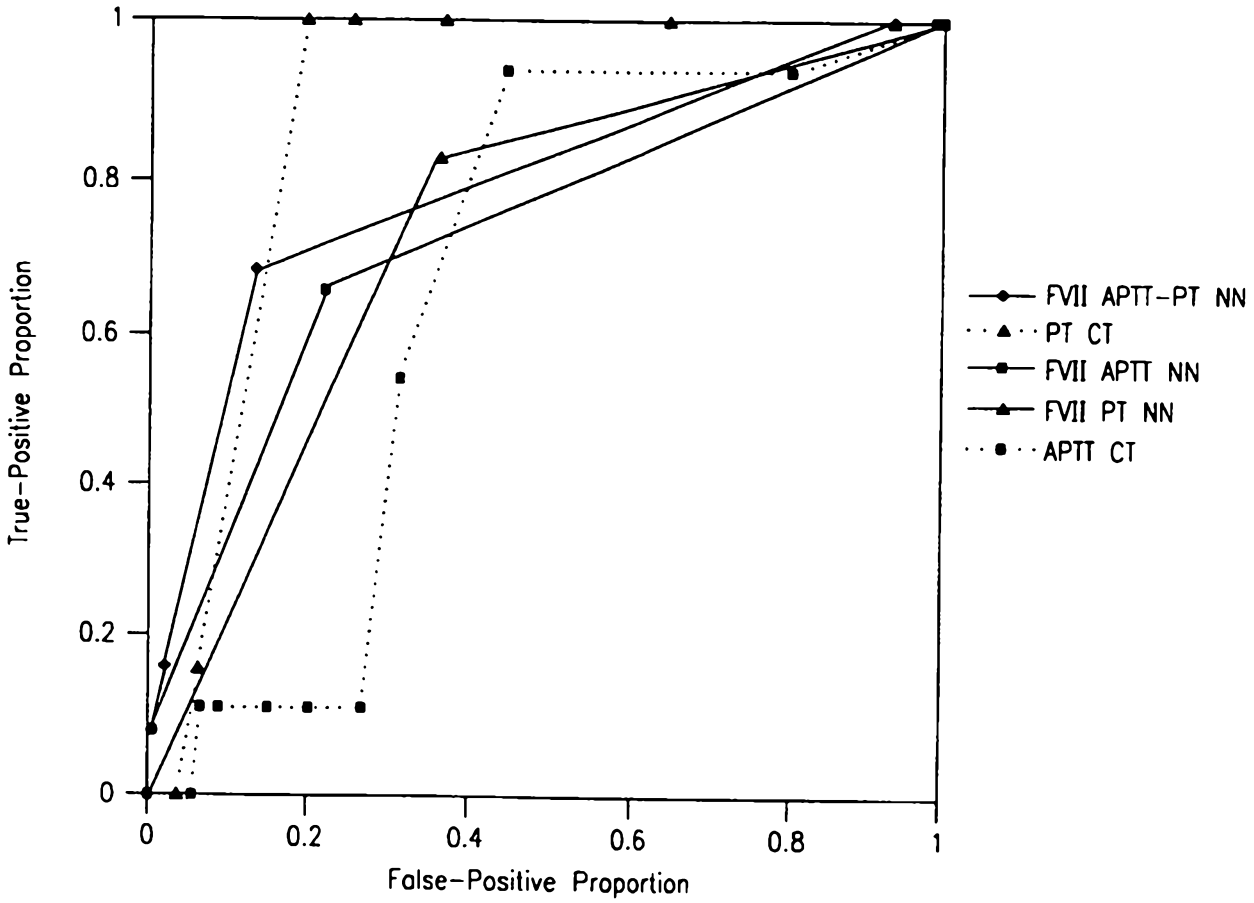
True-Positive Proportion
False-Positive Proportion
0
0.2
0.4
0.6
0.8
1
FVII APTT-PT NN
PT CT
FVII APTT NN
FVII PT NN
APTT CT

FIG. 16

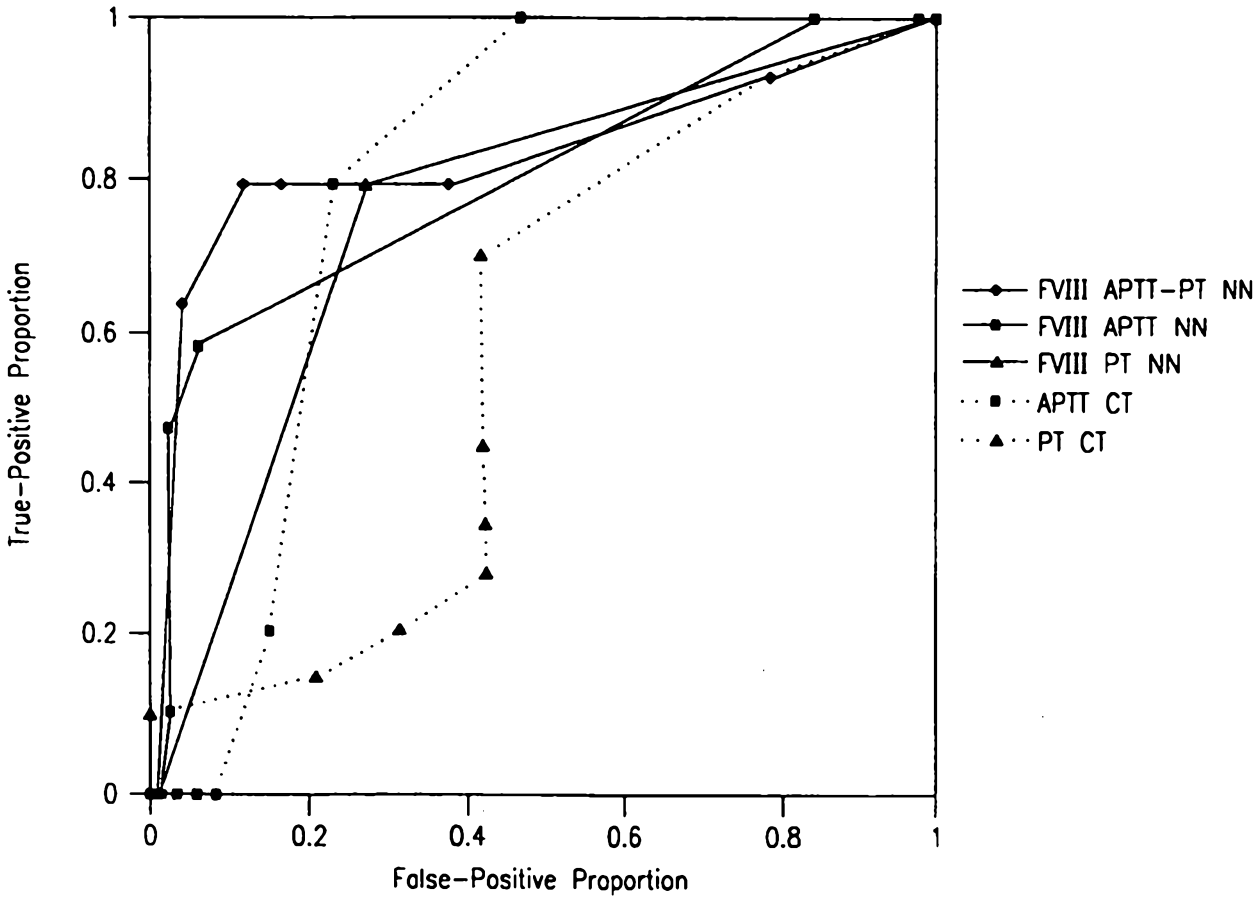
True-Positive Proportion
False-Positive Proportion
0
0.2
0.4
0.6
0.8
1
FVIII APTT-PT NN
FVIII APTT NN
FVIII PT NN
APTT CT
PT CT

FIG. 17

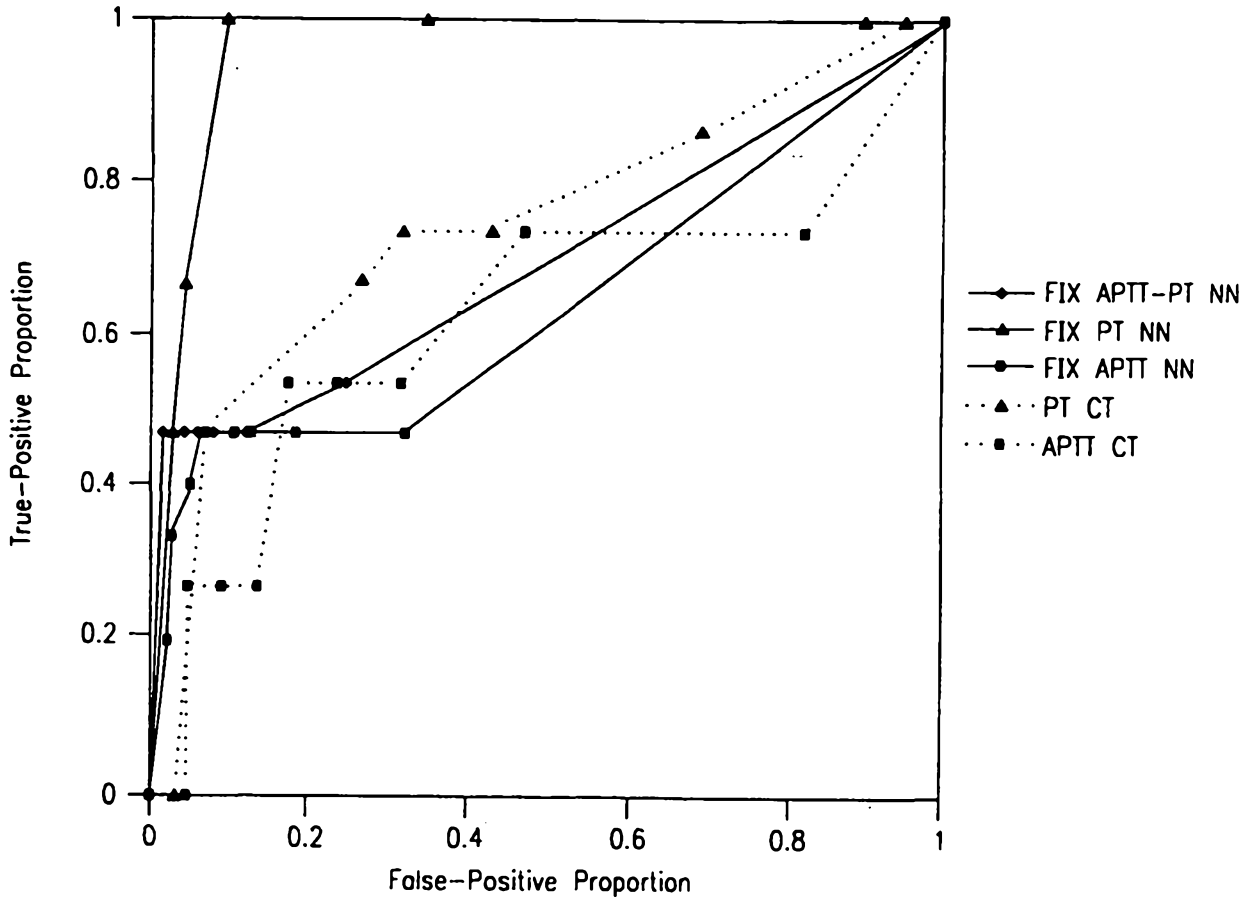
True-Positive Proportion
False-Positive Proportion
0
0.2
0.4
0.6
0.8
1
FIX APTT-PT NN
FIX PT NN
FIX APTT NN
PT CT
APTT CT

FIG. 18

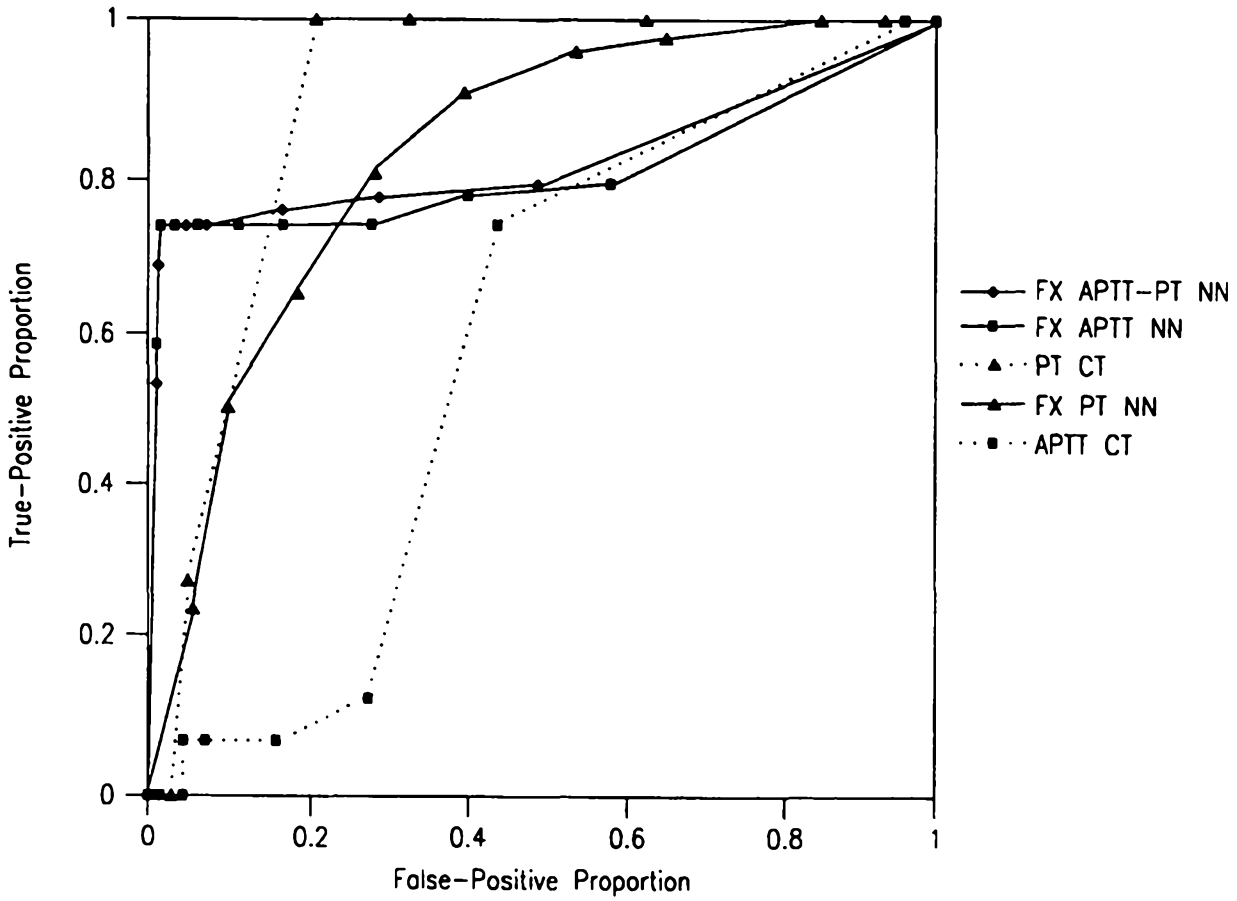
True-Positive Proportion
False-Positive Proportion
0
0.2
0.4
0.6
0.8
1
FX APTT-PT NN
FX APTT NN
PT CT
FX PT NN
APTT CT

FIG. 19

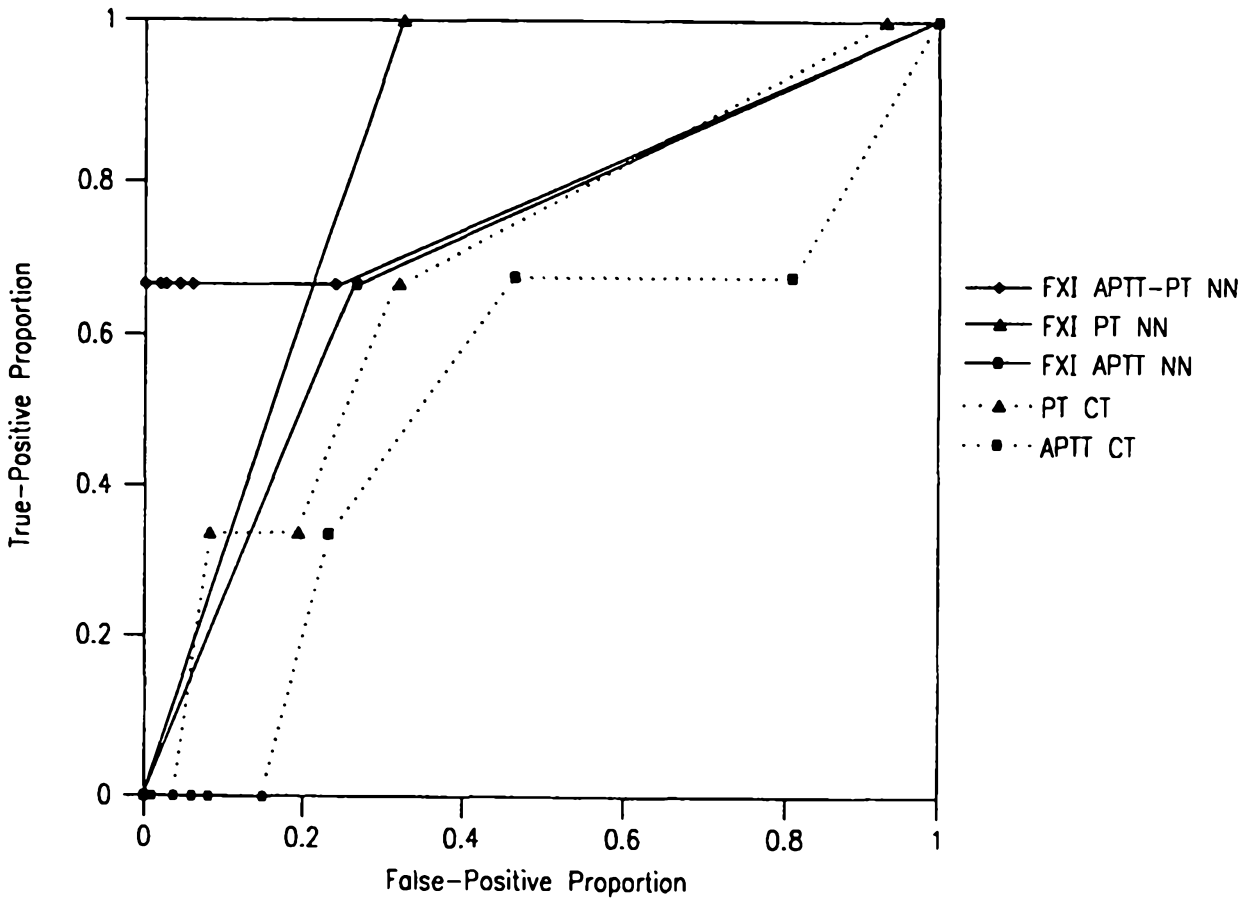
True-Positive Proportion
False-Positive Proportion
0
0.2
0.4
0.6
0.8
1
FXI APTT-PT NN
FXI PT NN
FXI APTT NN
PT CT
APTT CT

FIG. 20

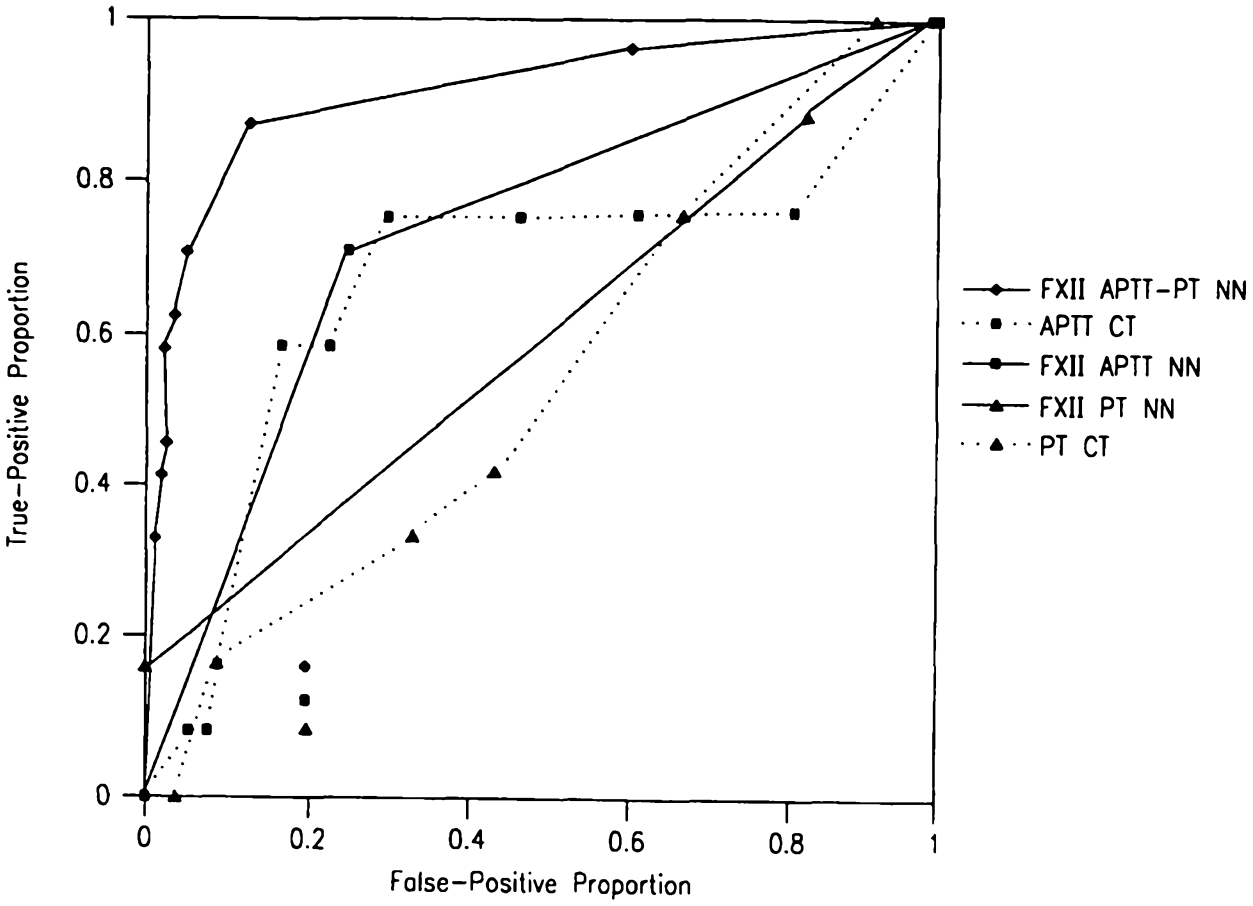

FIG. 21

Condition	Training Set		Cross-Validation Set	
	Negative	Positive	Negative	Positive
FII < 30%	346	32	362	19
FV < 30%	362	12	366	12
FVII < 30%	354	32	343	35
FVIII < 30%	342	32	367	19
FIX < 30%	344	26	360	15
FX < 30%	294	76	324	58
FX < 10%	338	32	369	13
FX < 50%	266	104	289	93
FXI < 30%	358	12	367	12
FXII < 30%	346	32	362	24

FIG. 22

Results of classification of coagulation factor deficiencies as determined from area under ROC curves. Results are shown for classification based on APTT and PT clot times (APTT CT and PT CT, respectively) and from neural networks using APTT optical data parameter sets (APTT NN), PT data parameters (PT NN) and combined data sets from both assays (APTT-PT NN). Results are expressed as area under ROC curves and the associated standard error (SE) calculated according to [19].

Condition		APTT-PT NN		APPTT NN		PT NN		APTT CT		PT CT		Comments
Factor	Cut-off	Area	SE	Area	SE	Area	SE	Area	SE	Area	SE	
FII	30%	0.999	0.001	0.998	0.002	0.876	0.032	0.594	0.044	0.922	0.016	Best results for APTT NN, APTT-PT NN
FV	30%	0.787	0.087	0.942	0.018	0.760	0.090	0.412	0.076	0.815	0.026	Best results for APTT NN
FVII	30%	0.791	0.045	0.724	0.049	0.728	0.041	0.661	0.036	0.882	0.017	NNs do not provide either greater area under curve or higher specificity (Fig. 5)
FVIII	30%	0.826	0.065	0.794	0.060	0.752	0.055	0.789	0.027	0.423	0.082	NNs do not give greater area under curve; do tend toward higher specificity (Fig. 6)
FIX	30%	0.691	0.087	0.634	0.090	0.961	0.011	0.622	0.090	0.738	0.073	Best results for PT NN
FX	30%	0.827	0.041	0.809	0.043	0.830	0.025	0.579	0.034	0.894	0.016	NNs do not give greater area under curve; do tend toward higher specificity (Fig. 11)
FXI	30%	0.790	0.093	0.692	0.080	0.826	0.033	0.509	0.091	0.675	0.077	Best results for APTT-PT NN if greater specificity is desired (Fig. 8)
FXII	30%	0.902	0.039	0.710	0.055	0.586	0.067	0.659	0.070	0.530	0.058	Best results for APTT-PT NN

FIG. 23

Areas under ROC curves for three networks trained to classify factor deficiencies based on three different diagnostics cutoffs (10%, 30%, and 50%). The area under the ROC curve for PT clot time is also included. ROC curves for APTT clot time are not shown due to the generally accepted insensitivity of APTT clot time to FX (as exhibited in Table II). SE is the standard error associated with the area.

Condition		APTT-PT NN		PT CT	
Factor	Cut-off	Area	SE	Area	SE
FX <	10%	0.994	0.004	0.951	0.016
FX <	30%	0.827	0.041	0.894	0.016
FX <	50%	0.748	0.035	0.900	0.016

FIG. 24

Results from linear regressions comparing factor concentrations estimated using neural networks with measured factor concentrations, including the slope, intercept, and the Pearson product moment correlation coefficient (r). Pearson correlation coefficients are also included for linear regressions comparing APTT and PT clot times with measured factor concentrations.

Factor	APTT-PT NN			APTT Clot Time	PT Clot Time
	Slope	Intercept	r	r	r
FII	0.53	46.7	0.62	0.05	0.05
FV	0.31	64.2	0.45	0.07	0.01
FVII	0.18	8.5	0.32	0.17	0.08
FVIII	-0.14	140.5	0.02	0.15	0.13
FIX	0.38	60.7	0.54	0.26	0.15
FX	0.50	53.2	0.60	0.11	0.13
FXI	0.20	75.4	0.37	0.27	0.08
FXII	0.35	54.8	0.51	0.10	0.08
Fibrinogen	0.89	61.9	0.97	0.07	0.07

FIG. 25

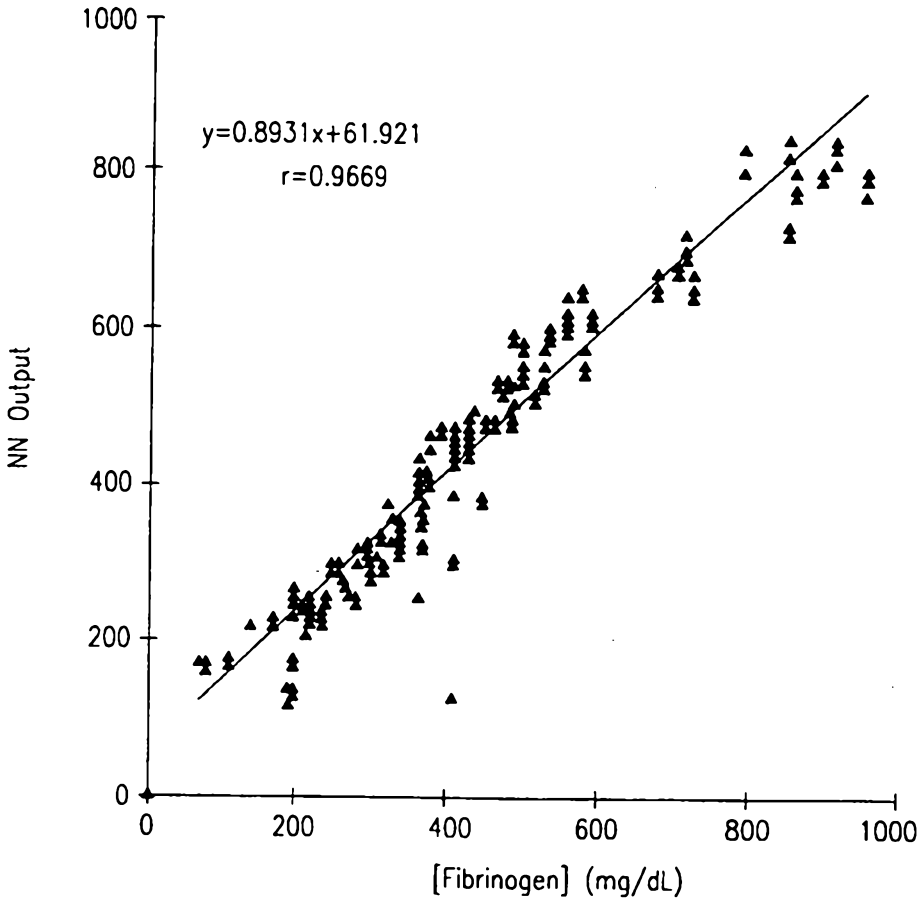
y=0.8931x+61.921
r=0.9669
NN Output
[Fibrinogen] (mg/dL)
0
200
400
600
800
1000

FIG. 26

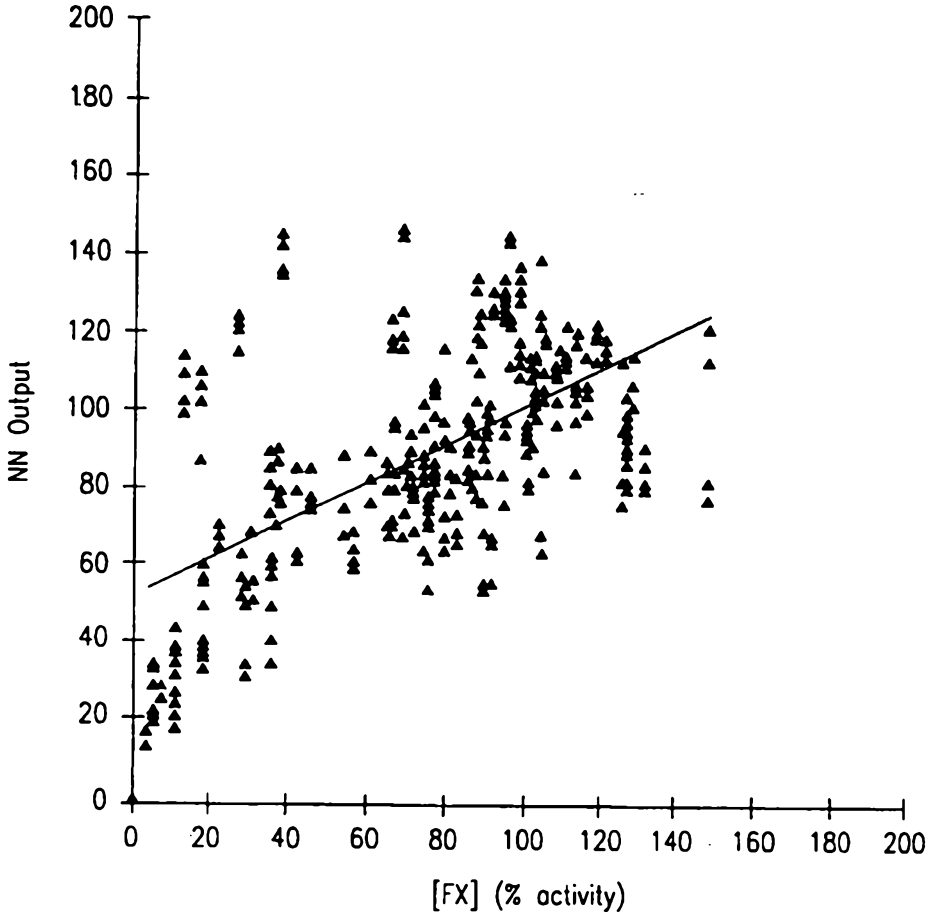
200
180
160
140
120
100
80
60
40
20
0
NN Output
0
20
40
60
80
100
120
140
160
180
200
[FX] (% activity)
y=0.5032x + 53.179
r=0.6007

FIG. 27

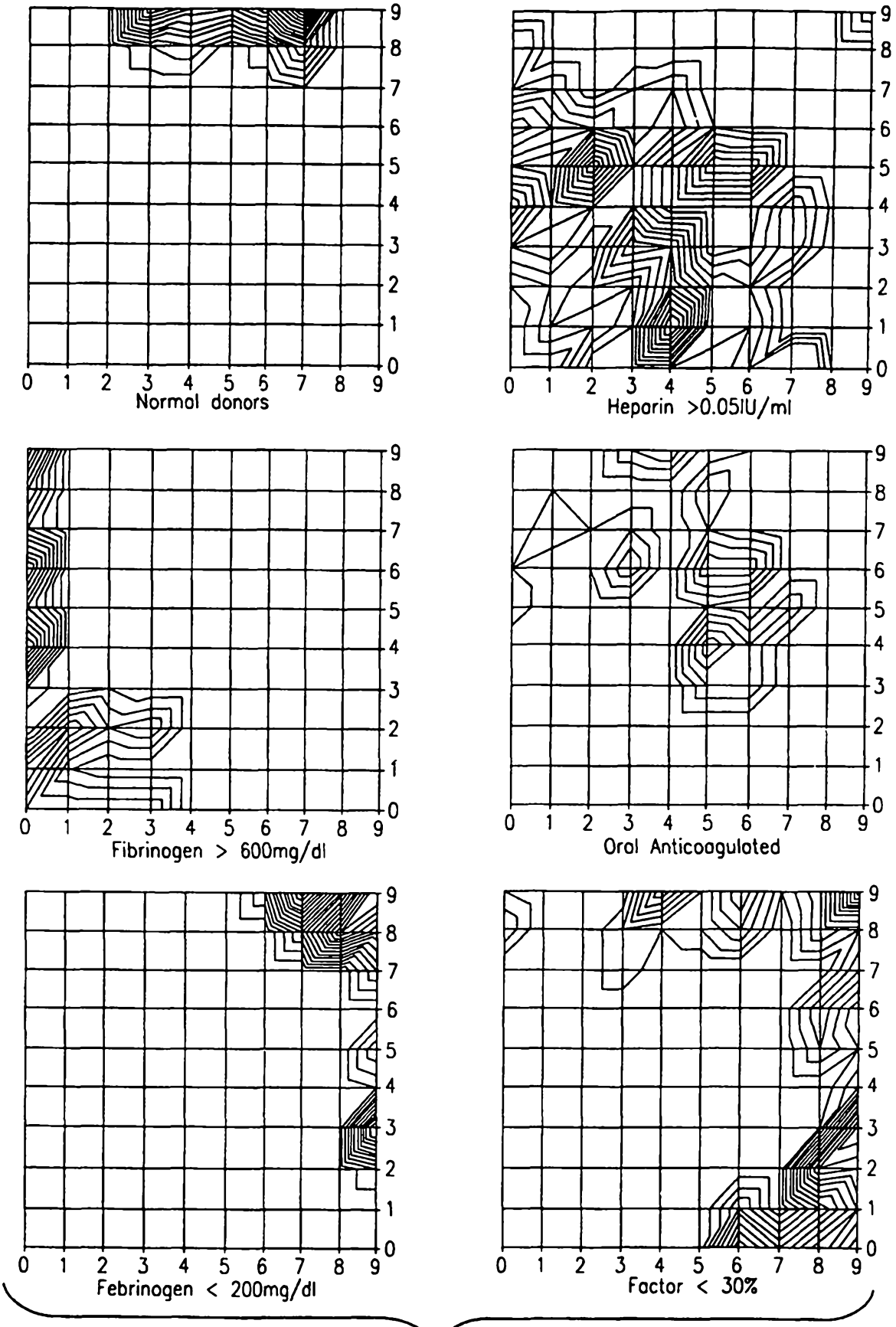
Normal donors
Heparin >0.05IU/ml
Fibrinogen > 600mg/dl
Oral Anticoagulated
Febrinogen < 200mg/dl
Factor < 30%

FIG. 28

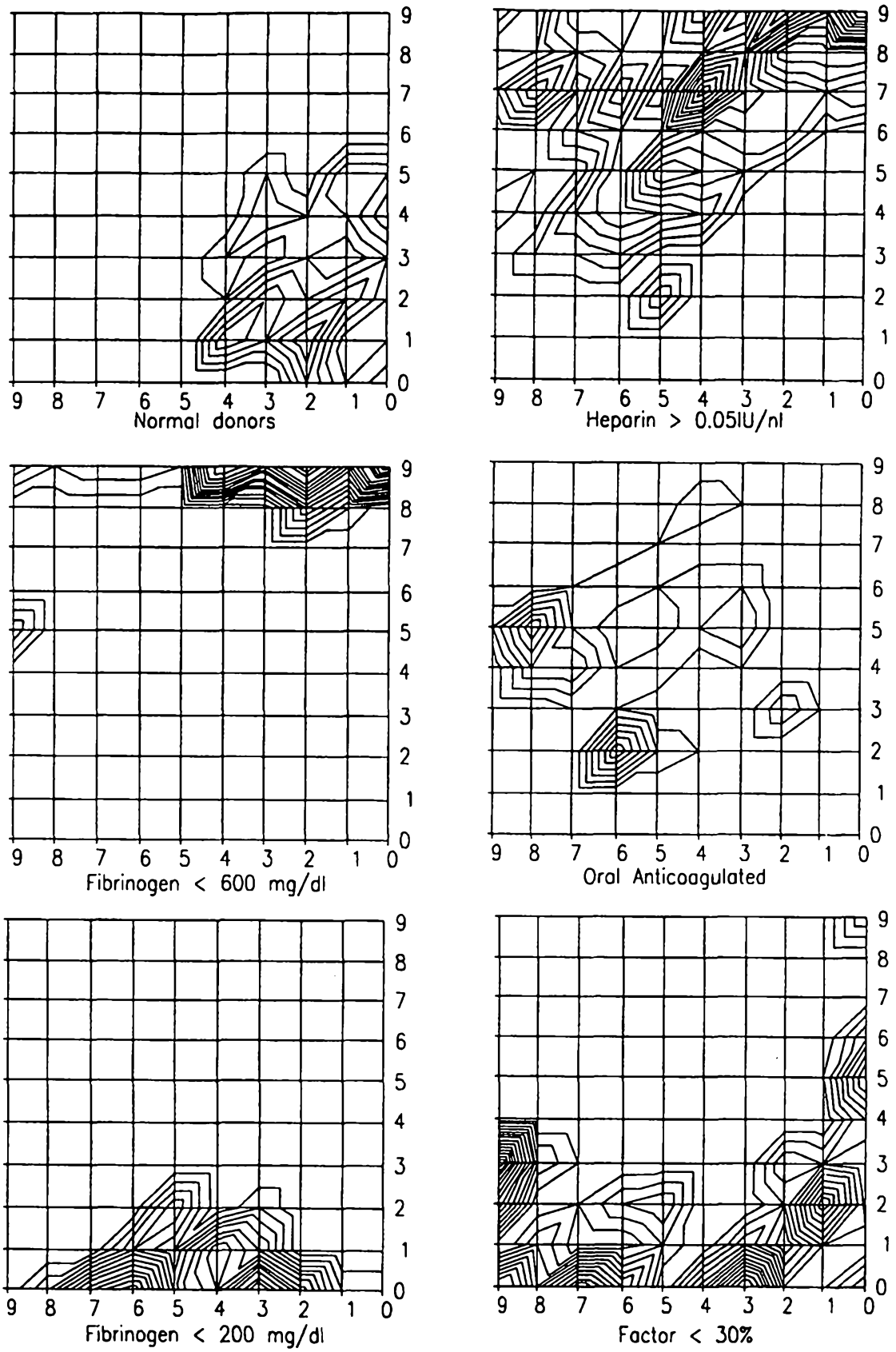
Normal donors
Heparin > 0.05IU/nl
Fibrinogen < 600 mg/dl
Oral Anticoagulated
Fibrinogen < 200 mg/dl
Factor < 30%

FIG. 29

Sensitivity, specificity, efficiency, predictive value of positive test (PPV), and predictive power of negative test (NPV) for self-organizing feature maps trained using learning vector quantization to predict factor-deficiencies or heparin therapy based on either APTT or PT parameters.

	APTT					PT				
Deficiency or Condition	Sensitivity	Specificity	PPV	NPV	Efficiency	Sensitivity	Specificity	PPV	NPV	Efficiency
FII < 30%	0.84	0.93	0.39	0.99	0.93	0.79	0.96	0.51	0.99	0.95
FV < 30%	0.00	0.98	0.00	0.97	0.95	0.00	0.99	0.00	0.97	0.96
FVII < 30%	0.22	0.97	0.42	0.92	0.90	0.03	0.97	0.09	0.91	0.88
FVIII < 30%	0.33	0.96	0.21	0.98	0.94	0.00	0.96	0.00	0.97	0.93
FIX < 30%	0.47	0.91	0.18	0.98	0.89	0.00	0.96	0.00	0.96	0.92
FX < 30%	0.62	0.85	0.43	0.93	0.82	0.66	0.86	0.46	0.93	0.83
FXI < 30%	0.67	0.96	0.35	0.99	0.95	1.00	0.96	0.45	1.00	0.96
FXII < 30%	0.79	0.90	0.34	0.98	0.89	0.50	0.92	0.29	0.97	0.89
Heparin < 0.051 U/ml	0.76	0.86	0.72	0.88	0.83	0.77	0.74	0.59	0.87	0.75

FIG. 30

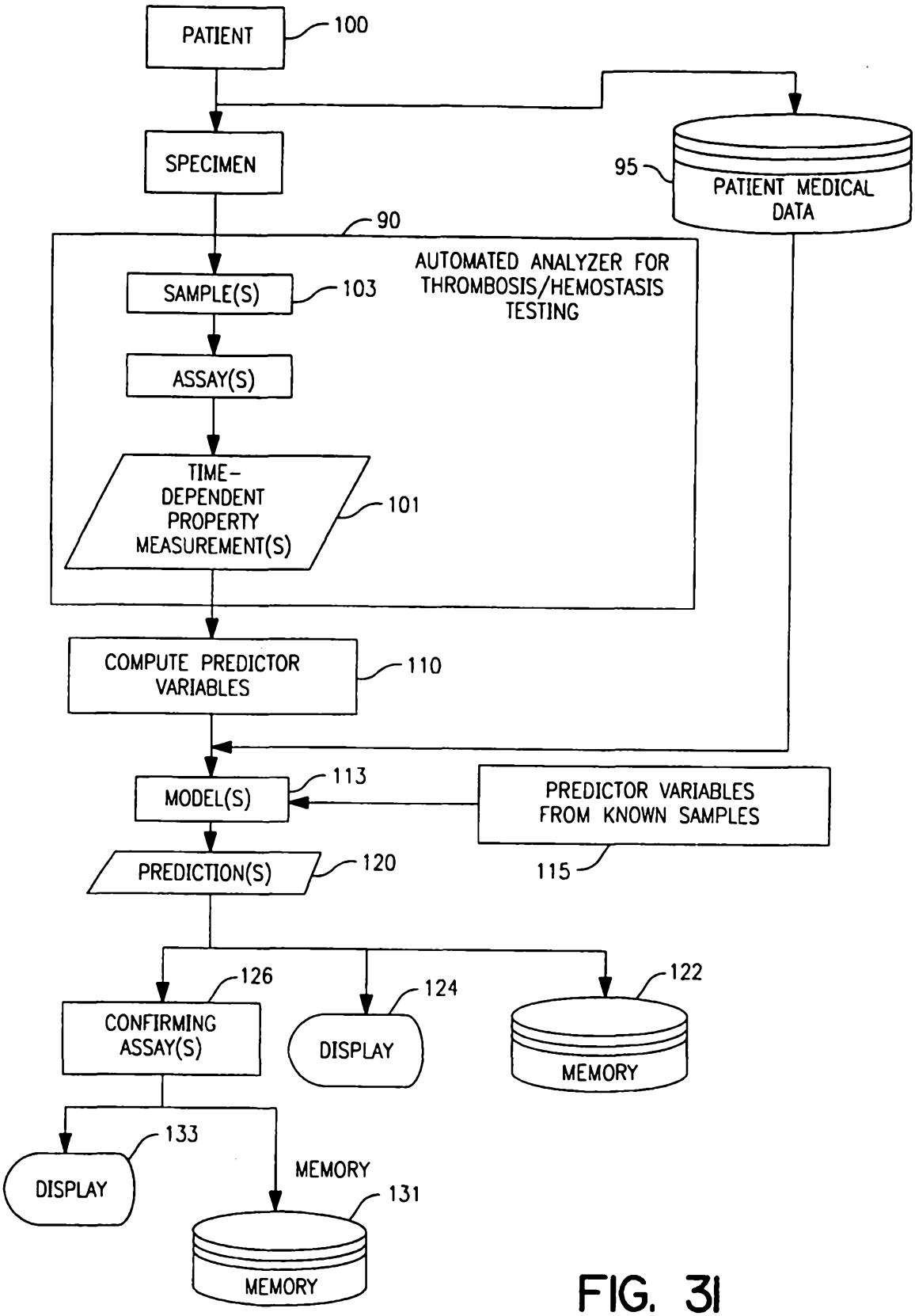
PATIENT
100
SPECIMEN
95
PATIENT MEDICAL DATA
90
AUTOMATED ANALYZER FOR THROMBOSIS/HEMOSTASIS TESTING
SAMPLE(S)
103
ASSAY(S)
TIME-DEPENDENT PROPERTY MEASUREMENT(S)
101
COMPUTE PREDICTOR VARIABLES
110
MODEL(S)
113
PREDICTOR VARIABLES FROM KNOWN SAMPLES
115
PREDICTION(S)
120
CONFIRMING ASSAY(S)
126
DISPLAY
124
MEMORY
122
DISPLAY
133
MEMORY
131
MEMORY

FIG. 31

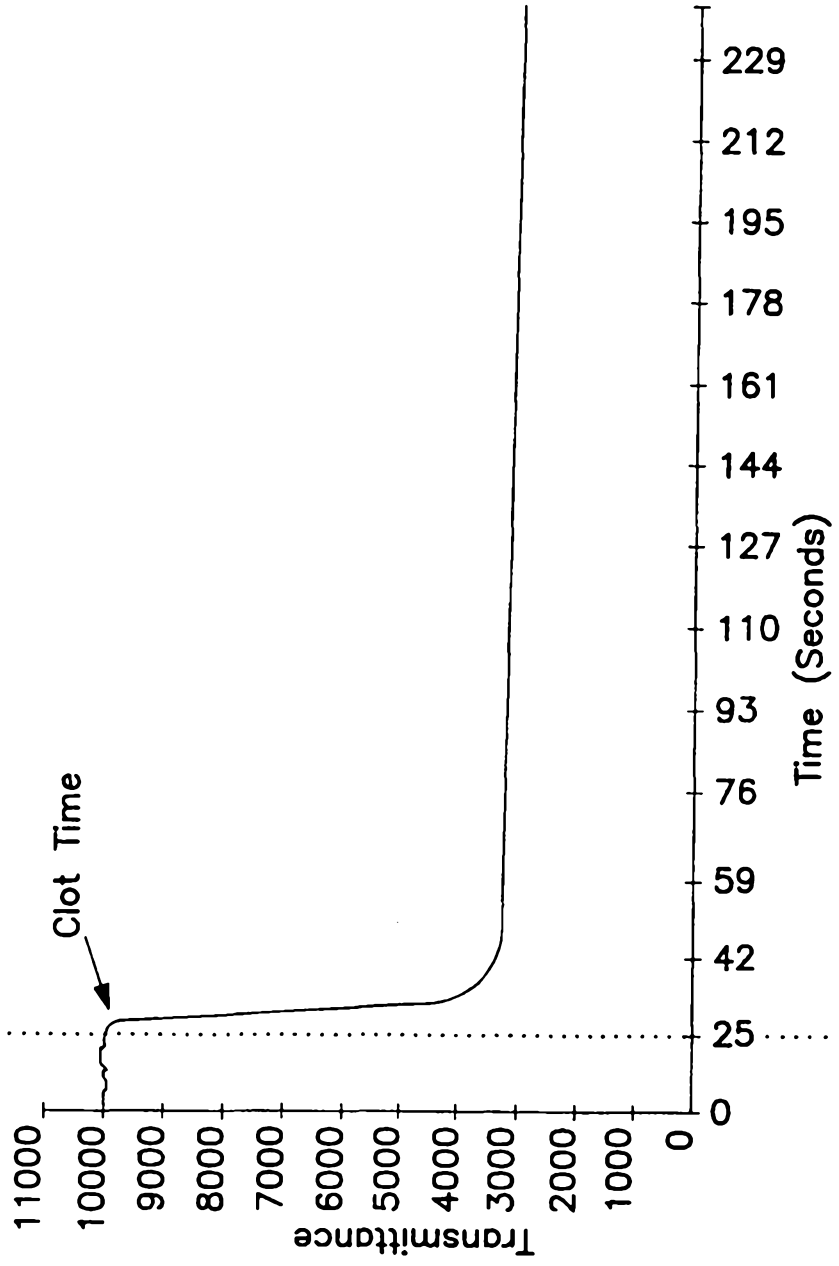
Clot Time
Transmittance
11000
10000
9000
8000
7000
6000
5000
4000
3000
2000
1000
0
Time (Seconds)
229
212
195
178
161
144
127
110
93
76
59
42
25
0

FIG. 32A

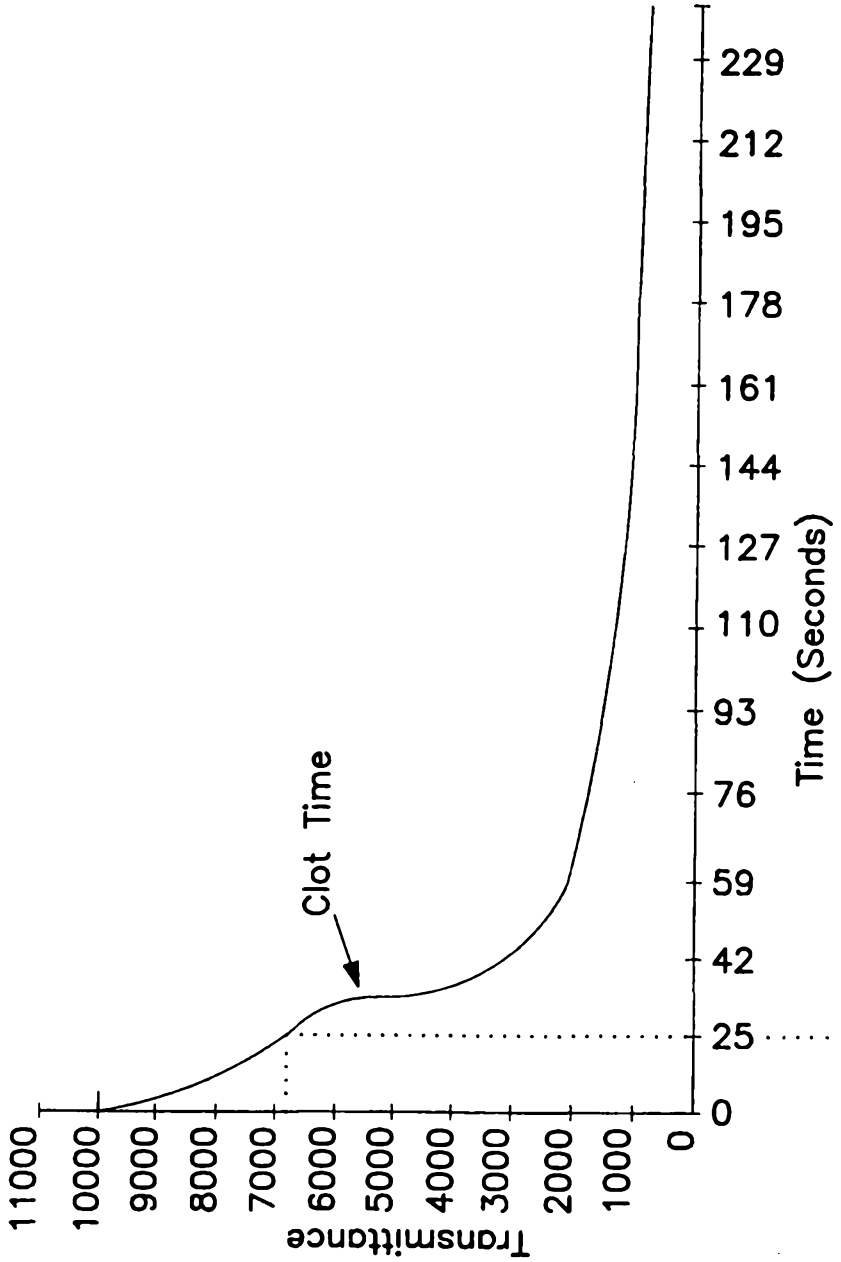
Transmittance
11000
10000
9000
8000
7000
6000
5000
4000
3000
2000
1000
0
Clot Time
Time (Seconds)
229
212
195
178
161
144
127
110
93
76
59
42
25
0

FIG. 32B

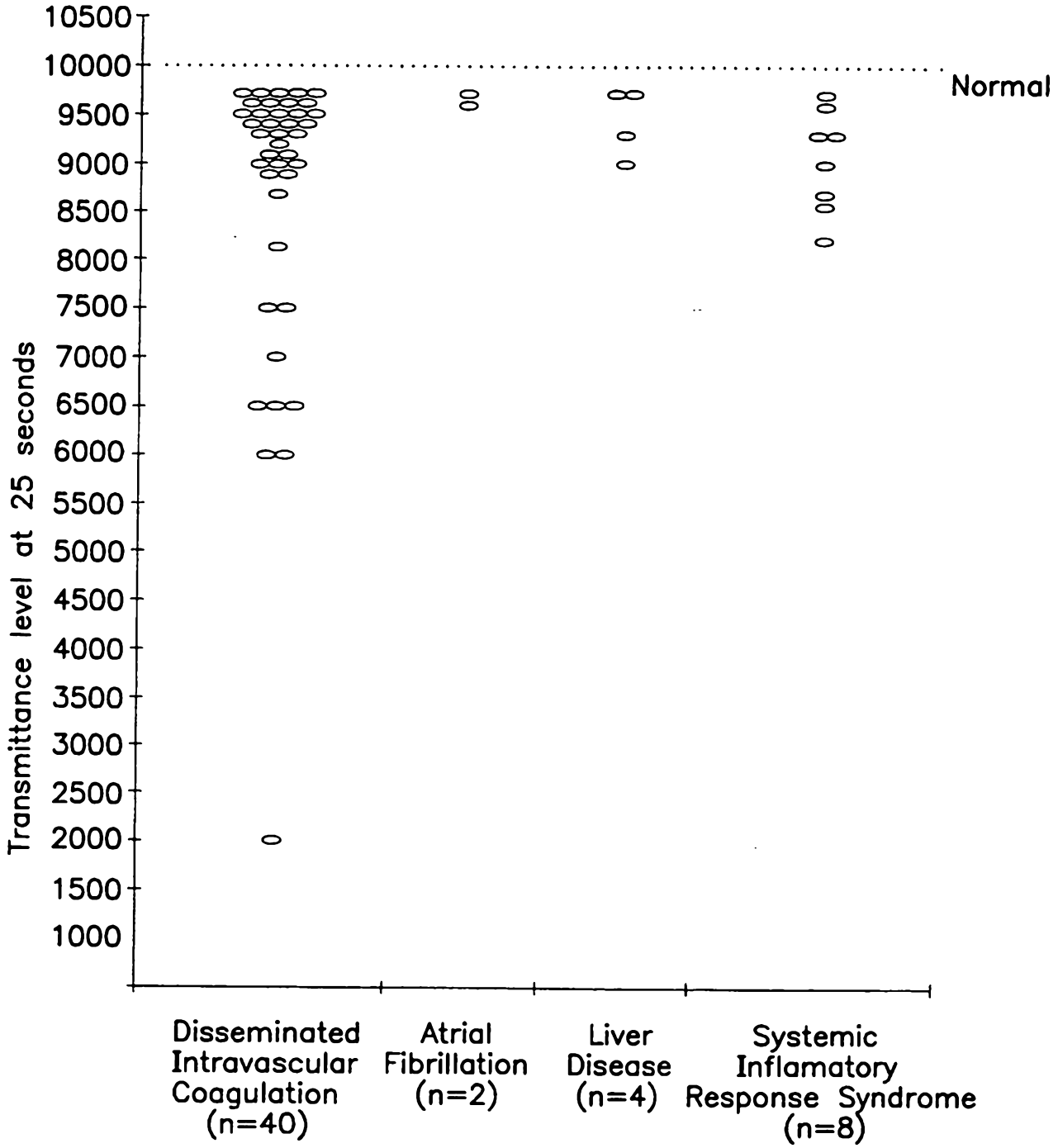
10500
10000
9500
9000
8500
8000
7500
7000
6500
6000
5500
5000
4500
4000
3500
3000
2500
2000
1500
1000
Transmittance level at 25 seconds
Normal
Disseminated Intravascular Coagulation (n=40)
Atrial Fibrillation (n=2)
Liver Disease (n=4)
Systemic Inflamatory Response Syndrome (n=8)

FIG. 33

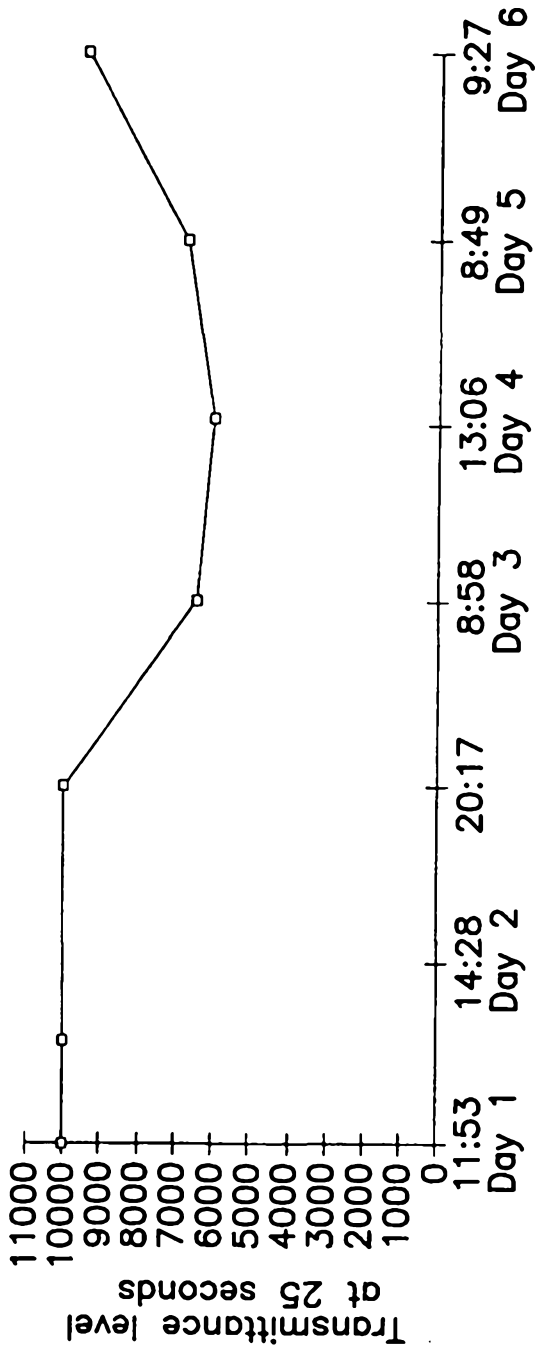
Transmittance level
at 25 seconds
11000
10000
9000
8000
7000
6000
5000
4000
3000
2000
1000
0
11:53
Day 1
14:28
Day 2
20:17
8:58
Day 3
13:06
Day 4
8:49
Day 5
9:27
Day 6

FIG. 34A

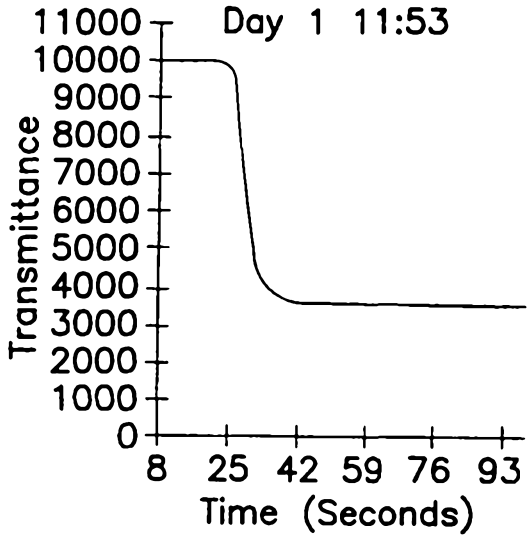

FIG. 34B

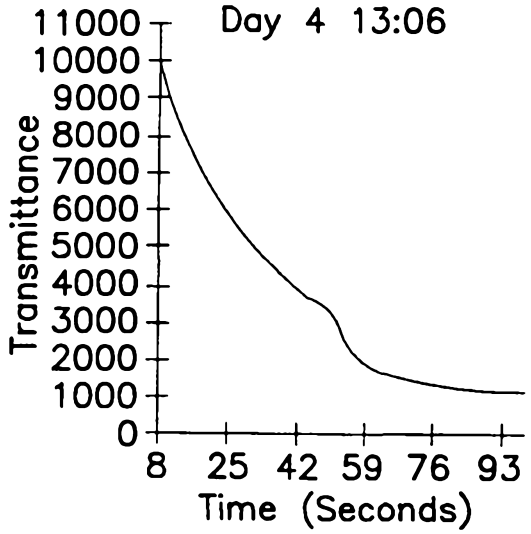

FIG. 34C

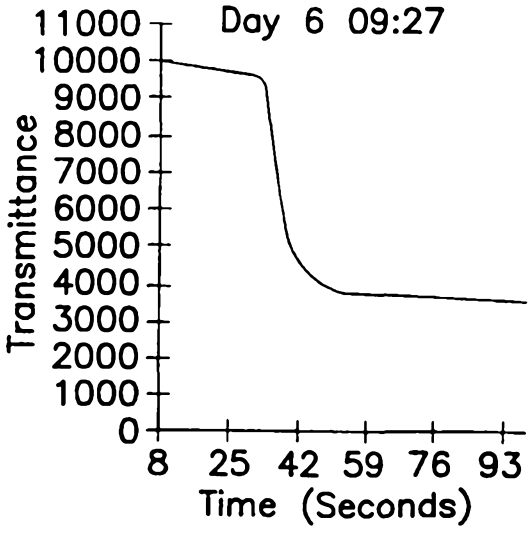

FIG. 34D

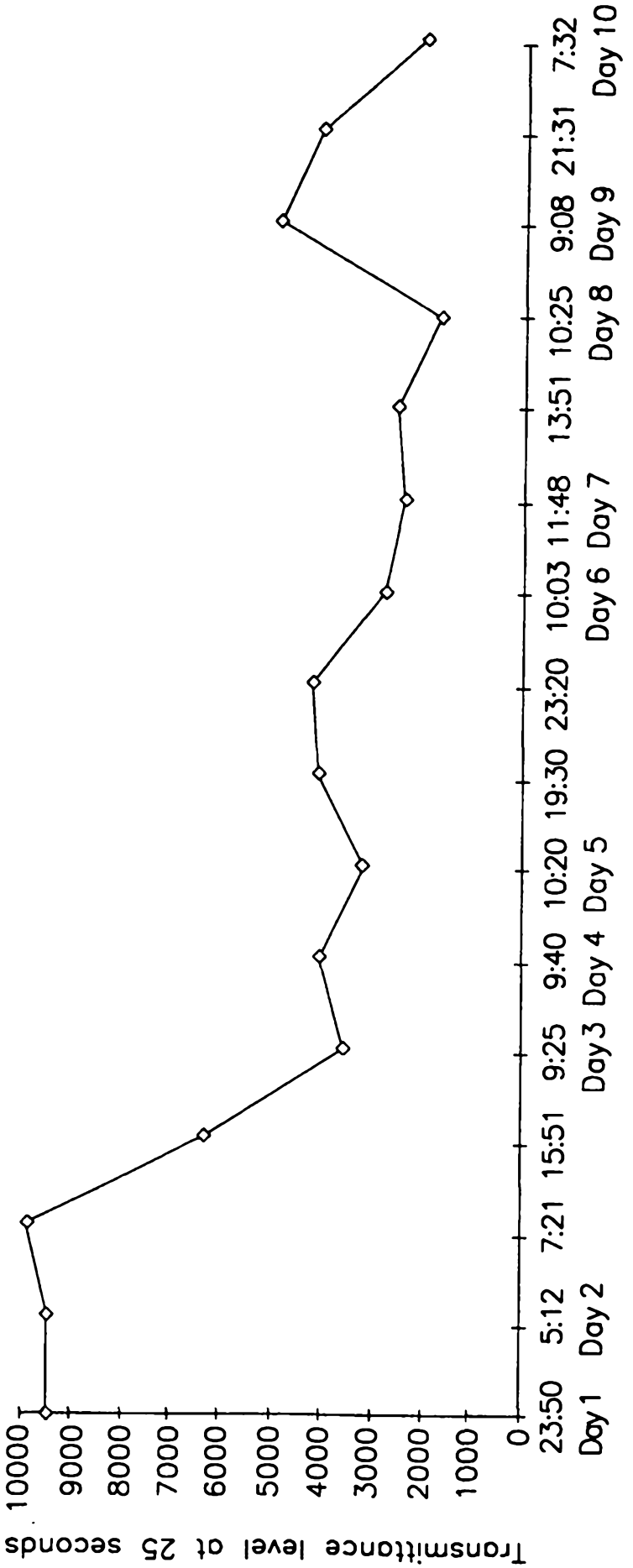
Transmittance level at 25 seconds
10000
9000
8000
7000
6000
5000
4000
3000
2000
1000
0
23:50 5:12 7:21 15:51 9:25 9:40 10:20 19:30 23:20 10:03 11:48 13:51 10:25 9:08 21:31 7:32
Day 1 Day 2 Day3 Day 4 Day 5 Day 6 Day 7 Day 8 Day 9 Day 10

FIG. 35A

FIG. 35B

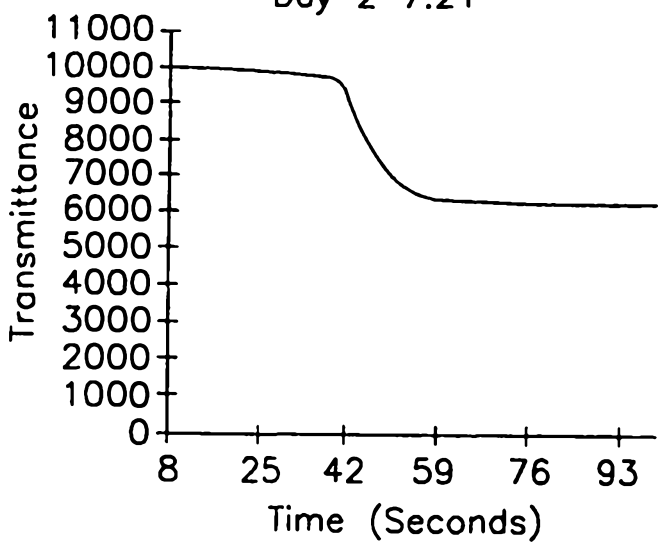

FIG. 35C

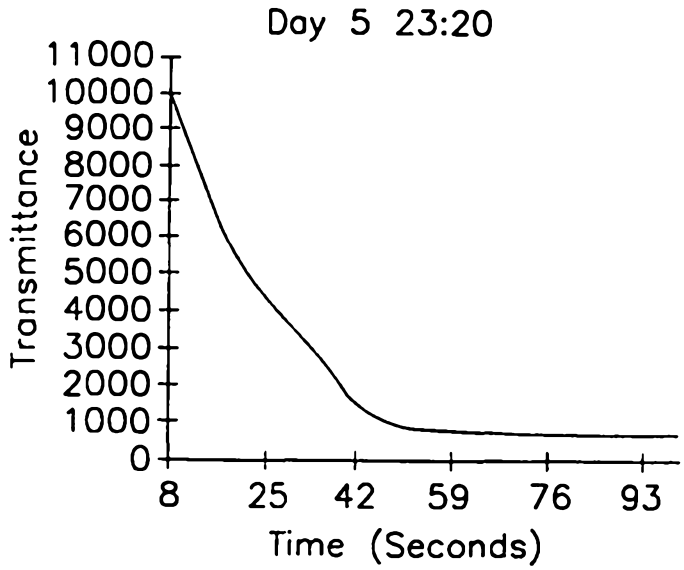

FIG. 35D

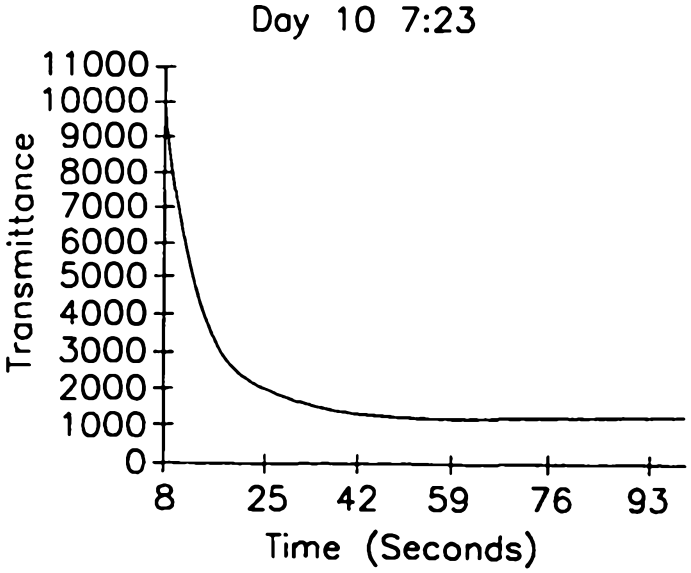

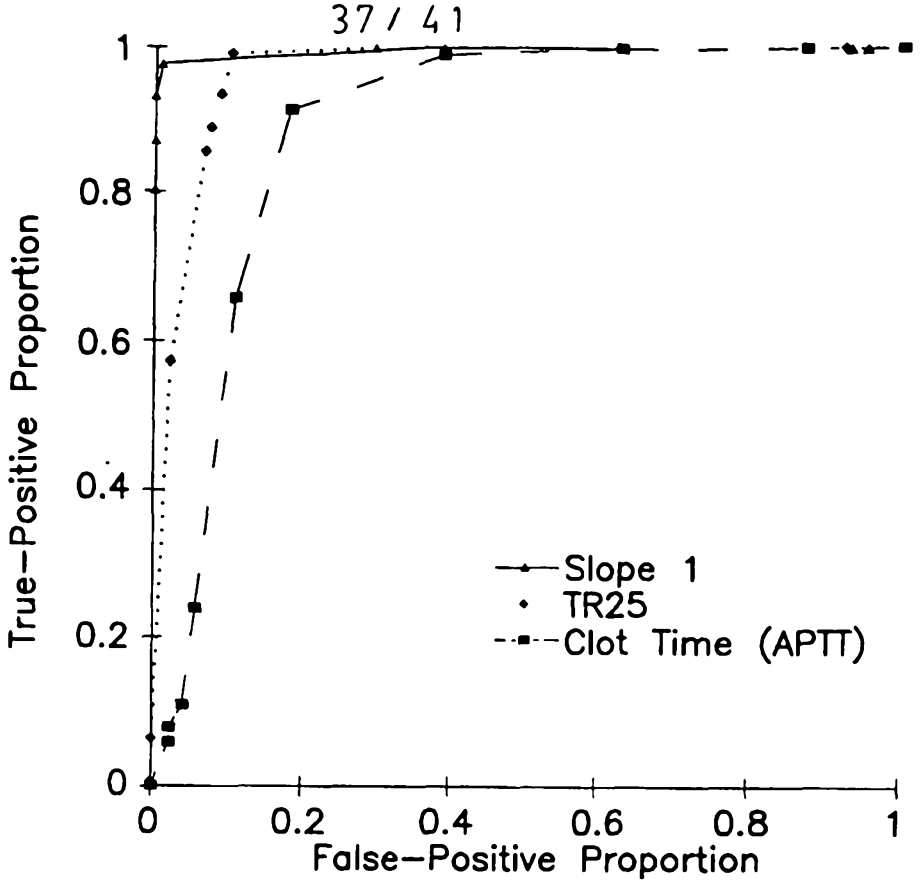
True–Positive Proportion
False–Positive Proportion
0
0.2
0.4
0.6
0.8
1
Slope 1
TR25
Clot Time (APTT)

FIG. 36

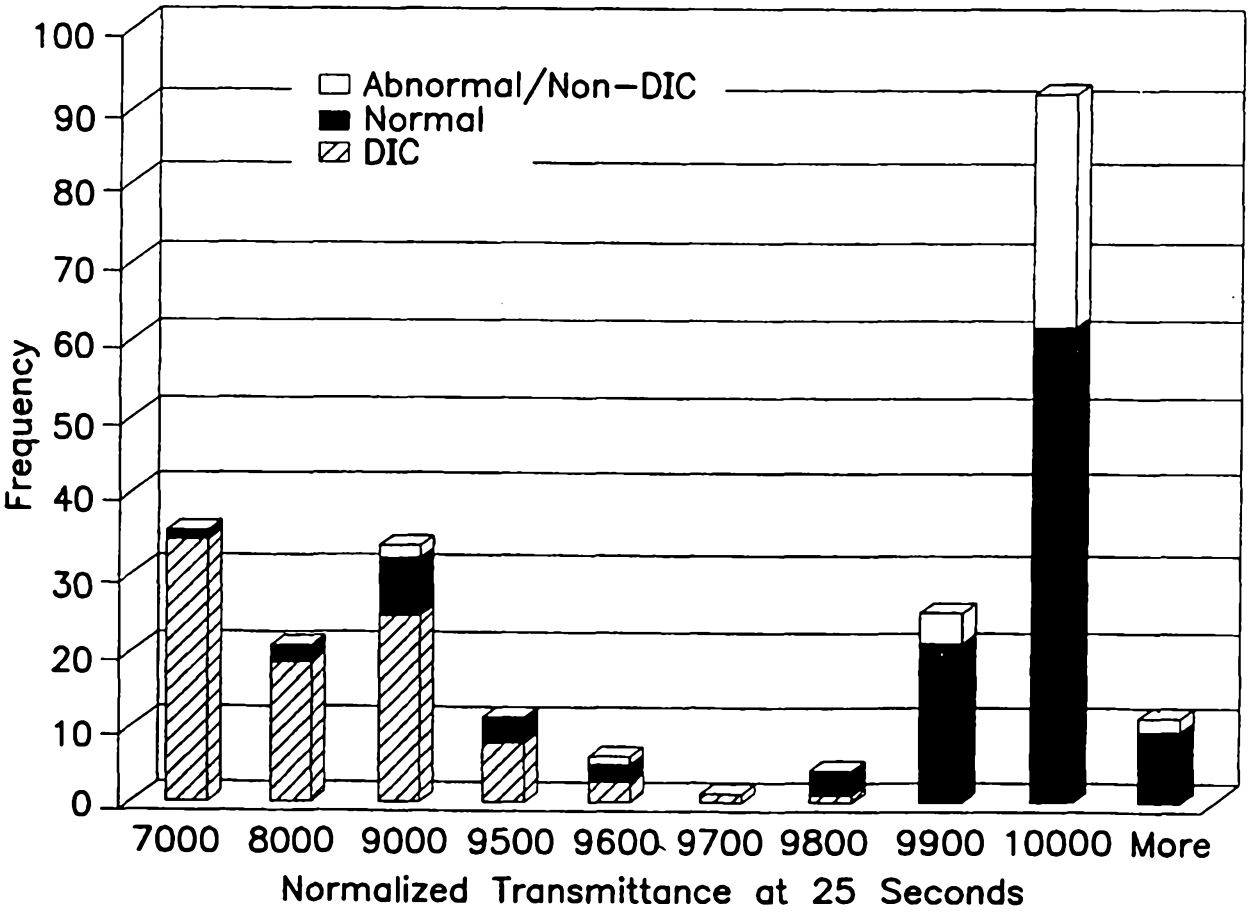
Abnormal/Non–DIC
Normal
DIC
Frequency
0
10
20
30
40
50
60
70
80
90
100
7000
8000
9000
9500
9600
9700
9800
9900
10000
More
Normalized Transmittance at 25 Seconds

FIG. 37

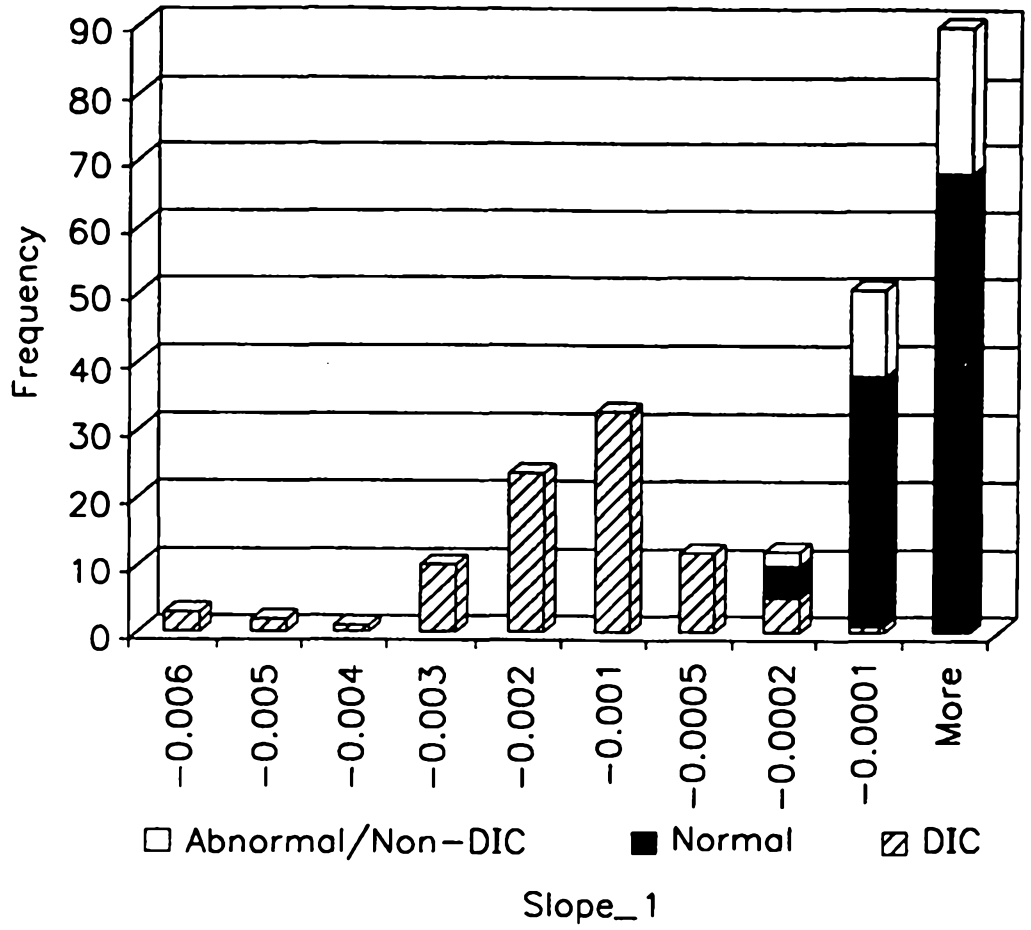
90
80
70
60
50
40
30
20
10
0
Frequency
-0.006
-0.005
-0.004
-0.003
-0.002
-0.001
-0.0005
-0.0002
-0.0001
More
Abnormal/Non-DIC
Normal
DIC
Slope_1

FIG. 38

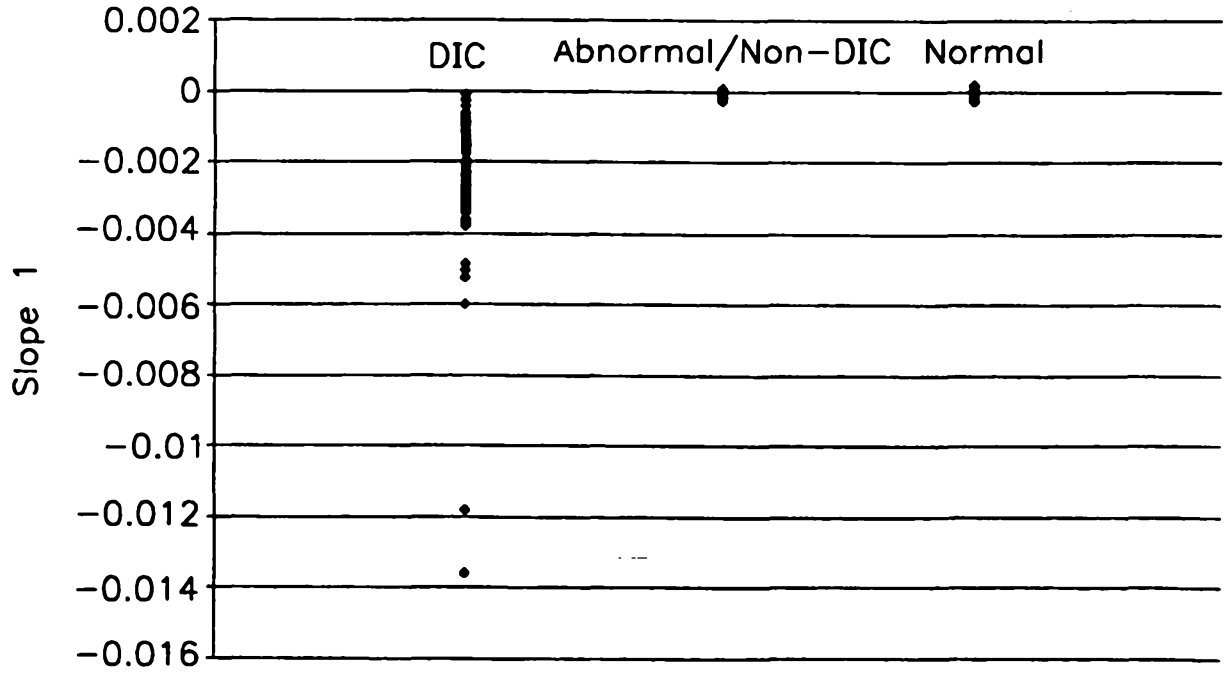
0.002
0
-0.002
-0.004
-0.006
-0.008
-0.01
-0.012
-0.014
-0.016
Slope 1
DIC
Abnormal/Non-DIC
Normal

FIG. 39

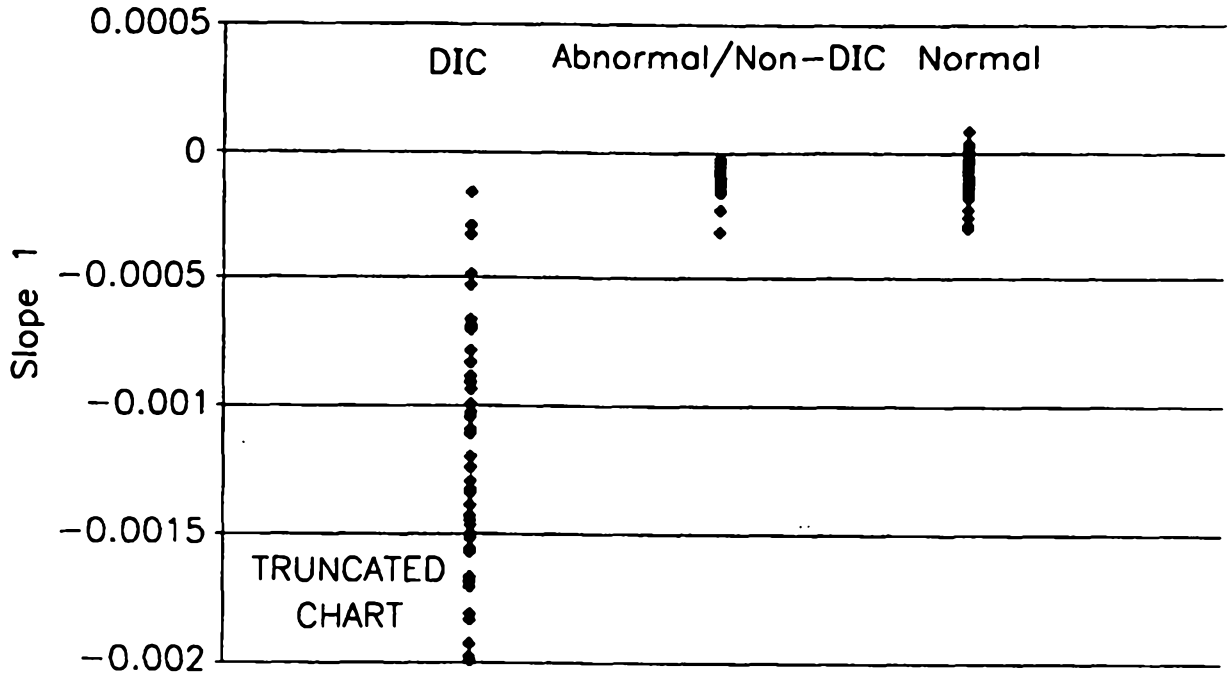
0.0005
0
−0.0005
−0.001
−0.0015
−0.002
Slope 1
DIC
Abnormal/Non−DIC
Normal
TRUNCATED
CHART

FIG. 40

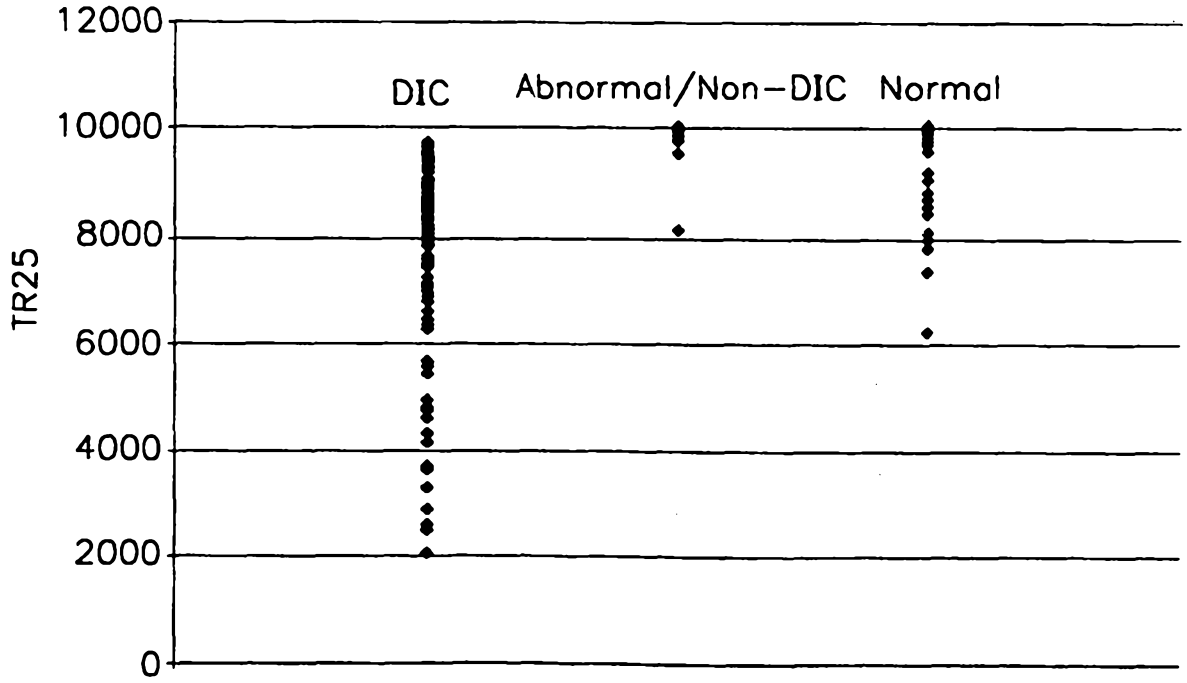
12000
10000
8000
6000
4000
2000
0
TR25
DIC
Abnormal/Non−DIC
Normal

FIG. 41

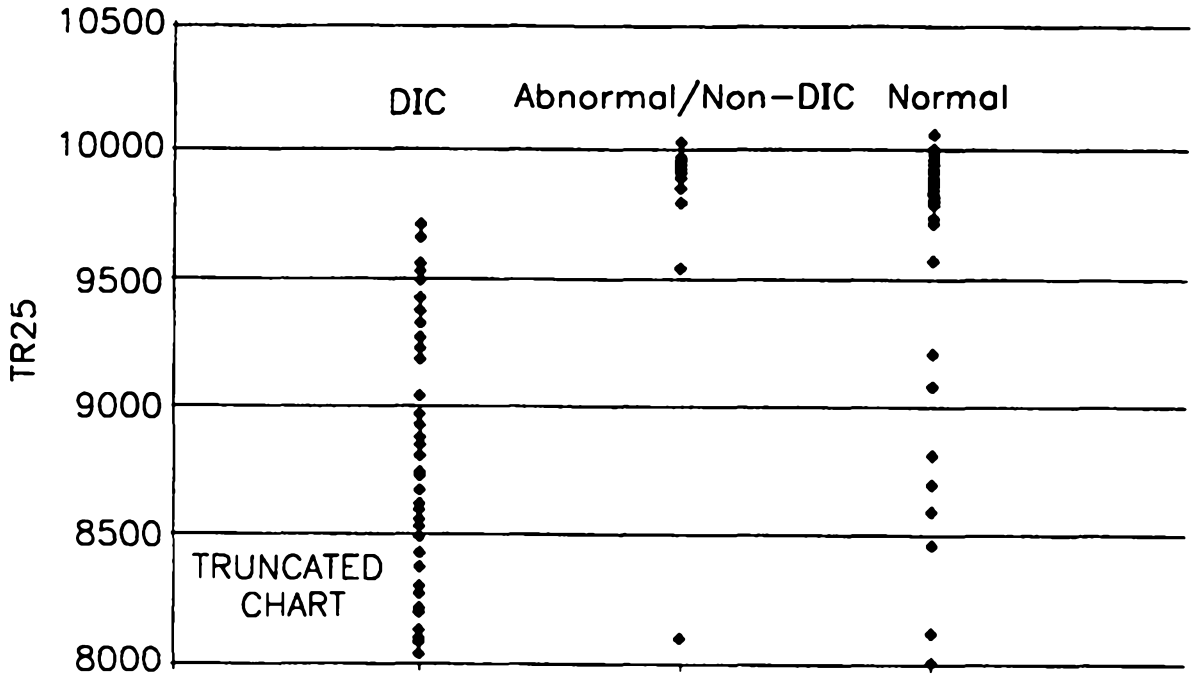
10500
10000
9500
9000
8500
8000
TR25
DIC
Abnormal/Non-DIC
Normal
TRUNCATED
CHART

FIG. 42

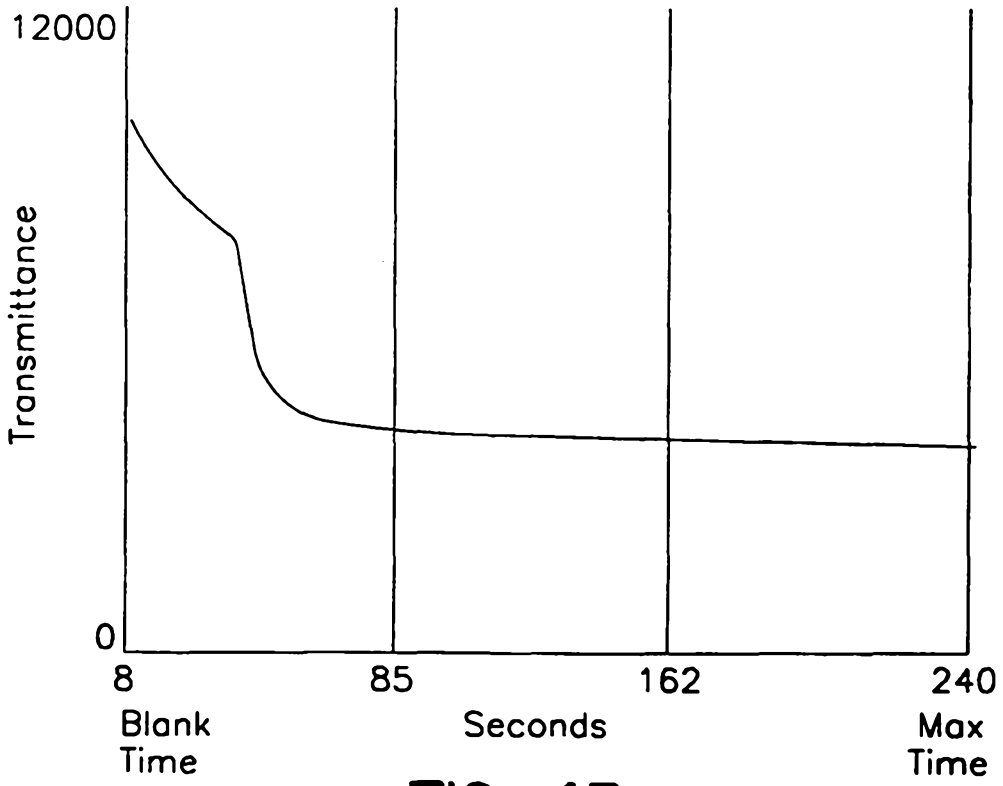
12000
0
Transmittance
8
85
162
240
Blank
Time
Seconds
Max
Time

FIG. 43

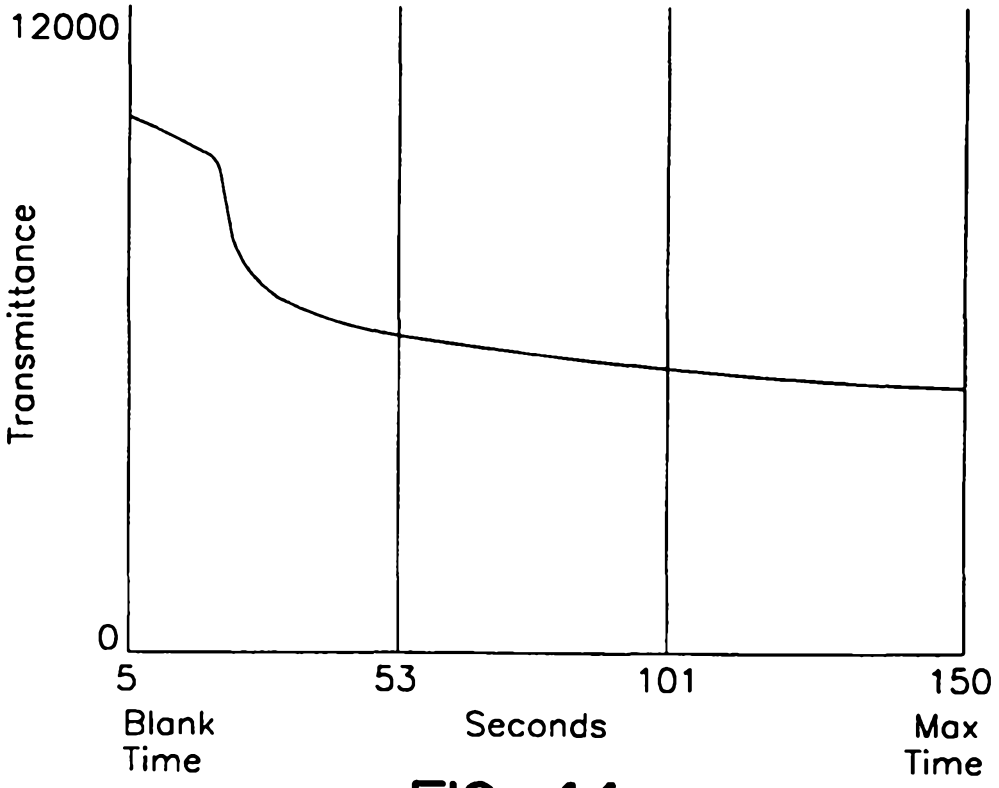
12000
Transmittance
0
5
53
101
150
Blank Time
Seconds
Max Time

FIG. 44

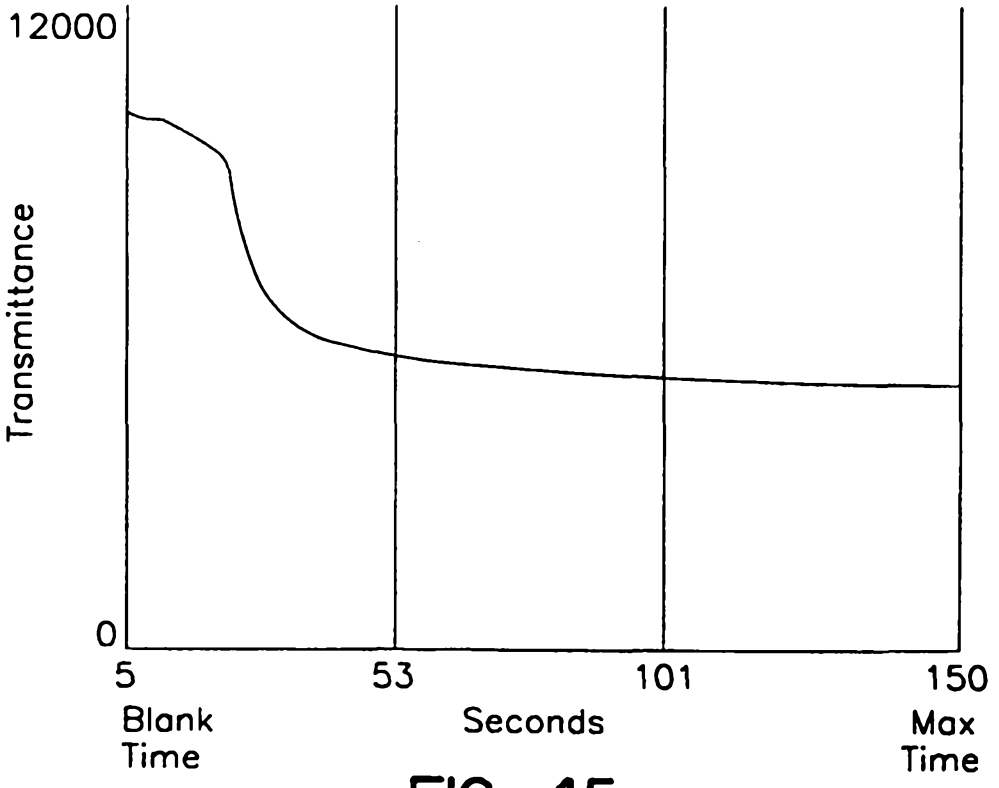
12000
Transmittance
0
5
53
101
150
Blank Time
Seconds
Max Time

FIG. 45